

Dissertation zur Erlangung des Doktorgrades
der Fakultät für Chemie und Pharmazie
der Ludwig–Maximilians–Universität
München

**The role of astrocytic amyloid
precursor protein in the regulation
of synaptic plasticity**



Sophie Crux

aus

Bad Soden am Taunus, Deutschland

2018

Erklärung

Diese Dissertation wurde im Sinne von §7 der Promotionsordnung vom 28. November 2011 von Herrn Prof. Dr. Jochen Herms betreut und von Herrn Prof. Dr. Martin Biel von der Fakultät für Chemie und Pharmazie vertreten.

Eidesstattliche Versicherung

Diese Dissertation wurde eigenständig und ohne unerlaubte Hilfe erarbeitet.

München, 23.08.2018

.....
Sophie Crux

Dissertation eingereicht am 23.08.2018

1. Gutachter: Prof. Dr. Martin Biel
2. Gutachter: Prof. Dr. Jochen Herms

Mündlichen Prüfung am 08.10.2018

Contents

Abbreviations	ix
Zusammenfassung	xv
Summary	xvii
1 Introduction	1
1.1 Morbus Alzheimer	2
1.1.1 History and epidemiology	2
1.1.2 Clinical symptoms	2
1.1.3 Neuropathological hallmarks	3
1.1.4 Risk factors	4
1.2 The amyloid cascade hypothesis	5
1.3 The amyloid precursor protein (APP)	7
1.3.1 Localisation and proteolytic cleavage	8
1.3.2 Functions of APP and its cleavage products	10
1.4 Synaptic plasticity	12
1.4.1 Structural plasticity of dendritic spines	13
1.4.2 Functional plasticity	14
1.5 Astrocytes	15
1.5.1 The tripartite synapse	15
1.5.2 Ca ²⁺ signalling in astrocytes	18
1.6 Methodology	20
1.6.1 Two-photon microscopy	20
1.6.2 Ca ²⁺ imaging	21

CONTENTS

1.7	Aim of this thesis	23
2	Results	25
2.1	The role of APP in synaptic plasticity in the cortex and hippocampus	26
2.1.1	APP is crucial for cortical dendritic spine plasticity without consequences on NMDA/AMPA receptor currents . . .	26
2.1.2	Hippocampal long-term plasticity depends on the presence of APP and cannot be restored by gliotransmitter D-serine	29
2.1.3	Conditional KO of APP in astrocytes influences spine density and morphology in the cortex and hippocampus	32
2.2	The role of APP in astrocytic function	35
2.2.1	Investigation of spontaneous astrocytic Ca^{2+} transients in the hippocampus and cortex	35
2.2.2	Altered mitochondrial network integrity in APP-KO astrocytes	42
2.2.3	Altered mitochondrial Ca^{2+} transients in APP-KO astrocytes	45
2.2.4	Investigation of mitochondrial proteins in primary astrocytes	48
2.2.5	Isolation and protein investigation of astrocytes derived from the adult mouse brain	50
3	Discussion	53
3.1	The role of APP in synaptic plasticity in the cortex and hippocampus	54
3.1.1	Lack of APP does not result in altered NMDA/AMPA receptor currents	54
3.1.2	Reduced LTP in APP-KO animals cannot be rescued by D-serine application	56
3.1.3	Astrocytic APP impacts spine density and morphology in the cortex and hippocampus	58
3.1.4	Conclusion I	60
3.2	The role of APP in astrocytic function	60

3.2.1	APP plays a role in perisynaptic Ca ²⁺ signalling in astrocytes	61
3.2.2	APP is crucial for mitochondrial network integrity	64
3.2.3	Mitochondrial Ca ²⁺ imaging in primary astrocytes	65
3.2.4	Mitochondrial proteins	65
3.2.5	Conclusion II	68
3.3	Relevance of APP studies for understanding AD	70
4	Materials and Methods	71
4.1	Genetically modified mouselines, genotyping and husbandry	72
4.1.1	Mouse lines	72
4.1.2	Genotyping	72
4.1.3	Husbandry	76
4.2	Genetic modifications via viruses and plasmids	76
4.2.1	Viruses	76
4.2.2	Plasmids	76
4.3	Stereotactic virus injection	77
4.3.1	Investigation of the role of APP in astrocytic Ca ²⁺ transients	78
4.3.2	Investigation of the role of APP in dendritic spine density and morphology	78
4.4	Electrophysiology in acute brain slices	78
4.4.1	Patch clamp recordings	78
4.4.2	LTP recordings	79
4.5	Astrocytic Ca ²⁺ imaging in acute brain slices	81
4.5.1	Two-photon Ca ²⁺ imaging in astrocytic protrusions	81
4.5.2	Analysis of astrocytic Ca ²⁺ transients	81
4.6	<i>Ex vivo</i> analysis of dendritic spines	82
4.6.1	Perfusion	82
4.6.2	Brain slicing	82
4.6.3	Immunohistochemical staining	82
4.6.4	Confocal microscopy	83
4.6.5	Dendritic spine counting and morphological investigation .	83
4.7	Primary astrocyte culture	83
4.7.1	Preparation	83

Table of Contents

4.7.2	Plamid transfection	84
4.7.3	Investigation of mitochondrial morphology	84
4.8	Mitochondrial Ca ²⁺ signals in cultured astrocytes	85
4.8.1	Two-photon imaging of mitochondrial Ca ²⁺ signals	85
4.8.2	Data analysis of mitochondrial Ca ²⁺ signals	86
4.9	Protein extraction and immunoblotting	86
4.10	Isolation of astrocytes from the adult mouse brain	87
4.11	Antibody list	88
4.12	Statistics	88
	Bibliography	89
	List of publications	106
	Acknowledgements	109

Abbreviations

°C	degree celsius
µg	microgram
µl	microliter
µm	micrometer
Aβ	amyloid beta peptide
1 st	first
2 nd	second
3 rd	third
AAV	adeno-associated virus
aCSF	artificial cerebrospinal fluid
AD	Alzheimer's disease
AEP	asparagine endopeptidase
AICD	amyloid precursor protein intracellular domain
AMPA	alpha-amino-3-hydroxy-5-methyl-4-isoxazolepropionic acid
AMPA	alpha-amino-3-hydroxy-5-methyl-4-isoxazolepropionic acid receptor
ANOVA	analysis of variance
AOM	acousto optical modulator
APP	amyloid precursor protein
APP CT	amyloid precursor protein C-terminus
APP NT	amyloid precursor protein N-terminus
APPsα	secreted amyloid precursor protein alpha
ATP	adenosine 5'-triphosphate
a.u.	arbitrary unit
AUC	area under the curve
AVG	average
BACE1	beta-secretase 1
BSA	bovine serum albumin
C57BL/6J	wild-type mouse line
Ca ²⁺	calcium ion
CA1	subfield of the hippocampus

Abbreviations

CLSM	confocal laser scanning microscope
CSF	cerebrospinal fluid
cyt C	cytochrome C
3D	three-dimensional
2D	two-dimensional
DG	dentate gyrus
DIV	days <i>in vitro</i>
DNA	deoxyribonucleic acid
DRP1	dynamin related protein 1
e.g.	for example; lat. <i>exempli gratia</i>
eGFP	enhanced green fluorescent protein
EPSC	excitatory postsynaptic current
ER	endoplasmatic reticulum
et al.	and others
F-actin	filamentous actin
FRET	Förster resonance energy transfer
fs	femtosecond
g	gram
GABA	gamma amino butyric acid
GCaMP	GFP-based Ca ²⁺ probe
GCaMP-Lck	membrane-tethered GCaMP
GECI	genetically encoded calcium indicator
GFAP	glial fibrillary acidic protein
GFP	green fluorescent protein
GPCR	G protein-coupled receptor
h	hour
hkprot	housekeeping protein
Hz	hertz
IM	inner mitochondrial membrane
IP3	inositol-1,4,5-trisphosphate
IP3R	inositol-1,4,5-trisphosphate receptor
i.p.	intraperitoneal
K ⁺	potassium ion
kDa	kilodalton
kg	kilogram
KO	knock-out
KD	knock-down
KPI	Kunitz-type protease inhibitor
LSM	laser scanning microscope
LTD	long-term depression
LTP	long-term potentiation
M	molar
MCU	mitochondrial calcium uniporter

mg	milligram
Mg ²⁺	magnesium ion
MHz	megahertz
min	minute
mitoGCaMP	mitochondria targeted GCaMP
ml	milliliter
mm	millimeter
mPTP	mitochondrial permeability transition pore
MRI	magnetic resonance imaging
MT5-MMP	membrane-type 5 metalloproteinase
MW	molecular weight
N	number
NA	numerical aperture
NaCl	sodium chloride
NaHCO ₃	sodium bicarbonate
NGS	normal goat serum
nl	nanoliter
nm	nanometer
NMDA	N-methyl-D-aspartate
NMDAR	N-methyl-D-aspartate receptor
OM	outer mitochondrial membrane
p	p-value
p3	postnatal day 3
PBS	phosphate buffered saline
PCR	polymerase chain reaction
pDRP1	phosphorylated dynamin related protein 1
PFA	paraformaldehyde
PMT	photomultiplier tube
PSEN 1/2	presenilin 1/2
PSD	postsynaptic density
ROI	region of interest
s	second
SEM	standard error of the mean
SNARE	soluble N-ethylmaleimide-sensitive-factor attachment receptor
STD	standard deviation
t	time
tg	transgene
Thy1	thymocyte antigen 1; CD90
TIM23	translocase of the inner mitochondrial membrane 23
TOM20	translocase of the outer mitochondrial membrane 20
TOM40	translocase of the outer mitochondrial membrane 40
TRPA1	transient receptor potential A1
VDAC	voltage-dependent anion channel

Abbreviations

vg vector genome
WT wild type

List of Figures

1.1	Histopathological hallmarks of the first Alzheimer patient Auguste Deter	3
1.2	The amyloid cascade hypothesis	6
1.3	Schematic domain structure of APP family members	7
1.4	Cellular processing pathways of APP	9
1.5	The tripartite glutamate synapse	17
1.6	One- and two-photon microscopy	21
1.7	Ca ²⁺ indicator Lck-GCaMP	22
2.1	NMDA/AMPA recordings in the cortex of APP-KO mice	27
2.2	NMDA/AMPA and paired-pulse currents do not differ in APP-KO mice	28
2.3	LTP is reduced in APP-KO mice	30
2.4	Reduced LTP in APP-KO hippocampus cannot be rescued by D-serine application	31
2.5	Conditional KO of <i>APP</i> in adult astrocytes surrounding GFP-M positive neurons	32
2.6	Conditional KO of <i>APP</i> in adult astrocytes alters morphology and density of dendritic spines	34
2.7	Imaging and analysis of astrocytic Ca ²⁺ transients in the hippocampus and cortex	37
2.8	Spontaneous astrocytic Ca ²⁺ transients are altered in the cortex of APP-KO mice	39
2.9	Spontaneous astrocytic Ca ²⁺ transients are altered in the hippocampus of APP-KO mice	41
2.10	Primary astrocytes harvested from APP-KO mice do not express APP	42
2.11	APP-KO astrocytes display fragmented mitochondrial morphology that can be rescued by reintroduction of APP	44
2.12	Stimulated mitochondrial Ca ²⁺ signals of APP-KO astrocytes display slower kinetics	46
2.13	Stimulated mitochondrial Ca ²⁺ signals of APP-KO astrocytes differ in distribution within the mitochondria network	47
2.14	Investigation of mitochondrial proteins implicated in energy metabolism, fission and Ca ²⁺ transport in primary astrocytes	49
2.15	Isolation of astrocytes derived from the adult mouse brain	50

List of Figures

2.16	Characterisation of astrocytes isolated from the adult brain and investigation of mitochondrial proteins	52
3.1	Potential interaction sites of APP with the ER and mitochondria that affect Ca^{2+} homeostasis	69

Zusammenfassung

Morbus Alzheimer ist die häufigste Form der Demenzerkrankung, die 47 Millionen Menschen weltweit betrifft. Zukünftig steigende Zahlen sind vorhergesagt, da die steigende Lebenserwartung das Risiko erhöht, an Morbus Alzheimer zu erkranken. So stellt die Krankheit eine enorme Belastung für unsere Gesellschaft dar. Eine Heilung wurde bisher noch nicht gefunden, trotz jahrzehntelanger Forschung.

Ein Kennzeichen der Erkrankung ist die Akkumulation vom β -Amyloid ($A\beta$), welches als molekulare Erklärung für die Krankheit gilt und deshalb Gegenstand intensiver Studien ist. Aktuelle therapeutische Strategien zielen auf die Symptome der Erkrankung und erste mechanistische Ansätze, die in die $A\beta$ -Produktion eingreifen, blieben jedoch bisher erfolglos. Daher bleibt es überaus wichtig, die Grundlagenbiologie zu verstehen, die Morbus Alzheimer zugrunde liegt, um erfolgreiche Therapien zu entwickeln. Obwohl $A\beta$ ein Spaltprodukt des β -Amyloid-Vorläuferprotein (APP) ist, ist die Funktion von APP weniger gut verstanden und bisherige Untersuchungen begrenzen sich hauptsächlich auf Neurone.

Der neuronale Informationsfluss zwischen Prä- und Postsynapsen ist stark von angrenzenden Astrozyten abhängig, die in synaptischer Plastizität, Informationsverarbeitung und -übertragung involviert sind. Die synaptische Plastizität gilt als Mechanismus für Lernen und Gedächtnis. Die vorliegende Arbeit untersucht die physiologische Funktion von APP im Rahmen neuronaler synaptischer Plastizität und den damit assoziierten Astrozyten. Hierfür wurden Modelle mit konstitutivem und konditionellem APP knock-out verwendet.

Im ersten Teil der Arbeit wird die Rolle von APP in struktureller und funktioneller synaptischer Plastizität im Hippokampus und Kortex beschrieben. Dabei zeigt sich, dass die Dichte und Morphologie postsynaptischer Spines im Kortex weniger Plastizität aufweist, wenn APP in Neuronen und Astrozyten fehlt. Diese Plastizitätsdefizite bleiben ohne Veränderung der exzitatorischen Rezeptordichte. Selektives Ausschalten von APP in Astrozyten führt zu verminderter Anzahl plastischer Spines im Kortex, wohingegen die Dichte der stabilen Spines im Hippokampus zunimmt. Außerdem führt das Fehlen von APP zu Defiziten der funktionellen Plastizität, die sich durch verminderte Signalverstärkung äußert. Diese funktionelle Plastizität wird vom Glutransmitter D-Serin potenziert, der von Astrozyten ausgeschüttet wird. Da APP-KO Tiere reduzierte D-Serin Werte im extrazellulären Raum aufweisen, wurde die funktionelle synaptische Plastizität unter Zugabe von D-Serin untersucht.

Der zweite Teil der Arbeit befasst sich mit der Rolle von APP in Astrozyten, unter dem Aspekt, dass diese aktiv bei der synaptischen Aktivität beteiligt sind. Ca^{2+} ist ein essentielles Signalmolekül, das viele zelluläre Prozesse reguliert; so auch die Gliotransmission. Hier wird gezeigt, dass APP eine wichtige Rolle in spontanen astrozytären Ca^{2+} -Strömen in den verästelten Kontaktbereichen zu Synapsen im Kortex und Hippokampus spielt. Die Ca^{2+} -Ströme in diesen perisynaptischen Strukturen werden durch Mitochondrien reguliert, die in APP-KO Astrozyten morphologische und funktionale Abweichungen aufweisen.

Zusammenfassend beschreiben die Ergebnisse dieser Arbeit eine physiologische Rolle von APP in synaptischer Plastizität und der damit zusammenhängenden Funktion von Astrozyten. Die Erkenntnisse sind wichtig für ein verbessertes Verständnis von Morbus Alzheimer und für die Entwicklung neuer therapeutischer Strategien.

Summary

Alzheimer's disease (AD) is the most common form of dementia affecting 47 million people worldwide and rising numbers are predicted for the future, as increasing life expectancy denotes increased risk of developing AD. The disease constitutes an enormous burden for our society. Despite numerous therapeutical approaches, a cure for AD has not been found yet.

One hallmark of AD is the accumulation of amyloid β ($A\beta$) which is intensively studied and widely considered as molecular explanation for the synaptic pathology in AD. Today's therapeutic strategies target AD symptoms and first mechanistic approaches, including interference with $A\beta$ production, are failing in clinical trials. Hence, it remains of utmost importance to further understand the fundamental biology of AD-related physiology in order to develop successful therapeutic strategies. $A\beta$ is a cleavage product of the amyloid precursor protein (APP). However, the physiological functions of APP remain less well understood and previous investigations have been mainly confined to neurons.

Neuronal information flow between pre- and postsynapse is strongly dependent on the adjacent astrocytes that are involved in synaptic information processing, transmission and plasticity. Synaptic plasticity is considered to be the underlying mechanisms of learning and memory. In the present work, the physiological role of APP was investigated both in synaptic plasticity and associated astrocytes in a constitutive and conditional knock-out model of APP (APP-KO).

In the first part of this work, the role of APP in structural and functional synaptic plasticity is characterised in the cortex and hippocampus. The density and morphology of postsynaptic compartments -the dendritic spines- display reduced plasticity when APP is lacking in both neurons and astrocytes of the cortex. The reduced plasticity does not involve excitatory receptor composition. Selective KO of APP in adjacent astrocytes results in decreased plastic spines in the cortex, while increased spine number and more stable spines are observed in the hippocampus. Additionally, APP-KO mice display functional plasticity deficits in the hippocampus manifested by reduced synaptic signalling strength. The gliotransmitter D-serine is released by astrocytes and potentiates functional plasticity in neurons. As extracellular levels of D-serine are reduced in APP-KO animals, application of D-serine was tested for rescue of the functional plasticity deficits.

The second part of this work focuses on the role of APP in astrocytes as active

Summary

partners in synaptic activity. Spontaneous Ca^{2+} activity, that is responsible for numerous cellular processes and gliotransmission, was investigated in the astrocytic contact sites to synapses. Ca^{2+} transients are shown to be reduced in the perisynaptic sites of APP-KO astrocytes in the cortex and hippocampus. The Ca^{2+} activity is regulated by mitochondria that are dysfunctional in APP-KO astrocytes evidenced by fragmented morphology and prolonged Ca^{2+} uptake and release duration.

In summary, these findings ascribe a physiological role to APP in synaptic plasticity and in associated astrocytic function. These insights are crucial for understanding the biology of AD and for developing new therapeutic strategies.

Chapter 1

Introduction

1.1 Morbus Alzheimer

1.1.1 History and epidemiology

In 1906, the German psychiatrist Alois Alzheimer described a special and until then unknown case of his patient Auguste Deter. He reported temporal and spatial disorientation and tremendous memory deficiencies. Moreover, he observed a severe atrophy in the brain after her death by the age of 55. The brain also displayed peculiar spots of accumulations and strongly stained neurofibrils which he correlated to her dementia. Today, these abnormalities are entitled amyloid plaques and neurofibrillar tangles and constitute the hallmarks of Alzheimer's disease (AD)(Figure 1.1)[1].

The term dementia is derived from the latin language and can be translated as "out of mind". It is descriptive for any kind of disease that includes loss of memory, thinking, orientation, comprehension, calculation, speech, ability to learn and judge [2].

Alzheimer's disease is ascribed to two-thirds of all dementia cases. The growing population and increasing life expectancy is a challenge of the today's world [3]: Today, 47 million people worldwide live with dementia and 131.5 million are predicted for 2050 [4]. The current estimated worldwide costs of dementia are 818 billion US dollar. However, many people with dementia have not received a diagnosis and therefore lack care and treatment [4]. This current and increasing burden for the world's society is an emotional, social, political and financial challenge. Therefore, it is of utmost importance to understand the disease and develop appropriate therapeutic strategies.

1.1.2 Clinical symptoms

AD is a neurodegenerative disease that is characterised by progressive dementia from a mild, moderate to severe stage [5]: Usually, about a decade passes by before the illness becomes severe and patients die as a tragic consequence [6]. Loss of neurons in the entorhinal cortex have been already detected during mild cognitive impairment [7] suggesting that some parts of the brain are earlier and more affected than others [6]. Reduced cortical thickness can be monitored via magnetic resonance imaging (MRI) in the living AD patients and correlated with cognitive decline [8].

There is evidence that AD does not simply cause neuronal loss resulting in silencing of neuronal networks, but rather altered network activity that might actively interfere with the complex processes underlying cognitive functions such as learning and memory [6]. For instance, AD patients display hyperperactivation of the neuronal network in the hippocampus during memory tasks [9]. This hyperactivity correlates with decreased hippocampal volume and cortical thinning in AD-related brain regions [10]. In brains of AD patients epileptic seizures can arise, which is most evident in patients with mild forms of the disease [11].

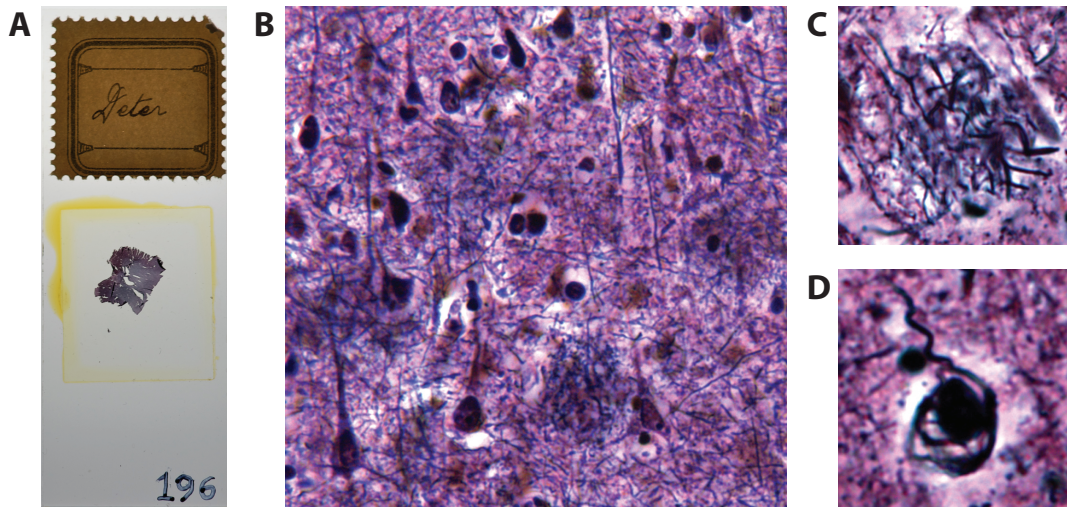


Figure 1.1. Histopathological hallmarks of the first Alzheimer patient Auguste Deter. (A) Histological brain slice preparation of Auguste Deter by courtesy of Prof. Dr. Dr. h. c. Hans Kretzschmar from the Institute for Neuropathology of the Ludwig-Maximilians-University Munich. (B-D) Microscopic images taken and thankfully provided by Dr. Dr. Mario Dorostkar. (B) Overview of Bielschowsky silver staining method for illustration of the AD hallmarks. Magnification of a $A\beta$ plaque (C) and neurofibrillary tangles (D).

1.1.3 Neuropathological hallmarks

Cortical thinning due to neuronal loss is one hallmark of AD and the atrophy can be detected before the onset of dementia [12]. Two major hallmarks of AD are amyloid- β ($A\beta$) plaques in the parenchyma and neurofibrillary tangles inside neurons (Figure 1.1). These deposits are associated with initiation of inflammatory processes involving microglia and astrocytes [13],[14]. Usually, the earliest neuritic plaques, neurofibrillary tangles, and neuropil threads appear in structures of the medial temporal lobe and expand in limbic and isocortical areas [15]. This has critical consequences on episodic memory function explaining the deficits in learning and memory in AD.

Neurofibrillary tangles are inclusions in neurons consisting of aggregated tau protein [16]. Tau is a microtubuli associated protein that stabilises microtubuli and is thereby important for transport of molecules along axons, axonal outgrowth, and cell polarity [17]. Hyperphosphorylation of tau leads to dissociation of tau from microtubuli resulting in destabilisation of those [18]. The hyperphosphorylation of tau also favours its accumulation in β -sheet configuration which forms neurofibrillary tangles and dystrophic neurites, as tau accumulates in somatodendritic compartments instead of functioning in axons.

The formation of distinct plaques consisting of accumulated $A\beta$ [19] is another hallmark of AD. $A\beta$ accumulation is an intensively studied hallmark in AD and will be further described in the context of the amyloid cascade hypothesis. However, the

1. Introduction

level of cognitive impairment correlates with the burden of neocortical neurofibrillary tangles [20].

The entailed atrophy visible through decreased brain volume and weight results from shrinkage and loss of neuronal processes, synapses and neurons [6]. Much evidence suggests that synapses and dendrites are predominantly affected by AD. Loss of neuronal connections can better explain cognitive decline in AD than neuronal loss [21].

Brain tissue samples from brains of AD patients and animal models of AD displayed alterations in levels of proteins and genes directly involved in neuronal Ca^{2+} signalling suggesting a perturbed Ca^{2+} homeostasis with detrimental consequences such as excitotoxicity and apoptosis [22]. Importantly, memory deficits in AD patients correlate best with synapse loss rather than $\text{A}\beta$ plaque burden or neurofibrillary tangles [23].

1.1.4 Risk factors

AD is probably caused by obscure interplay among numerous genetic, epigenetic and environmental factors [6]. A general risk factor of AD is increasing age, as from the age of 65 the probability to develop AD doubles [24].

In inherited familial cases of AD autosomal dominant mutations in amyloid precursor protein gene (*APP*), presenilin *PSEN1*, and *PSEN2* lead to familial early-onset AD (<60 years) while *APOE* isoforms (the *APOE4* allele) [25] and *TREM2* variants [26] are known as the most important risk factors for sporadic late-onset AD. The mutations in *APP* and *PSEN* (encodes the catalytic center of γ -secretase) impact *APP* processing resulting in increased production of aggregation prone $\text{A}\beta$ peptides [25]. Moreover, overexpression of *APP* alone leads to $\text{A}\beta$ accumulation. Consequently, patients with Down Syndrome (trisomy 21) harbouring a third copy of *APP*, due to the presence of *APP* on chromosome 21, show evidences of AD at early age [27],[19], [28].

A healthy life style has protective effects against dementia [29], while a history of stroke increases the risk of dementia in the older population [30].

There is currently no treatment to cure dementia or alter the disease progression (World Health Organisation, WHO 2018)[31]. The WHO recognises dementia as a 'public health priority'. In a 'Global action plan on the public health' the organisation responses to dementia for the years 2017-2025. However, there are numerous ongoing treatment approaches in different stages of clinical trials that target, among others, proteolytic cleavage of the amyloid precursor protein (*APP*) (e.g. BACE1 inhibition) or $\text{A}\beta$ accumulation (antibody therapy) [32].

1.2 The amyloid cascade hypothesis

The amyloid cascade hypothesis postulates that accumulation and deposition of $A\beta$ is the driving factor of the pathological courses of AD [33],[34],[35].

Later, the hypothesis was refined by stating that gradual changes in the levels and conformation of $A\beta$ in the brain are thought to initiate the amyloid cascade. Thus, due to an imbalance of $A\beta$ production and clearance, $A\beta$ forms soluble oligomers which are delineated to be the toxic structures that cause synaptic dysfunction. Further formation of insoluble amyloid plaques results in an immun response that involves activation of microglia and astrocytes. Subsequently, microtubule associated protein tau gets hyperphosphorylated and oligomerises forming insoluble aggregates. Further progression of the disease results in dysfunction and loss of neurons. The final hallmark of the disease is the tangle and plaque pathology (Figure 1.2)[36].

The combination of pathology and genetics in humans constitute the pillars of the hypothesis ascribing the primary role in the etiology of AD to $A\beta$. Basis for the hypothesis was provided by sequencing of the amino acid sequence of $A\beta$ as the main component of the pathological hallmark plaque [19] and cerebral angiopathies [37] from brains of AD patients. Since neuropathological hallmarks of AD were found in Down syndrome patients and the protein sequence resembled the one from sporadic AD patients [38],[39], the *APP* gene was cloned and localised on chromosome 21 shortly after [40],[41]. Due to a third copy of chromosome 21 in Down Syndrome patients, $A\beta$ production is increased which leads to $A\beta$ deposition and dementia at an early age. The identification of a mutation in the *APP* gene in early-onset AD patients that is pathologically identical to sporadic, late-onset AD, was an important step in understanding the disease cause [42]. Missense mutations in *PSEN* genes were identified responsible for early-onset AD [43],[25]. They are catalytic components of γ -secretases a cleaving enzyme of APP [44]. Nowadays, hundreds of mutations in *PSEN1* and *PSEN2* and *APP* are identified that can cause early-onset familial AD [45]. With regard to sporadic late-onset AD, isoforms of *APOE4* gene increase the risk for spontaneous AD by interfering with the clearance of $A\beta$ [46],[47],[25]. Furthermore, a coding mutation (A673T) in the *APP* gene was discovered that protects against AD and cognitive decline in the elderly without AD [48],[49].

Physiological production [51] and clearance of $A\beta$ [52] and synapse change associated with soluble $A\beta$ in AD brains [53] led to revision of the amyloid cascade hypothesis suggesting $A\beta$ oligomers as toxic component in the development of AD [50],[36]. As $A\beta$ is the initiating cause of AD, the hypothesis implies that inhibition of excessive production and removal of toxic $A\beta$ would prevent or cure the disease. The early recognition of the disease needs to be advanced [54] so that the therapy can start with the first changes in $A\beta$ levels 25 years before expected symptom onset [55].

Despite many approaches targeting $A\beta$ levels to improve symptoms, there is no cure of the disease yet [56],[57] and clinical studies targeting $A\beta$ have been failing [32]. Hence, the amyloid hypothesis is under debate and alternative approaches are taken into consideration [58].

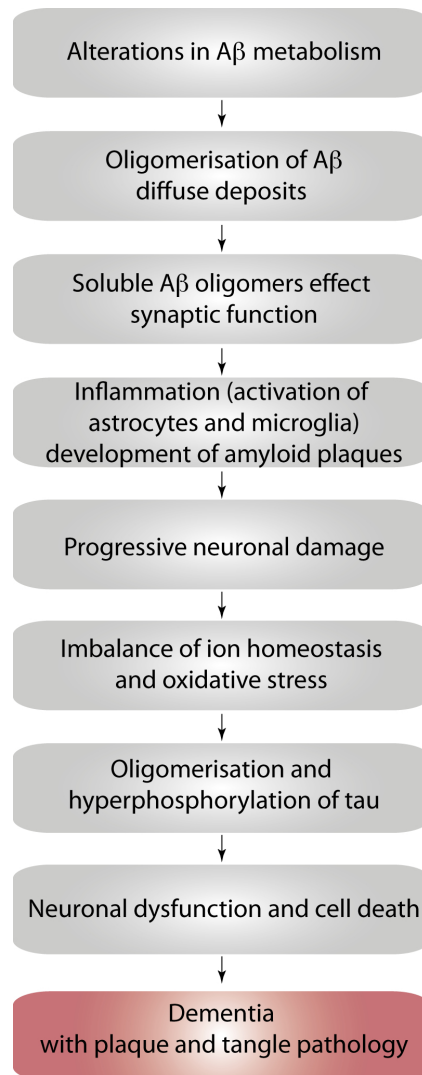


Figure 1.2. The amyloid cascade hypothesis. The course of Alzheimer's disease according to the amyloid cascade hypothesis. Illustration adapted from Hardy et al. [50] and Haass et al. [36].

1.3 The amyloid precursor protein (APP)

The amyloid precursor protein (APP) is a type I transmembrane protein that plays a crucial role in the pathogenesis of AD. It belongs to a small gene family further including the amyloid precursor-like proteins APLP1 [59] and APLP2 [60] in mammals [61],[62].

All three family members share conserved extracellular domains E1 (growth-factor like domain (GFLD), copper-binding domain (CuBD)) and E2 and acidic domain [63],[64]. Additionally, the Kunitz-type protease inhibitor domain (KPI) is harboured by isoforms of APP and APLP2 (Figure 1.3)[60],[63]. Processing by several secre-

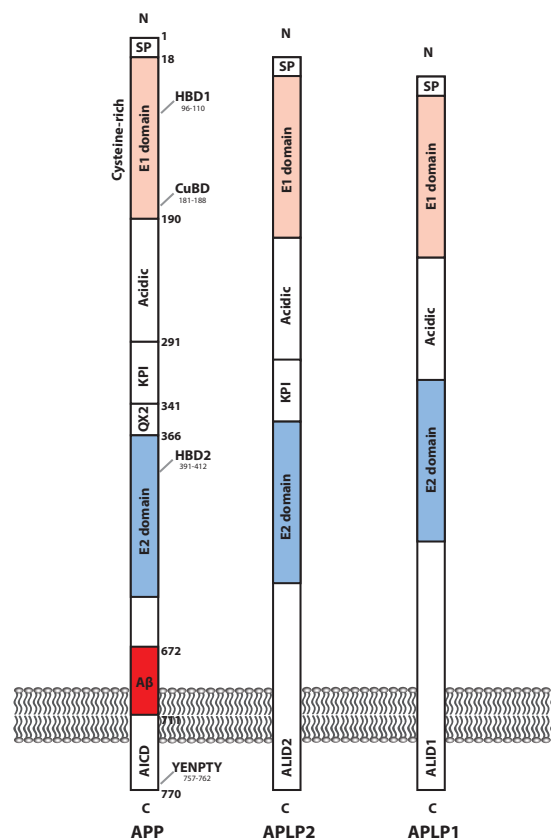


Figure 1.3. The structure of APP family members. The amyloid precursor protein (APP) and the family members amyloid precursor-like proteins 2 and 1 (APLP2 and APLP1). All APP family members harbour a conserved extracellular domain 1 (E1) consisting of a heparin-binding domain (HBD1) and a copper-binding domain (CuBD), a conserved E2 domain and an acidic domain. Isoforms of APP and APLP2 contain a Kunitz-type protease inhibitor domain (KPI). APP exclusively contains the A β peptide. The short intracellular domain carrying the YENPTY motif is present in all APP family members (AICD: APP intracellular domain, ALID2: APP-like intracellular domain 2, ALID1: APP-like intracellular domain 1).

1. Introduction

tases results in various extra- and intracellular APP fragments [65]. The intracellular YENPTY motif differs among all three family members: APP contains the APP intracellular domain (AICD), APLP2 the APP-like intracellular domain 2 (ALID2), and APLP1 the APP-like intracellular domain 1 (ALID1) [63]. APP family members interact with multiple proteins via their extracellular and intracellular domains [63],[64].

Even though the family members differ in their constitution, α -, β - and γ -secretases process them in a similar way. Importantly, proteolytic processing of only APP releases the AD-related $A\beta$ peptide [65].

1.3.1 Localisation and proteolytic cleavage

APP is a ubiquitous protein that is expressed in systemic organs and in the brain in different cell types [66],[67]. APP localises at the plasma membrane of various cell organelles, such as endoplasmic reticulum (ER), Golgi apparatus [68], and mitochondria [69],[70].

In the brain, the relative abundance of the different APP isoforms are distributed in a cell- and region-specific manner. There are three different isoforms APP770 /APP751 /APP695 whose mRNAs appear in a ratio of approximately 1:10:20 in the cerebral cortex [71]. Isoforms APP770 and APP751 have been shown to be more abundant in certain brain areas of AD patients [71]. APP is also expressed in astrocytes and microglia [72]. For instance, the mRNAs of KPI containing isoforms APP770/751 were found to be elevated in astrocytes in comparison to neurons [73].

In neurons, APP is described to be synthesised and localised in synaptosomes and growth cones [74], postsynaptic density [75], and is transported along axons [66] and dendrites.

APP undergoes post-translational modifications in the Golgi apparatus including glycosylation, sulphation, phosphorylation and palmitoylation [76],[77]. Posttranslational modifications are taking place during the secretory pathway, when APP passes from the ER to the plasma membrane. This is also the major compartment, where APP undergoes proteolytic processing [78]. Only a fraction of the expressed full-length APP resides the plasma membrane while about 90% stays in the Golgi network. If APP is not shed at the plasma membrane, the YENPTY internalisation motif is present which triggers endocytosis [79]. Subsequently, APP is transported to endosomes and is partly recycled to the plasma membrane or degraded in lysosomes [80].

In principle, there are two proteolytic processing pathways in which APP is cleaved by different secretases: In the amyloidogenic pathway β - and γ -secretases processing of APP results in $A\beta$. In contrast, in the non-amyloidogenic pathway APP is cleaved by the α -secretase and further by γ -secretase (Figure 1.4)[81]. Alternative APP processing can take place, as several other proteases can cleave APP at specific sites such as asparagine endopeptidase (AEP), membrane-type matrix metalloproteases (MT5-MMP) and meprin β [82].

The different proteolytic processing pathways are localised to different subcellular compartments. While the non-amyloidogenic pathway presumably occurs on the cell

1.3 The amyloid precursor protein (APP)

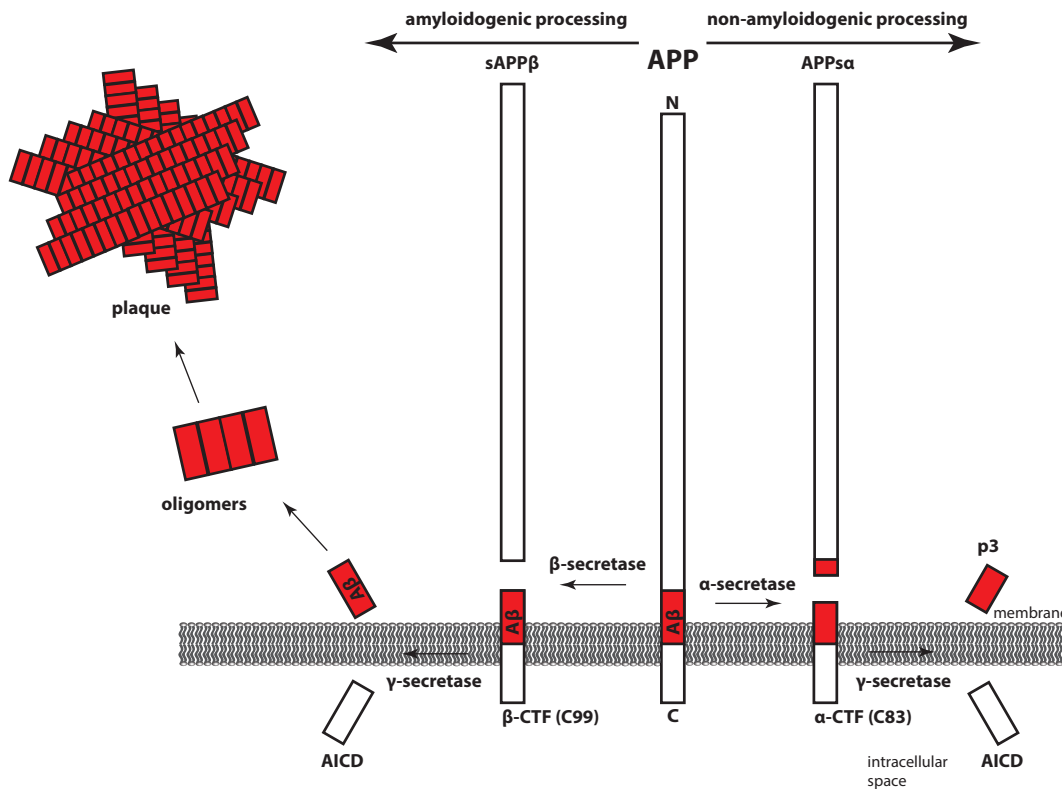


Figure 1.4. Cellular processing pathways of APP. APP can be proteolytically processed by two different pathways: The non-amyloidogenic pathway includes proteolytic cleavage by α - and γ -secretase, precluding $A\beta$ generation. This pathway is initiated by α -secretase and produces APPs α and the α -carboxyl-terminal fragment, α -CTF or C83. C83 can be further processed by γ -secretase and produces P3 and AICD. The amyloidogenic pathway involves β -secretase cleavage that produces secreted APPs β , and the β -carboxyl-terminal fragment, β -CTF or C99. C99 can be further cleaved by γ -secretase, giving rise to $A\beta$ and AICD. In Alzheimer's disease $A\beta$ forms oligomers that further accumulate to plaques, a hallmark of the disease.

membrane, the amyloidogenic processing is taking place in the endosomal compartment [83].

Proteolytic processing of APP produces $A\beta$ which plays a central role in the pathogenesis of AD, as its accumulation to oligomers, fibrils and plaques is a central hallmark of the disease [65],[81]. Specifically, it is crucial to understand the source and the generation of $A\beta$ in order to develop strategies for targeting its excessive abundance in AD.

As the deposition of the APP cleavage product $A\beta$ is a hallmark of AD, APP expression and cleavage sites are in focus of attention. However, the physiological function of APP still remains largely unknown [67].

1.3.2 Functions of APP and its cleavage products

The proteolytic cleavage of APP gives rise to the A β peptide that is the component of the amyloid plaques in AD patients. In order to profoundly understand the disease and develop therapeutic strategies, decoding the physiological functions of APP and its cleavage fragments is of major importance.

In addition to the numerous APP fragments with varying effects on neural function, also the APP full-length form has important functions [84],[64]. APP has an impact on cell proliferation, differentiation, neurite outgrowth [85], cell adhesion and synaptogenesis [67]. Moreover, it acts as a cell surface receptor [86] and growth factor [87]. APP participates both intracellularly and extracellularly in diverse mechanisms [67]: APP is also a typical cell surface G protein-coupled receptor (GPCR) [84] and is important during the development of the brain [74]. Furthermore, the amyloid precursor protein intracellular domain (AICD) plays a role in numerous processes such as nuclear signalling, transcriptional regulation, cell death, DNA repair and cell cycle re-entry [88]. Both the amyloidogenic and the non-amyloidogenic pathways are able to generate AICD.

APP by itself does not play an essential role in development, as APP-KO mice are viable and fertile. However, APP-KO mice display reduced locomotor activity and grip strength, reactive gliosis and reduced body weight and neuronal plasticity deficits [89],[64].

Functions of APP at the synapse

APP and APP cleavage products play important roles in numerous synaptic processes [64]. On the pre- and postsynapse, APP is also suggested to play a role in cell adhesion thereby stabilising synapses [90],[84]. In hippocampal neurons, cell-associated APP accounts for neuron viability, axonogenesis, and arborisation. Furthermore, secretory products of APP modulate axon growth, dendrite branching and counts [91].

Moreover, APP is implicated in modulation of synaptic transmission by regulating the receptor composition at the synapse: Increased levels of NR2A and NR2B subunits of the NMDA receptor are associated with increased levels of APP and its other family members [92],[93] and full-length APP enhances synaptic activity, synapse formation, and dendritic spine formation [94]. In contrast, the lack of APP in autaptic hippocampal neurons results in increased AMPA and NMDA receptor currents [95].

Furthermore, APP is essential for constitutive and adaptive synaptic plasticity of dendritic spines [96],[97]. This APP-dependent plasticity is regulated by the gliotransmitter D-serine implicating a role of astrocytes [96].

Diverse levels of the cleavage product A β can have different consequences on neuronal function. High levels are well known for their detrimental effects in synaptic function leading to dementia [36], while picomolar levels of monomeric and oligomeric A β have a positive modulatory effect on neurotransmission and memory [98].

Other APP cleavage products such as secreted APP α (APPs α) are important for excitatory principal neurons for mediating normal dendritic architecture, spine density

and morphology, synaptic plasticity and cognition. APPs α is derived from the non-amyloidogenic processing pathway (Figure 1.4)[84]. APPs α is generated by α -secretase processing and thereby secreted into the extracellular space where it is associated with neuronal and synaptic function [99],[100]. It is neuroprotective, neurotrophic and regulates cell excitability and synaptic plasticity [101],[102]. A neuroprotective role of APPs α in stress signalling, dendritic degeneration and neuronal cell death has also been reported [103]. APPs α has been shown to have trophic effects, for instance knock-in of APPs α into APP-KO animals is sufficient to prevent the reduced spine density observed in APP-KO mice [104]. Moreover, APPs α knock-in in APP-deficient mice can rescue anatomical, behavioural and electrophysiological phenotypes [101].

Especially the extracellular part of APP seems to be important for synapse function, as mice lacking the intracellular domain of APP show no plasticity deficits and increased levels of APP at the cell surface [101].

Functions of APP associated with Ca²⁺ homeostasis

APP and its cleavage products are associated with mitochondria and endoplasmic reticulum (ER) function. Both organelles operate in a strict interplay and their dysregulation is also linked to AD [105]. As energy deficiency and mitochondrial dysfunction have been recognised as a prominent, early event in AD, it is crucial to understand the physiological role of APP and its cleavage products in energy metabolism.

Full-length APP and its cleavage products play a role in mitochondrial function when they localise in mitochondria-associated ER membranes [106] and in the mitochondrial import channel [107]. Moreover, once inside mitochondria A β interacts with several proteins inside the organelle which leads to mitochondrial dysfunction [108].

APP and its cleavage products are important for mitochondrial integrity: Overexpression of APP and thus overproduction of A β has been shown to play a role in mitochondrial morphology, function and protein composition [109]. Alterations in the electron transport chain and energy production have been reported in mouse models of AD [70].

In more detail, APP contains a mitochondrial targeting signal and it forms stable complexes with the translocase of the outer mitochondrial membrane 40 (TOM40). TOM40 acts as an import channel and forms a complex with the translocase of the inner mitochondrial membrane 23 (TIM23). Together, they are regulating the import of proteins into the mitochondrial lumen [107].

It is suggested that AICD is involved in cytosolic calcium ion (Ca²⁺) homeostasis and energy production, as decrease or lack of AICD leads to an enhanced Ca²⁺ concentration in the cytosol, reduced ATP levels and mitochondrial hyperpolarisation [110]. Reduced levels of AICD were shown to diminish Ca²⁺ signalling via a mechanism that implicates ER Ca²⁺ store modulation [111]. These observations suggest a tight interaction of ER and mitochondria and that impairment of one organelle might entail imbalance of the whole Ca²⁺ homeostasis machinery. Studies investigating the role of APP in terms of cellular Ca²⁺ homeostasis in APP-KO astrocytes revealed

1. Introduction

that resting cytosolic Ca^{2+} is not altered, whereas stimulated Ca^{2+} release from ER is reduced [112].

Another aspect, that is linked to Ca^{2+} buffering and therefore to mitochondrial function, is mitochondrial morphology. Mitochondria are highly dynamic structures that adapt constantly to local energy demands. Hence, they undergo fission and fusion and get transported to the locus where they are needed. Fragmentation of mitochondria is associated with dysfunction and diseases [70]. Mitochondrial fission arrest has been reported in AD [113] also suggesting an impaired balance between fission and fusion [114]. It has been shown that functional KO of APP leads to a fragmented morphology of mitochondria [115]. Likewise, overexpression of WT and mutant APP causes fragmented structure of mitochondria and changed levels of fission and fusion proteins such as DLP1, OPA1 and Fis1. Moreover, APP overexpression leads to elevated reactive oxygen species levels, decreased mitochondrial membrane potential and reduced ATP production [109].

Hence, APP and its cleavage products interact with organelles that are involved in Ca^{2+} homeostasis.

1.4 Synaptic plasticity

Synapses are the specialised connecting sites that allow neurons to forward information by communicating with each other. The human brain contains 10^{12} neurons which themselves form thousands of synapses. The resulting great network of 10^{15} neuronal connections reaches further complexity by the specialisation of individual synapses. Synapses display diverse communication between pre- and postsynapse via transmitters. Transmitters are released by the presynapse, diffuse through the synaptic cleft and initiate diverse activation of the postsynapse. The complexity of the network drives the various and sophisticated features of the brain such as perception, emotion, thought, and behaviour [116].

Synaptic plasticity is a term for experience-dependent adjustments of synapses that are manifested by morphological and molecular rearrangements in the pre- and postsynaptic compartments. Thereby, neurons adapt to new conditions by strengthening or weakening synaptic pathways. This adaptation is considered as the underlying mechanism of learning and memory [116]. Here, the term synaptic plasticity is further specified in structural and functional plasticity depending on the experimental approach. Neural circuits are configured by formation, elimination and morphological adjustments of synapses. Thereby new connections are formed and preexisting ones weakened, abolished and strengthened. These modifications are termed structural plasticity. These processes are accompanied by molecular changes such as rearrangements of synaptic components and gene expression adaptations [116]. When molecular changes result in strengthening or weakening of synaptic signalling measured by modified neuronal activity, the term functional plasticity is used.

1.4.1 Structural plasticity of dendritic spines

Structural plasticity of synapses refers to morphological changes that come along with signalling alterations between pre- and postsynapse. For instance, the postsynapse of excitatory glutamatergic synapses forms a distinctive dendritic spine that receives excitatory input from the presynapse of pyramidal cells and many other principal neurons [117].

A dendritic spine is a small (1–2 μm long) specialised protrusion of the dendritic shaft. Dendritic spines were discovered in 1888 by Santiago Ramón y Cajal with the Golgi staining method which was a groundbreaking revelation in the history of neuroscience [118]. In dendritic spines, filamentous actin (f-actin) determines the spine shape, arranges the postsynaptic signalling machinery, and promotes changes in spine structure and spine stability [119]. Moreover, the postsynaptic density (PSD) is a protein dense structure in the postsynaptic spine, close to the synaptic cleft that receives the information from the presynapse (Figure 1.5).

Based on the morphology, different spine classes can be distinguished: thin spines are fine and long and can have a small head; stubby spines have a large head without a neck; mushroom spines have bulbous head and thin neck; filopodia are thin protrusions without PSD [120] and are therefore classically not considered as dendritic spine [121],[122]. The morphology of dendritic protrusions provides evidence about its stability: Filopodia only exist for several hours and are very motile. Thin spines are more stable than filopodia, but still less stable than mushroom spines.

During development dendritic spines form and turn over dynamically, while they are stable for months and years in the adult brain. The stability of dendritic structures is important for accurate brain function and a dysregulation is associated with psychiatric or neurodegenerative diseases [123]. Experience-dependent dendritic spine plasticity (morphology, formation and elimination) provides the structural mechanism for learning and memory. Hence, altered spine plasticity is a hallmark of injuries and neurological diseases accompanied by intellectual disabilities [124].

Dendritic spines are playing a substantial role in modulating neuronal networks to an extent that includes complex mechanisms such as learning and memory [125]. Their electrical properties enable neural circuits to gain a high connectivity, with individually integrated inputs in order to generate an emergent functional conglomerate [126].

In vivo two-photon microscopy reveals fundamental insights into spine plasticity, as it allows chronic observation of the same dendritic spine [120], e.g. during experience-dependent plasticity [127],[124] or during development of the brain [128].

Synaptic plasticity enables neuronal networks to function in a highly dynamic manner. Thus, structural plasticity investigations of neuronal networks become a targeted matter in neuron-associated diseases.

1.4.2 Functional plasticity

Molecular rearrangements in the pre- and postsynaptic compartments can strengthen or weaken synaptic signalling. The mechanisms underlying the various forms of long-term potentiation (LTP) and long-term depression (LTD) are associated with diverse functions both during development and forms of experience-dependent plasticity, including learning and memory [129],[130]. During synaptic plasticity, receptor composition on the postsynaptic membrane undergoes changes that result in increased or decreased transmission of synaptic signals.

The most compelling form of such plasticity is NMDAR-dependent LTP which is widely studied in the Schaffer collateral-CA1 synapses of the hippocampus [130],[131],[132],[133]. This mechanism involves AMPARs and NMDARs, the two major classes of ionotropic glutamate receptors at the postsynaptic neuron [134].

In an experimental setting, this phenomenon can be achieved by different induction protocols implicating a strong electrophysiological stimulation of the presynapse resulting in strong depolarisation of the postsynapse via alpha-amino-3-hydroxy-5-methyl-4-isoxazolepropionic acid receptor (AMPA)[131]. During the depolarisation of the postsynapse NMDARs get activated: Binding of glutamate to NMDARs together with depolarisation of the postsynaptic membrane releases the magnesium ion (Mg^{2+}) block of the NMDAR. The successional opening of the NMDAR channel promotes entry of Ca^{2+} and rise of Ca^{2+} level in the postsynapse (Figure 1.5)[132],[135]. The resulting rise in Ca^{2+} within the dendritic spine also associates with further downstream consequences that involve the modulation of the AMPAR function, its trafficking to the postsynaptic membrane, and transcriptional modifications. This complex process is regulated by a large number of proteins [132].

In contrast to LTP, prolonged NMDAR activation, that is below the threshold for inducing synaptic potentiation, can induce synaptic depression: long-term depression (LTD).

Long-lasting synaptic changes such as LTP are accompanied by cytoskeletal modifications of dendritic branches and spines [136].

1.5 Astrocytes

Alongside with oligodendrocytes and microglia, astrocytes belong to the group of glial cells which are important regulators of brain homeostasis [137]. They regulate the volume and composition of the extracellular space, thus manage the brain environment. Moreover, astrocytes also play a crucial role in regulating the blood brain barrier [138] and are implicated in ion and metabolic brain homeostasis [139]. They have important roles in key aspects of brain development and function, such as neuronal metabolism, synaptogenesis, homeostasis of the extracellular milieu, or cerebral microcirculation.

Astrocytes are intercellularly coupled by gap junctions [140] which are relevant for astrocytic and neuronal signalling. Gap junctions are crucial for glutamate transport within the astrocytic network that depends on the release of glutamate from active neurons [141]. During high neuronal activity and high metabolic demand, astrocytic metabolic coupling is essential for maintaining glutamatergic synaptic transmission [142].

The highly ramified non-overlapping processes of astrocytes contact the surrounding neuropil. It is estimated that one astrocyte might contact around 100 000 synapses in hippocampal region CA1 in the rat brain [143]. In line, astrocytes play functionally relevant roles in synaptic physiology and glial function is essential for properly operating neurons. Hence, glial dysfunction significantly contributes to brain pathology [137].

1.5.1 The tripartite synapse

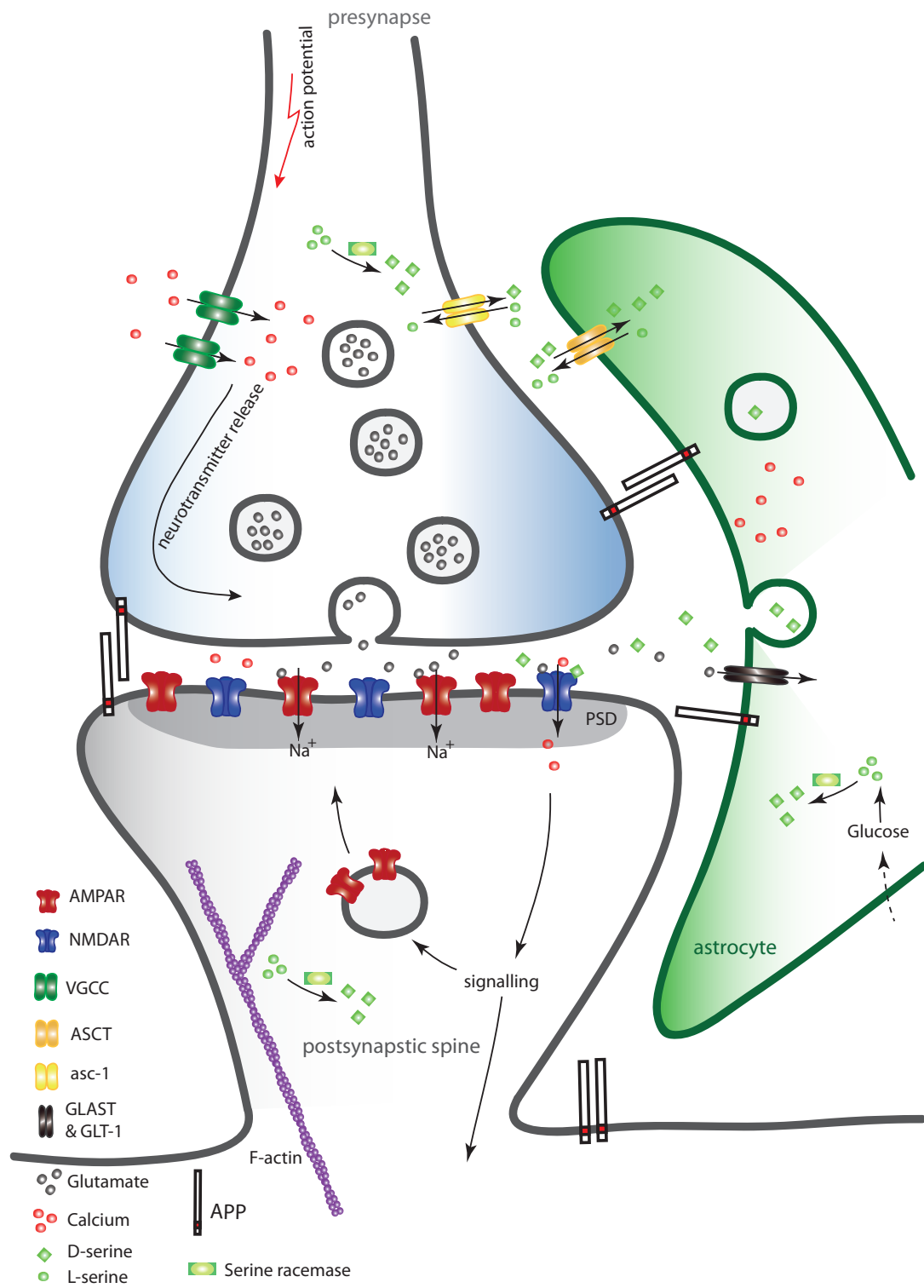
The classical view that brain functions are exclusively driven by neuronal activity is obsolete, since accumulating evidence suggests a complex interplay of neurons and astrocytes that constitutes and monitors the sophisticated functions of the brain. The tripartite synapse refers to the concept that a synapse is a functional unit consisting of pre- and postsynapse and an astrocytic perisynaptic process (Figure 1.5). Astrocytes exchange information with the synapse, react to synaptic activity and also regulate synaptic transmission. Thus, astrocytes are highly integrated in the procedure of information processing, transfer and storage by the nervous system. However, astrocytic Ca^{2+} transients occur spontaneously and can be independent from synaptic activity, but are also evoked by neurotransmitters released during synaptic activity [144],[145].

Hence, the elaborate brain functions emerge not only from the complexity of different synapse types but also from the balanced activity of a network of neurons and synapse associated glia cells [146],[144],[147].

Interaction of astrocytes with dendritic spines

The cellular basis of learning is constituted by experience-dependent changes of synaptic transmission, termed plasticity. This impressive feature of the brain is accompanied by morphological adaptations of dendritic spines. This structural plasticity implicates

1. Introduction



the change of the cytoskeleton and thereby the appearance of the dendritic spine. These modifications in spine size and density are thought to reflect changes in the strength of synaptic transmission [148],[149].

Astrocytes operate in very close interaction with excitatory and inhibitory synapses by structurally engulfing them, functionally reacting to neurotransmitters, and releasing gliotransmitters that modulate synaptic transmission [150],[151]. Perisynaptic astrocyte processes can favour synaptic modulation during development and in the adult brain [152]. Thereby, astrocytic protrusions targeting synapses are very highly motile, even more than dendritic spines [153]. It has been shown that activity of the neuronal network regulates structural relationships between dendritic spines and astrocytic processes. This is associated with synaptic plasticity and consequences on the astrocytic regulation of synaptic transmission. This phenomenon requires presynaptic activity, mGluR activation, and G protein-coupled receptor (GPCR) mediated Ca^{2+} elevations in astrocytes [152].

3D reconstructions of synapses in the hippocampus have described higher astrocyte coverage of thin spines than of larger spines. These findings suggest selective synapse-astrocyte interaction in dynamic and forming spines, rather than in persisting ones [154].

As astrocytes are extensive and close interactors of synapses, disruption of this relationship has profound consequences ascribed to numerous disorders [155],[156]. Hence, it is important to understand the interplay physiologically in order to selectively target the disease-related disturbances.

Figure 1.5 (preceding page). The tripartite glutamate synapse. The glutamatergic tripartite synapse comprises a presynaptic terminal, a postsynaptic spine, and an astrocytic process. When an action potential reaches the presynapse, voltage gated Ca^{2+} -channels (VGCC) open and allow Ca^{2+} influx in the presynaptic compartment. Following, vesicles filled with the neurotransmitter glutamate fuse with the presynaptic membrane and release the transmitter into the synaptic cleft. Glutamate binds to AMPA receptors, which function as a Na^+ -channel, leading to depolarisation of the postsynaptic membrane. Binding of glutamate to NMDA receptors additionally results in influx of Ca^{2+} which leads to further signalling cascades: towards the nucleus implicating gene expression modulation and travelling of AMPA receptors to the postsynaptic membrane increasing the sensitivity to glutamate. For activation of the NMDA receptor, a certain level of depolarisation of the postsynapse and binding of D-serine is required for potentiation of the receptor. The adjacent astrocyte plays a role in modulation of synaptic signalling: glutamate is cleared from the synaptic space through amino acid transporters (GLAST and GLT-1). Moreover, D-serine is released in an activity-dependend manner via vesicles that require Ca^{2+} elevations in the astrocyte. D-serine is produced from L-serine by serine racemase. L-Serine is produced in astrocytes shuttles to neurons through alanineserinecysteine transporter 1 (asc-1) and is converted into D-serine by serine racemase. D-serine shuttles from neurons to astrocytes, where it is packed in glial vesicles until it is released. D-serine is removed from the synaptic cleft via ASCT and asc-1 transporters.

The role of astrocytes in synaptic signalling and plasticity

Astrocytes integrate and process synaptic information and control synaptic transmission. They react to neuronal activity and neurotransmitters by activating metabotropic receptors. This in turn can release gliotransmitters such as ATP, D-serine, glutamate and GABA which modulate neuronal activity [144]. For instance, synaptic transmission is modulated by astrocyte-derived ATP or its metabolite adenosine implicated in sleep and cognition [157].

In general, astrocytes function in slower time dimensions than neurons. While one action potential has a duration of 1 ms, astrocytic Ca^{2+} signals last several seconds. Also the influence on synaptic transmission is a transient control of the synaptic strength during seconds [158],[144]. Thereby, astrocytes contribute to synaptic plasticity such as LTP during which the release of gliotransmitter D-serine is crucial for the generation of LTP [159]. This is taking course via D-serine binding to the glycine-binding site of neuronal NMDAR.

Astrocytes control their membrane potential via inward rectifier K^+ (Kir) channels [160]. The potential is close to the equilibrium potential of K^+ . Thus, when extracellular K^+ rises, K^+ ions flow into astrocytes through these inward rectifiers.

Astrocytes express neurotransmitter glutamate [161] and GABA [162] transporters. Thereby, astrocytes do not only participate in modulating synaptic transmission by clearing the extracellular space from neurotransmitters but also by providing the presynapse with a recycled source of transmitters [142]. For instance, the glutamate that is taken up by astrocytes is converted into glutamine which is then released to the neurons modulating neuronal activity [163],[142].

During high neuronal activity and high metabolic demand, astrocytic metabolic coupling is essential for maintaining glutamatergic synaptic transmission [142]. Moreover, astrocytes are highly involved in energy supply of neurons. They take up glucose and either store it as glycogen or metabolise it to lactate [164] releasing either one or the other when needed.

1.5.2 Ca^{2+} signalling in astrocytes

Astrocytes exhibit spontaneous and synaptically evoked Ca^{2+} signals [144]. The synaptically evoked Ca^{2+} signals occur in most brain areas and in response to the release of numerous neurotransmitters and factors such as norepinephrine, ATP, GABA, glutamate, acetylcholine, nitric oxide, endocannabinoids [144],[165],[142]. Notably, the common transmitter among astrocytes and neurons is glutamate which has modulatory effects on both cells [166].

The transmitters bind to high-affinity astrocytic metabotropic GPCRs in the astrocytic membrane that provoke inositol-1,4,5-trisphosphate (IP3) production and Ca^{2+} release from the endoplasmic reticulum (ER)[144],[165]. Moreover, transient receptor potential A1 (TRPA1) channels at the cell membrane are implicated in Ca^{2+} signals in astrocytes, as their opening allows Ca^{2+} influx from the extracellular space into the

cell lumen [167]. The functional consequence of Ca^{2+} signals in astrocytes is the release of gliotransmitter which have modulatory actions on other glial, neuronal or vascular cells [165]. The release occurs via regulated exocytosis that depends on docking and fusion of vesicles with the plasma membrane. This process requires Ca^{2+} and the formation of the soluble N-ethylmaleimide-sensitive fusion protein attachment protein receptor (SNARE) complex [168].

The consequences of astrocytic contribution to neuronal signalling are exceedingly diverse: modulation of stimulation or inhibition of synaptic transmission, involvement in LTP or LTD, heterosynaptic facilitation or depression and homeostatic plasticity [142]. Astrocytes react to synaptic activity with Ca^{2+} elevations [169]. Moreover, it has been shown that spontaneous astrocytic Ca^{2+} oscillations can spread as waves to neighbouring astrocytes and initiate slowly decaying NMDA receptor-mediated inward currents in adjacent neurons [170]. This indicates that astrocytes are involved in neuronal ion homeostasis.

The Ca^{2+} signals in astrocytes can be of two different kinds: the somatic Ca^{2+} transients are differing from the ones in astrocytic protrusions. The Ca^{2+} events in the soma are less frequent but of longer duration and larger in amplitude than those in the processes [165],[171]. In the astrocyte processes the Ca^{2+} signals originate in spatially restricted areas termed microdomains [172].

Within astrocytes, organelles are tightly associated with each other to regulate intracellular Ca^{2+} levels. ER-induced Ca^{2+} rise is followed by increased mitochondrial Ca^{2+} levels [173]. Glutamate release from astrocytes is also controlled by rising Ca^{2+} levels that are modulated by mitochondria [174].

While neurons have a certain resting potential and reach a threshold when they elicit an action potential, astrocytes base their cellular activity on variations of Ca^{2+} concentration in the cytoplasm.

Astrocytic Ca^{2+} signalling modulates neuronal information in diverse spatiotemporal dimensions to reach a higher degree of brain integration. Thereby astrocytes display a complex compartmentalisation and highly dynamic Ca^{2+} transients [165].

1.6 Methodology

In order to answer the neurobiological questions concerning the physiological role of APP in synaptic plasticity associated with astrocytic function, diverse technical approaches were made: intracellular and extracellular electrophysiological recordings of neurons, immunohistological stainings, region-specific delivery of viruses encoding different genetic tools, primary astrocyte cultures, *ex vivo* confocal laser scanning microscopy, *ex vivo* two-photon Ca^{2+} imaging.

1.6.1 Two-photon microscopy

Imaging of living tissue for detailed visualisation of biological processes and structures is of crucial benefit for decoding biological complexity. This advance of technical tools enables us to better understand physiology and pathophysiology in neuroscience. Fluorescent labelling and modern microscopy allows selective visualisation of molecules. Especially, the technique two-photon microscopy enables imaging studies of specific protein localisation and of the structure and function of living single cells in intact tissue [175], [176]. Two-photon microscopy enables high resolution imaging deeply in the tissue in 3D with low phototoxicity and high sensitivity at several time points [177]. The technique applied on biological samples was firstly described by Denk and colleagues [178]. Hereby, the excitation of the fluorophore in the tissue is taking place by nearly simultaneous absorption of two photons. The photons feature a long wavelength close to infrared and are therefore of low energy. The addition of two photons results in an excited energy state and elicits a photon of higher energy than the exciting photons (Figure 1.6A). This non-linear effect of two-photon absorption (Figure 1.6B) increases the excitation probability by high light intensity [179]. Hence, a specialised laser is required which is typically a ultrafast pulsed Titanium-sapphire (Ti:sapphire), with a pulsing rate of ~ 100 MHz. Multiphoton absorption is termed nonlinear because the absorption is of higher power than first power of the light intensity [179].

One advantage of two-photon microscopy is longer wavelength laser light that is less absorbed and scattered, therefore it can penetrate the tissue more deeply and is additionally less phototoxic. Moreover, the excitation only takes place in a focal volume which additionally reduces phototoxicity and bleaching. Furthermore, also scattering photons are collected, as there is no pinhole that blocks scattered photons, in contrast to a confocal microscope [180],[181],[182].

One-photon microscopy with linear absorption requires one higher-energetic photon with smaller wavelength (typically blue or green) and is more scattered in the tissue (Figure 1.6A). Confocal laser scanning microscopy applies one-photon excitation and is also based on optical sectioning. Fluorophores get selectively excited by a spatially restricted laserbeam. The laserbeam scans the probe which consecutively excites image points. The emitted light from the fluorophores passes a pinhole that blocks scattered light outside the focal plane before it reaches the detector [182].

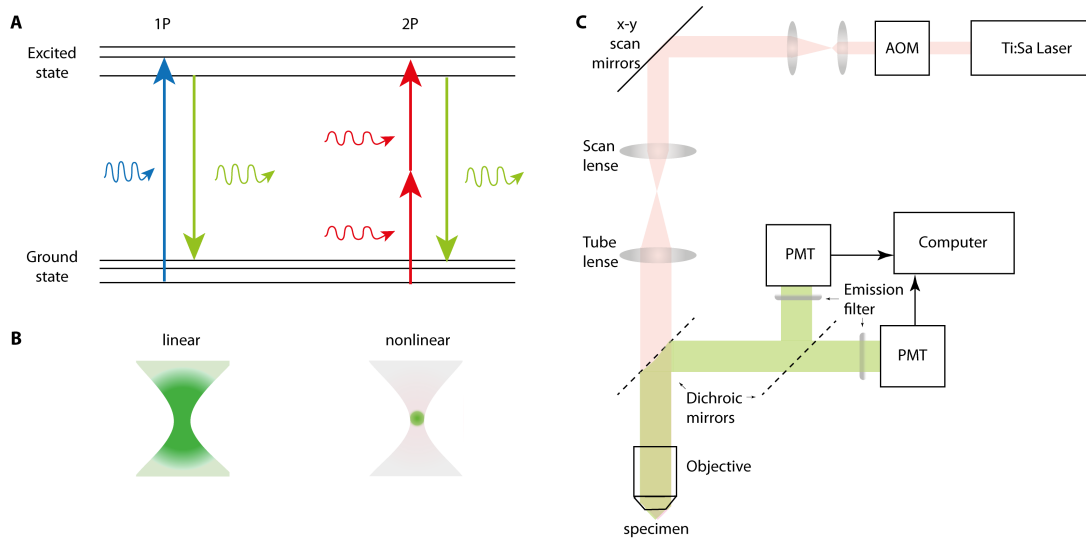


Figure 1.6. One- and two-photon microscopy. **(A)** Illustration of the fluorescence excitation by one and two-photon absorption in a simplified Jablonski diagram. The one-photon excitation (1P, blue) is described as a photon of a short wavelength (blue) gets absorbed by a molecule which promotes it to an excited state and when it returns to its ground state, a photon of a slightly lower energy gets emitted (green). The two-photon excitation (2P, red) takes advantage of two photons of half the energy/double wavelength arriving nearly simultaneously (~ 0.5 fs) at a molecule where they combine their energy for promoting the molecule to an excited state. For this nonlinear effect a very high photon density is needed. **(B)** Light cone of 1P (left) and 2P (right) excitation. 1P excitation is taking place within the entire cone of the focussed light beam. In contrast, 2P excitation is confined to a perifocal region, as sufficient photon density is only given there. **(C)** Nonlinear laser-scanning microscope. A Ti:Sa laser provides the photon density necessary for nonlinear excitation in near-infrared ultrashort pulses. The acousto-optic modulator (AOM) regulates the intensity and a telescope the size of the laser beam. The scan mirrors and several lenses direct the laser beam that is then focused on the specimen by the objective. The emitted fluorescence is separated from the excitation light and directed to photomultiplier tubes (PMTs) via dichroic mirrors. Emission filters in front of the PMTs ensure detection of a specific wavelength.

1.6.2 Ca^{2+} imaging

Ca^{2+} is a ubiquitous signalling molecule that is mediating various cellular processes, ranging from development and differentiation to cell death [183],[184]. Sources and sinks of intracellular Ca^{2+} can be channels in the plasma membrane, the ER and mitochondria. Ca^{2+} concentration gradients (outside ~ 2 mM, cytosol ~ 100 nM), created by energy-dependent Ca^{2+} transport across cellular membranes promote the conditions for Ca^{2+} signalling [185]. Free and active cytosolic Ca^{2+} can bind to Ca^{2+} buffering proteins in the cytosol and can initiate signalling to the nucleus modulating transcription [183].

In order to visualise the alternating levels of cellular Ca^{2+} , highly Ca^{2+} -selective

1. Introduction

chelators fused to a fluorescent molecule are nowadays employed. The most recent breakthrough are protein-based genetically encoded Ca^{2+} indicators (GECIs) that are based on green fluorescent protein (GFP) [186] and calmodulin [187],[188]. GECIs translate Ca^{2+} binding into an optical signal, as Ca^{2+} binding changes the optical properties of the protein [189]. Spatial and temporal resolution of Ca^{2+} processes can be achieved, as GECIs can be targeted to specific cell types or subcellular compartments [190],[189]. There are two different kinds of GECIs: I) FRET-based indicators change their conformation when Ca^{2+} is binding in order to induce Förster resonance energy transfer (FRET). This leads to a shift in emitted wavelength (e.g. from 480 nm to 530 nm). II) Single fluorophore GECIs are high-affinity Ca^{2+} indicators composed of a single GFP fused to calmodulin (CaM). The so-called GFP-based Ca^{2+} probe (GCaMP) provides a low signal-to-noise ratio [191],[188].

The latest generation of GCaMPs are GCaMP6 that bind Ca^{2+} with ultrasensitive affinity and provide new spatial and temporal resolution of Ca^{2+} transients [192]. A modified membrane-tethered GCaMP (GCaMP-Lck) allows visualisation of Ca^{2+} fluctuations in small volume compartments, such as near the cell membrane and in distal and ramified cell processes of astrocytes [193]. GCaMP-Lck can be expressed via an adeno-associated virus (AAV) [194] or in a genetically modified mouse line (Figure 1.7)[195],[196].

A recent 3D Ca^{2+} imaging study of a whole astrocyte revealed that most of the basal Ca^{2+} activity occurs in the processes, some in the endfeet, while small proportion is detectable in the soma [171]. Thereby, the gliapil constitutes $\sim 75\%$ of the astrocytic volume [171]. In order to understand the role of APP in Ca^{2+} signalling in the perisynaptic sites of astrocytes, a GCaMP6-Lck was used in APP-KO animals and by that two-photon microscopy [177] allows visualisation of Ca^{2+} transients in the intact tissue.

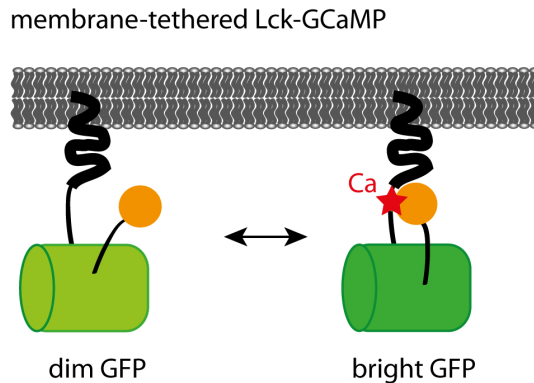


Figure 1.7. Lck-CaMP. Single-fluorophore genetically encoded Ca^{2+} indicator (GECI) that is tethered to the plasma membrane. Binding of Ca^{2+} to GCaMP leads to an increase in emitted fluorescence.

1.7 Aim of this thesis

The aim of this thesis is to decipher the physiological role of astrocytic APP in synaptic plasticity with regard to neuronal function and the associated astrocytic contribution. Even though the presence of APP in astrocytes has been proven, the investigations of APP functions have been mainly confined to neurons. As astrocytes are active partners in neuronal signalling and comply with other tasks related to brain homeostasis, their adequate function is of utmost importance. Understanding the physiological role of APP in the entire brain is essential for fundamental biology and in regard to potential therapeutic strategies for the treatment of AD.

Chapter 2

Results

2.1 The role of APP in synaptic plasticity in the cortex and hippocampus

2.1.1 APP is crucial for cortical dendritic spine plasticity without consequences on NMDA/AMPA receptor currents

Dendritic spines are sites of input typically found on excitatory neurons. Synaptic activity determines their formation, plasticity, and sustainment [197]. Hence, they are of major importance for the connection of neuronal circuits [117]. In order to examine the physiological function of APP on synaptic function in the cortex, a constitutive knock-out (KO) mouse model of APP was used that lack APP in every cell type [198],[101].

Chronic *in vivo* two-photon imaging investigated the plasticity of dendritic spines in layer I/II of layer V pyramidal neurons in the somatosensory cortex of adult APP-KO mice [96]. Reduced spine turnover rate (formation and elimination) was observed in APP-KO animals in comparison to wild type (WT) mice in standard environment. When exposed to enriched environment, WT mice displayed increased spine density which could not be observed in APP-KO [96]. These observations came along with decreased thin spine and increased mushroom spine proportion.

It has been shown that human AD cases and AD animal models display increased levels of the endogenous NMDAR co-agonist D-serine in the brain and the cerebrospinal fluid (CSF) [199]. Moreover, APPs α and A β is suggested to induce D-serine production and release from glia cells [200],[201]. For this reason, extracellular and total D-serine levels were investigated in the cortex of APP-KO mice. Decreased extracellular but increased intracellular levels were found, suggesting a release problem in the absence of APP [96].

Here, the application of D-serine via drinking water was tested whether it could be of benefit for the spine plasticity impairments in APP-KO mice. Indeed, the treatment with D-serine increased the spine turnover rate in standard environment and spine density in enriched environment which correlated with increased thin spines and decreased mushroom spines [96].

These observations raised the questions whether APP-KO mice display alterations in excitatory synaptic transmission in terms of decreased NMDAR currents, as D-serine potentiates NMDARs by binding to the glycine binding site and NMDARs have been shown to be increased in mushroom spine type [202].

For functional investigation whether NMDAR density is altered in principal neurons of the cortex of APP-KO animals, evoked NMDAR and α -amino-3-hydroxy-5-methyl-4-isoxazolepropionic acid receptor (AMPA) currents were recorded and put into ratio. Therefore, acute coronal brain slices of 300 μ m were prepared from 3-months old APP-KO and WT mice. After recovery, the slice was placed in a submerged recording chamber containing picrotoxin for blockage of inhibitory currents. A stimulation

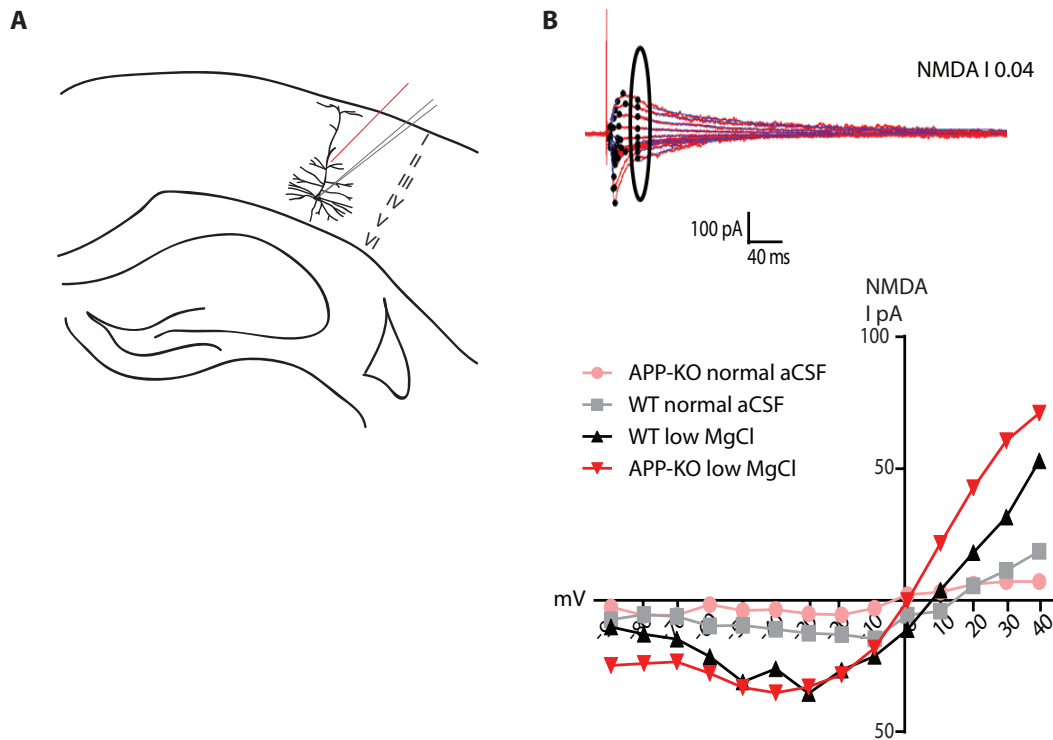


Figure 2.1. NMDA/AMPA recordings in the cortex of APP-KO mice. (A) Illustration of the experimental setting of evoked NMDA/AMPA EPSC in the acute brain slice. The stimulation electrode (red line) was placed in close proximity to the soma of layer V pyramidal neurons. Following, one pyramidal neuron was patched in the whole cell patch mode (black lines) and stimulated EPSCs were recorded. (B) Top: Illustration of NMDA currents at different holding potentials (-90 to +40 mV). Black circle indicates the 40 ms after the stimulation as measurement point of the NMDAR current amplitude. Bottom: NMDA current amplitude at different holding potential in slices of WT and APP-KO animals with common aCSF (2 mM MgCl₂) and low Mg²⁺ aCSF (0.5 mM MgCl₂); n = 2-6.

electrode was placed in close proximity (layer III/IV) to the soma of layer V pyramidal neurons. Subsequently, the adjacent soma was patched in whole-cell configuration (Figure 2.1A) from which excitatory postsynaptic currents (EPSCs) were recorded. An increase in current after stimulation (stimulus response) verified neuronal connection to the patched neuron. Firstly, the artificial cerebrospinal fluid (aCSF) conditions were tested for ideal investigation of NMDAR currents. As NMDARs harbour a Mg²⁺ block inside the channel, which is released upon reaching a certain depolarisation threshold, the NMDAR current was tested under two aCSF conditions: commonly used 2 mM MgCl₂ and low 0.5 MgCl₂. The neuron was clamped at different holding potentials from -90 mV to +40 mV investigating the slower NMDAR component of the response current amplitude 40 ms after the stimulus. Under normal MgCl₂ conditions, the NMDAR current amplitude was very low and barely increased with increasing hold-

2. Results

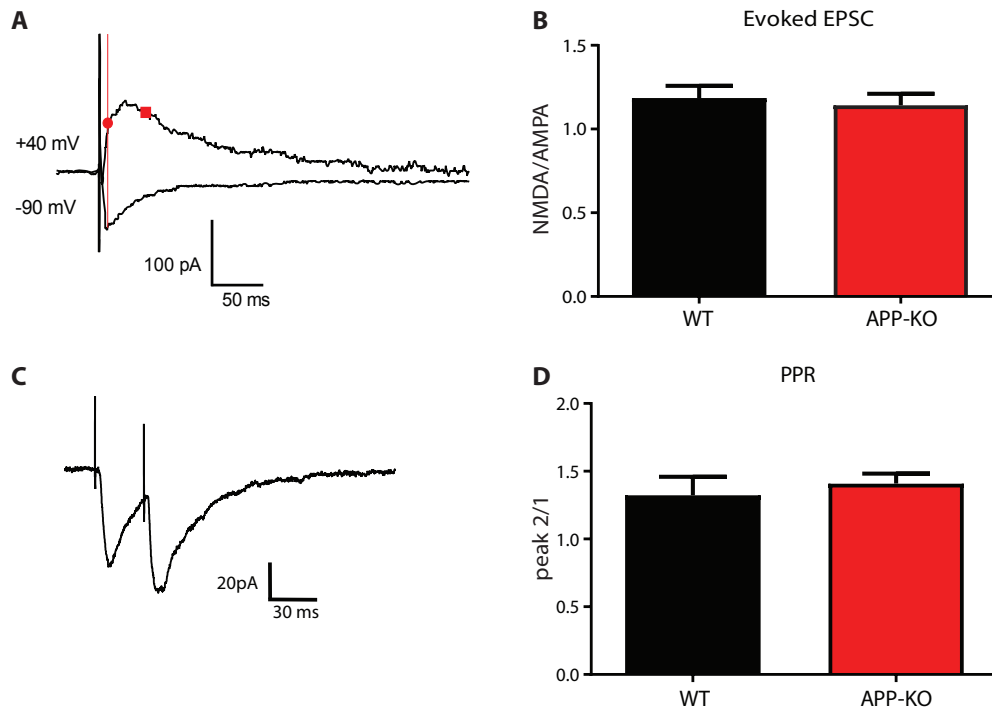


Figure 2.2. NMDA/AMPA and paired-pulse currents do not differ in APP-KO mice. (A) Example traces for determination of the NMDA/AMPA EPSC ratio at -90 mV and +40 mV. Red line shows the position of the AMPAR response peak at -90 mV. This position is used for the AMPAR current value in the recording at +40 mV (red dot). The NMDAR current value is taken from the mean of 40 to 50 ms after the stimulation (red square, mean of 10 ms). **(B)** Bar graph of the NMDA/AMPA EPSC ratio of WT and APP-KO animals. Two-tailed *t*-test, $t(29) = 0.4178$; $p = 0.679$; $n = 14-17$. **(C)** Example traces of paired-pulse recording with 30 ms inter pulse interval. **(D)** Bar graph of the PPR of the response amplitude of the second peak/first peak of WT and APP-KO. Two-tailed *t*-test, $t(13) = 0.6115$; $p = 0.5514$; $n = 5-10$.

ing potential (Figure 2.1B) in APP-KO and WT. When recordings were performed under low $MgCl_2$ conditions the amplitude of the NMDAR current was larger and remarkably changing over the different holding potentials (Figure 2.1B). Hence, the subsequent NMDA/AMPA recordings were obtained with low Mg^{2+} aCSF.

Four stimulated transients were consecutively recorded at -90 mV in order to define the position of the AMPAR response peak. Subsequently, four stimulated transients at +40 mV were recorded for a combined AMPAR and NMDAR current of which the AMPAR response amplitude could be determined from the position of the peak at -90 mV (Figure 2.2A, red line and dot). The NMDAR current amplitude was employed from 40 to 50 ms after the stimulus artefact (Figure 2.2A, red square). The ratio of NMDAR and AMPAR current amplitude of WT and APP-KO did not reveal any differences (Figure 2.2B)(mean \pm SEM: WT = 1.184 ± 0.07405 ; APP-KO = 1.142 ± 0.06896 ; $p > 0.05$). Moreover, paired-pulse facilitation (PPF) recordings

were performed with a stimulus interval of 30 ms. PPF is a short form of synaptic plasticity: It is a phenomenon of an increase of the 2nd EPSC when the stimulation closely follows a prior stimulation. PPF arises due to increased presynaptic Ca²⁺ concentration resulting in a greater release of neurotransmitters from the presynapse that is measurable as increased 2nd EPSC. The paired-pulse ratio (PPR) of 2nd and 1st peak was unchanged between WT and APP-KO pyramidal cells (mean \pm SEM: WT = 1.323 ± 0.1358 ; APP-KO = 1.409 ± 0.07358 ; $p > 0.05$) (Figure 2.2C,D) indicating unchanged presynaptic release.

The lack of APP does not result in a change of NMDA/AMPA ratio and PPR in layer V pyramidal cells of the somatosensory cortex in contrast to the observed spine plasticity deficits in APP-KO. Hence, APP is crucial for dendritic spine plasticity without consequences on synaptic signalling in terms of NMDA/AMPA density and PPF currents.

2.1.2 Hippocampal long-term plasticity depends on the presence of APP and cannot be restored by gliotransmitter D-serine

It has been shown that impaired spine plasticity in the cortex of APP-KO animals could be related to reduced levels of D-serine [96] and that astrocytic D-serine is crucial for the induction of LTP [159]. The described LTP reduction in APP-KO animals [101],[203] was hypothesised to result from a reduction of D-serine in the hippocampus. Hence, a LTP rescue after D-serine application was tested, as demonstrated before [167],[159].

Acute sagittal brain slices of 350 μ m thickness from 3-months old mice were used for local field LTP recordings in the Schaffer collateral projections to CA1 area of the hippocampus. Two stimulation electrodes were placed in the Schaffer collaterals stimulating the fibers in both directions (anterograde and retrograde). A recording electrode was positioned between the stimulation electrodes receiving anterograde and retrograde input from both sides (Figure 2.3A). The LTP protocol defined a 20 min stable baseline, followed by LTP induction by tetanus stimulation (100 pulses during 1s) and further LTP recording over 60 min. For the analysis, the slope of the field potential was taken into account (Figure 2.3A) and the change normalised to the baseline is displayed in percent. The recordings confirmed a LTP reduction in APP-KO animals (Figure 2.3B) (mean \pm SEM in %: WT = 136 ± 4.082 ; APP-KO = 120.8 ± 3.339 ; $p < 0.05$). However, the lack of APP did not alter presynaptic release probability examined by PPF with inter-pulse intervals of 20, 30, 50, 75, 100 and 200 ms (Figure 2.3C) (PPR mean \pm SEM: 20 ms: WT = 1.657 ± 0.07693 ; APP-KO = 1.564 ± 0.04944 . 30 ms: WT = 1.864 ± 0.05692 ; APP-KO = 1.84 ± 0.0604 . 50 ms: WT = 1.915 ± 0.05112 ; APP-KO = 1.938 ± 0.06043 . 75 ms: WT = 1.877 ± 0.02832 ; APP-KO = 1.868 ± 0.06112 . 100 ms: WT = 1.819 ± 0.01758 ; APP-KO = 1.799 ± 0.04419 . 200 ms: WT = 1.539 ± 0.03202 ; APP-KO = 1.537 ± 0.02736 . n = 6 animals,

2. Results

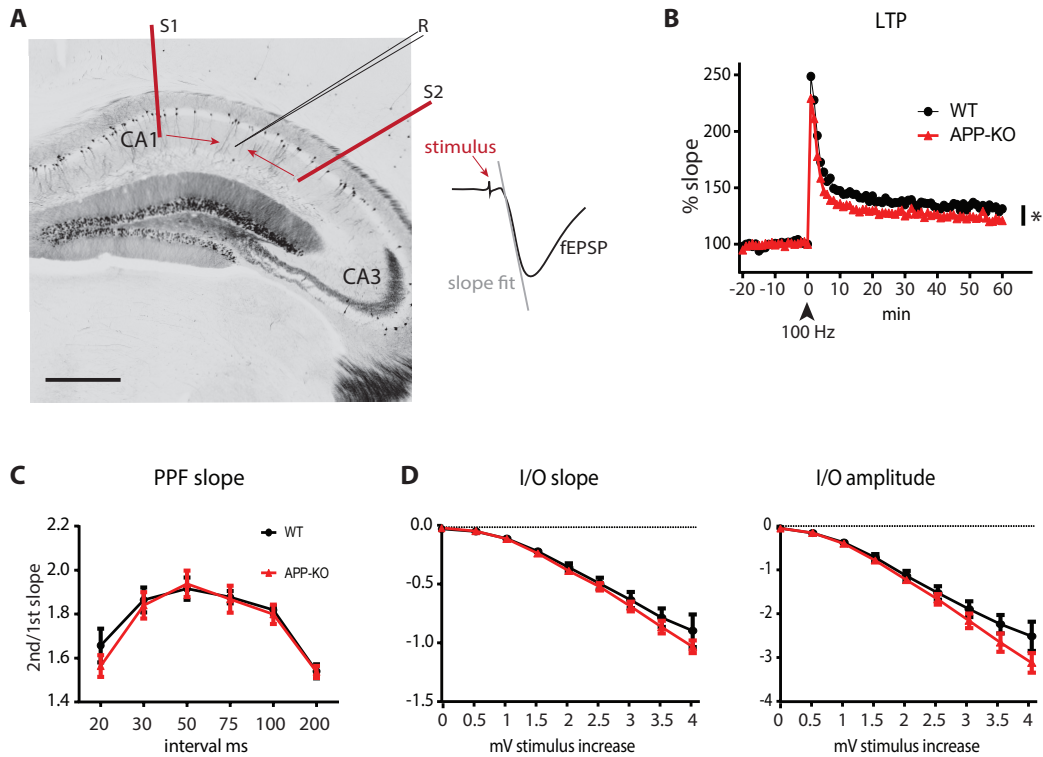


Figure 2.3. LTP is reduced in APP-KO mice. (A) Illustration of the experimental setting of local field long-term potentiation (LTP) recordings in the hippocampus of acute brain slices. The confocal picture with sparsely labelled neurons serves for demonstrating the electrode positions. Two stimulation electrodes are placed in the CA1 region on the Schaffer collaterals, one closer to CA3 and one more far from CA3. Then, the recording electrode is placed between the two stimulation electrodes detecting the local field potential that are elicited from both stimulation electrodes (arrows). The example trace on the left shows the analysis of the local field potential by a straight line along the slope. The change in the slope grade is taken into account for LTP analysis. Scale bar = 500 μ m. (B) The LTP is reduced in APP-KO mice in comparison to WT. Analysis of % employed from min 50 to 60. One-way ANOVA: $p = 0.0244$; $n = 16-17$ slices. (C) Paired-pulse facilitation recording with different stimulus intervals plotted along the x-axis. A ratio of the 2nd and the 1st slope serves as facilitation interpretation. There is no difference between APP-KO and WT ($n = 6$ animals). (D) Input/output (I/O) curve of the response slope along stimulus increase 0-4 mV. There is no difference in the response to stimuli increase between WT and APP-KO ($n = 6$ animals).

$p > 0.05$).

Moreover, the amplitude and the slope of the input/output (I/O) measuring the local field potential response to increasing stimuli did not reveal a change between WT and APP-KO animals (Figure 2.3D). These findings suggest a plasticity related phenotype that is independent of presynaptic release or basic postsynaptic stimulus response.

2.1 The role of APP in synaptic plasticity in the cortex and hippocampus

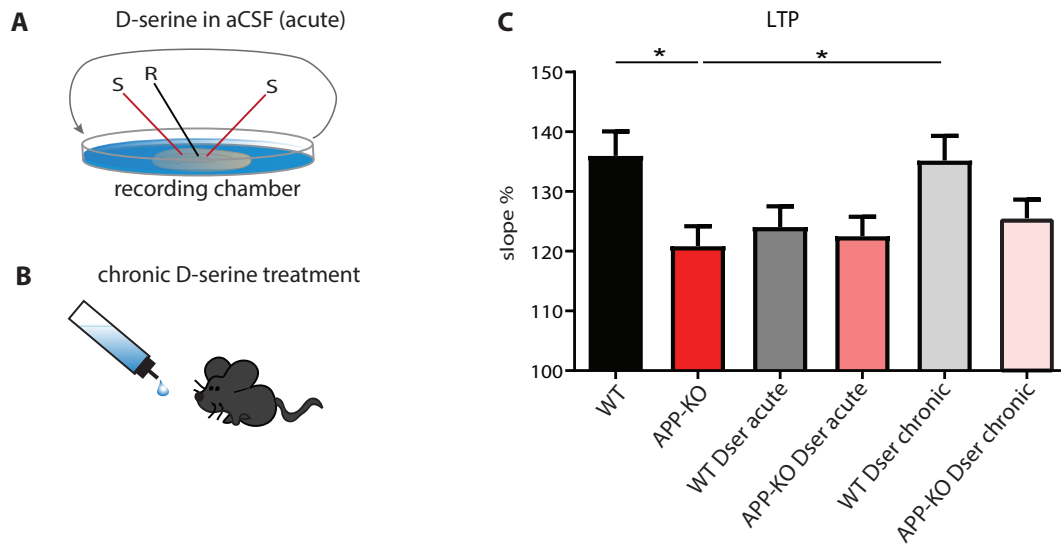


Figure 2.4. Reduced LTP in APP-KO hippocampus cannot be rescued by D-serine application. (A) Illustration of the experimental setting of acute 10 μ M D-serine application via aCSF perfusion in der submerged recording chamber, containing the acute slice with stimulation and recording electrode. (B) Illustration of chronic 5.2 mM D-serine application via the drinking water over 4 weeks. (C) LTP recordings of WT, APP-KO without treatment, D-serine in the recording chamber (acute) and D-serine treatment (chronic) via drinking water. APP-KO animals display reduction in LTP in comparison to WT untreated (WT vs. APP-KO: $F_{(5,94)} = 1.468$, $p = 0.0244$). WT animals treated with D-serine (WT treated with D-serine vs. APP-KO: $F_{(5,94)} = 1.435$, $p = 0.0237$). One-way ANOVA, $n = 16-21$.

In order to test whether D-serine can rescue the reduction of LTP in APP-KO animals, 10 μ M D-serine was acutely washed in the recording chamber (Figure 2.4A) or chronically applied via the drinking water for 4 weeks (Figure 2.4B). Neither of the D-serine applications could rescue the phenotype of APP-KO (Figure 2.4C) (mean \pm SEM: WT = 136 ± 4.082 ; APP-KO = 120.8 ± 3.339 ; WT D-serine acute = 124.1 ± 3.446 ; APP-KO D-serine acute = 122.5 ± 3.275 ; WT D-serine chronic treatment = 135.2 ± 4.128 ; APP-KO D-serine chronic treatment = 125.5 ± 3.159 ; $p > 0.05$). Surprisingly, acutely applying D-serine in the recording chamber resulted in a slight decrease of LTP in the WT which was neither significantly different to WT nor to APP-KO. In contrast, chronic treatment with D-serine in the drinking water had no effect on LTP in WT slices (significantly different to APP-KO)(Figure 2.4C).

In conclusion, APP is not essential for basic synaptic transmission involving pre- and postsynapse (PPF, I/O) but for functional plasticity (LTP) in the hippocampus. The ineffective application of D-serine indicates that other or additional factors are involved.

2.1.3 Conditional KO of APP in astrocytes influences spine density and morphology in the cortex and hippocampus

Morphology and distribution of dendritic spines are dynamically and tightly regulated [125] and profoundly influenced by neuronal activity [204]. Astrocytes are in close proximity to synapses and are supporting partners in synaptic function [144].

Previous studies report a crucial role of APP in spine stability in the cortex and hippocampus [205],[206],[97],[96]. However, the role of astrocytic APP in spine stability in the context of the tripartite synapse has been neglected so far. Hence, the

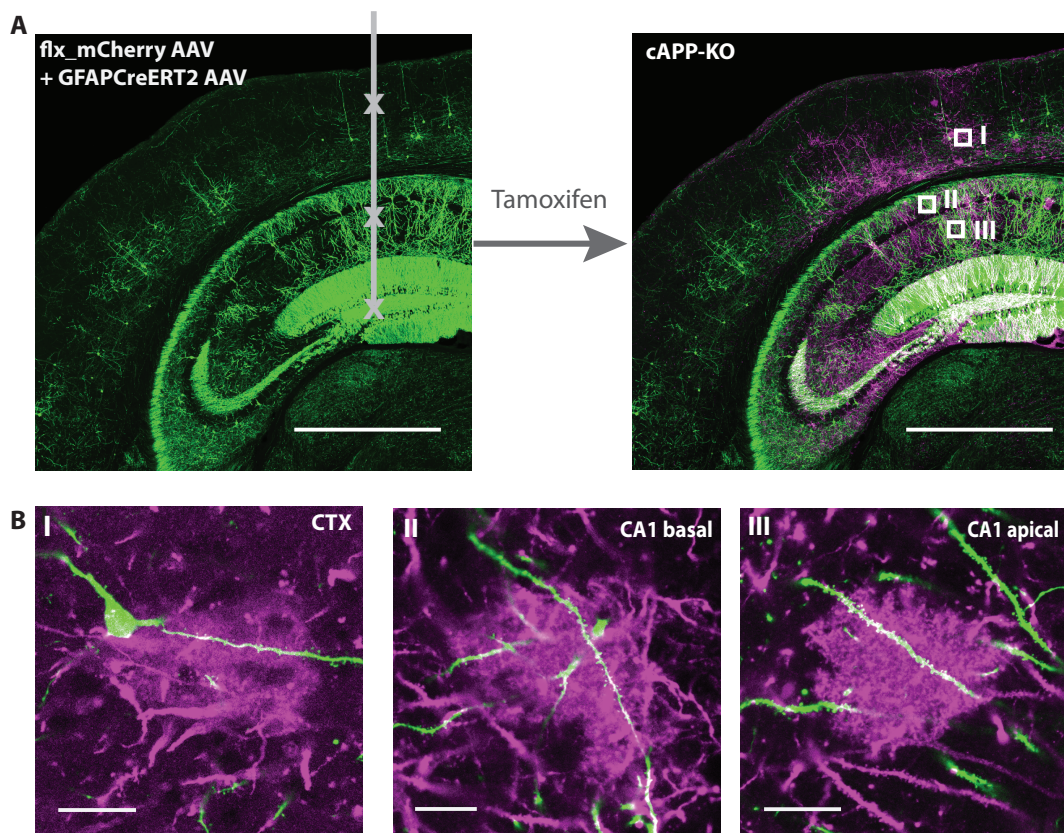


Figure 2.5. Conditional KO of APP in adult astrocytes surrounding GFP-M positive neurons. (A) Confocal picture of the cortex and hippocampus illustrating injection sites: Grey line indicates injection needle and crosses the injection sites where AAV Brainbow and AAV GFAPCreERT2 were applied in $APP^{+/+} \times GFP-M$ and $APP^{fl/fl} \times GFP-M$. Tamoxifen application (10 weeks later) activated Cre recombinase which entailed fluorophore expression and KO of APP. Another 10 weeks later, the perfused brain was used for *ex vivo* confocal studies. Scale bar = 1000 μm . (B) Example picture of sparsely labelled dendrites passing through one astrocyte lacking APP in the cortex (I), hippocampus CA1 basal (II) and apical (III) region. Scale bar = 20 μm .

question was raised which role astrocytic APP plays in spine density and morphology. For this purpose, animals with a floxed *APP* gene locus [207] were bred with eGFP-M animals expressing eGFP in a subset of principal neurons [208]. Stereotactic injection of adeno-associated virus (AAV) encoding a floxed mCherry fluorophore (AAV9 Brainbow, reporter virus) and GFAPCreERT2 (AAV5 inducible Cre expression in astrocytes) in the hippocampus and cortex enables selective and conditional KO of *APP* in astrocytes after tamoxifen application. After recombination, the mCherry fluorophore is expressed and provides an indication of Cre recombinase activity and therefore indicates KO of *APP* (Figure 2.5A). The sparse labelling of neurons with eGFP was used for spine analysis on dendrites that are surrounded by a mCherry positive and APP deficient astrocyte. Hereby, the density and morphology of the basal cortical dendrites and basal and apical dendrites of CA1 in the hippocampus were investigated (Figure 2.5B).

The basal cortical dendrites did not display any alterations in spine density (mean spines/ $\mu\text{m} \pm \text{SEM}$: WT = 0.9402 ± 0.05368 ; cAPP-KO = 0.9162 ± 0.06287 , $p > 0.05$). However, the basal and apical dendrites of the hippocampus showed increase in spine density when *APP* was knocked out in the surrounding astrocyte (mean spines/ $\mu\text{m} \pm \text{SEM}$: basal WT = 1.38 ± 0.06862 ; basal cAPP-KO = 1.653 ± 0.07941 ; apical WT = 1.795 ± 0.07798 ; apical cKO = 2.067 ± 0.06255 , $p < 0.05$) (Figure 2.6B).

Classification of the spine types mushroom, thin and stubby spines, revealed decrease of thin spines in the cortex as a consequence of lack of APP in the adjacent astrocyte (mean cortical thin spines/ $\mu\text{m} \pm \text{SEM}$: WT = 0.4858 ± 0.03673 ; cAPP-KO = 0.3455 ± 0.03827 , $p < 0.05$). In contrast, the increase in spine density in the basal and apical CA1 area exclusively resulted from elevated numbers of mushroom spines (mean CA1 mushroom spines/ $\mu\text{m} \pm \text{SEM}$: basal WT = 0.7332 ± 0.04195 ; basal cAPP-KO = 0.9566 ± 0.07516 , $p < 0.05$; apical WT = 1.034 ± 0.05337 ; apical cAPP-KO = 1.21 ± 0.05944 , $p < 0.05$) (Figure 2.6C).

The results depict an astrocytic role of APP in regulating structural plasticity of excitatory synaptic spines varying across brain regions.

2. Results

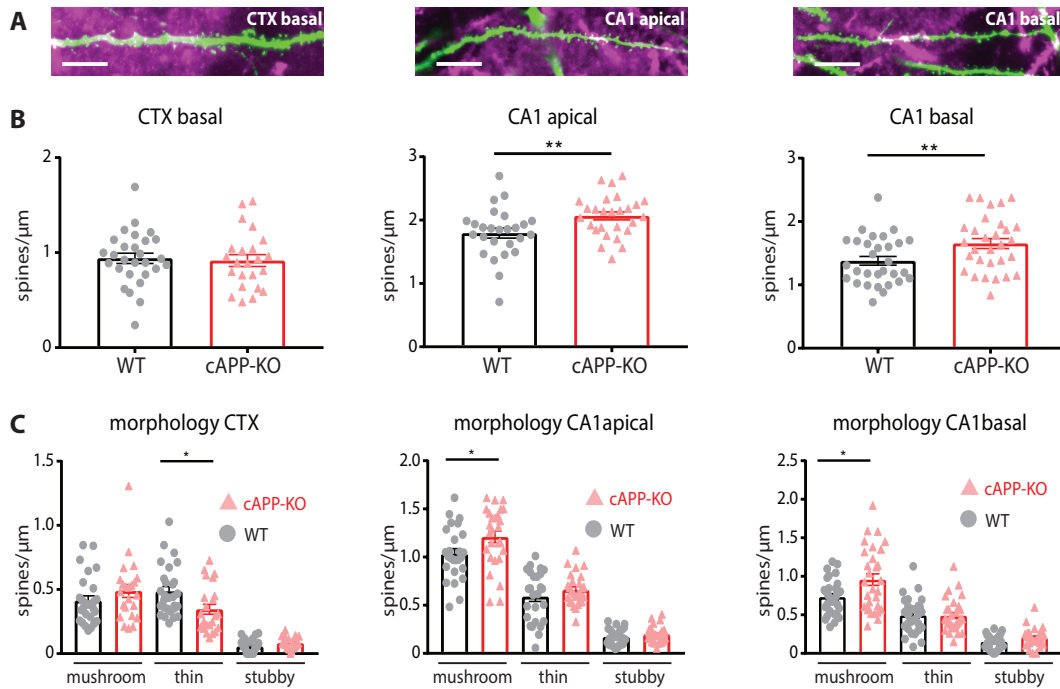


Figure 2.6. Conditional KO of APP in adult astrocytes alters morphology and density of dendritic spines. **(A)** Analysed example dendrites. Only the part of the dendrite passing through a labelled astrocyte was analysed. Scale bar = 10 μm . **(B)** Bar graphs of spine densities (spines/ μm) on dendrites after conditional KO of APP (cAPP-KO) in the adjacent astrocyte. Spine density of cortical dendrites is not changes between cAPP-KO and WT ($t(49) = 0.2916$, $p = 0.7718$, $n = 23-28$). Hippocampal dendrites display increase in spine density in cAPP-KO, CA1 apical ($t(51) = 2.731$, $p = 0.0087$, $n = 26-27$) and CA1 basal ($t(58) = 2.602$, $p = 0.0117$, $n = 30$, two-tailed Students t -test). **(C)** Morphological alterations of dendritic spines in cAPP-KO. Cortical dendritic spines exhibit a decrease in thin spines in cAPP-KO ($t(49) = 2.629$, $p = 0.0114$, $n = 23-28$). In the hippocampus dendrites show an increase in spines of the mushroom type both in apical ($t(51) = 2.19$, $p = 0.0311$, $n = 26-27$) and basal ($t(58) = 2.595$, $p = 0.012$, $n = 30$, two-tailed Students t -test) areas.

2.2 The role of APP in astrocytic function

APP-KO animals display a neuronal plasticity phenotype [64] that is supposedly associated with dysfunction of astrocytic Ca^{2+} signalling. For instance, reduced levels of extracellular D-serine were associated with structural synaptic plasticity impairments in APP-KO animals [96]. D-serine is Ca^{2+} dependently released by astrocytes during functional synaptic plasticity [159],[167],[209], which was shown to be reduced in APP-KO animals [101]. Moreover, primary APP-KO astrocytes display deficits in Ca^{2+} homeostasis and energy supply [112],[110]. Generally, astrocytic Ca^{2+} increase can be induced during synaptic activity by neurotransmitter or spontaneously in the absence of neuronal activity [144]. It has been shown that stimuli for LTP induction enhance the motility of synapse-associated astrocytic processes. This motility depends on G-protein-mediated Ca^{2+} elevations in astrocytes [152].

Taken together, several lines of evidence suggest a crucial role of APP in astrocytic Ca^{2+} signalling impacting synaptic function. Hence, spontaneous astrocytic Ca^{2+} transients and related mitochondrial function were investigated within fine perisynaptic processes of APP-KO astrocytes.

2.2.1 Investigation of spontaneous astrocytic Ca^{2+} transients in the hippocampus and cortex

As the focus of this thesis lies in aspects of communication between neurons and astrocytes in the view of the tripartite synapse, Ca^{2+} signals were measured in the highly ramified processes of astrocytes that are the contact sites to neurons. Therefore, an AAV GFAP_Lck_GCaMP6 encoding a membrane-tethered Ca^{2+} indicator GCaMP6 [194] was used. The virus was stereotactically injected in the hippocampus (dentate gyrus and CA1) and overlying somatosensory cortex of 2-months old APP-KO and WT control animals (Figure 2.7A). The brain was harvested for two-photon imaging of 350 μm acute coronal slices 4-5 months later. Acute brain slices were prepared as for LTP recordings and transferred into the submerged recording chamber of the two-photon microscope. The expression of the Ca^{2+} indicator was checked by epifluorescence and an appropriate ROI ($67 \times 67 \mu\text{m}$, 5 min, 2 Hz) in the cortex or hippocampus was chosen for two-photon imaging (Figure 2.7A). The imaged astrocytes displayed Ca^{2+} elevations within small spatially restricted areas that lasted several seconds. Preparation for analysis included a shift correction followed by cropping the image sequence to $60 \times 60 \mu\text{m}$. For the analysis of the active areas (Figure 2.7B), termed microdomains, the image sequence was filtered in 3D from the background noise. Next, a detection threshold was set by projecting the image sequence along the time axis to a single image of average intensity (AVG) and standard deviation (STD). The STD image was added $3\times$ to the AVG image and a threshold was defined. Subsequently, this threshold was used for a summary and STD projection of the image sequence. The addition of both threshold projections were filtered and gave rise of microdomains/ROIs that were

2. Results

applied onto the raw image series in order to extract the Ca^{2+} transients. Notably, not all detected microdomains display transient activity. Only active microdomains were manually selected and considered for analysis. The Ca^{2+} traces were further analysed in terms of Ca^{2+} event frequency and kinetics with the MiniAnalysis programme (Figure 2.7B).

Imaging of perisynaptic astrocytic Ca^{2+} transients enables investigations of astrocytic activity as an important partner in synaptic function.

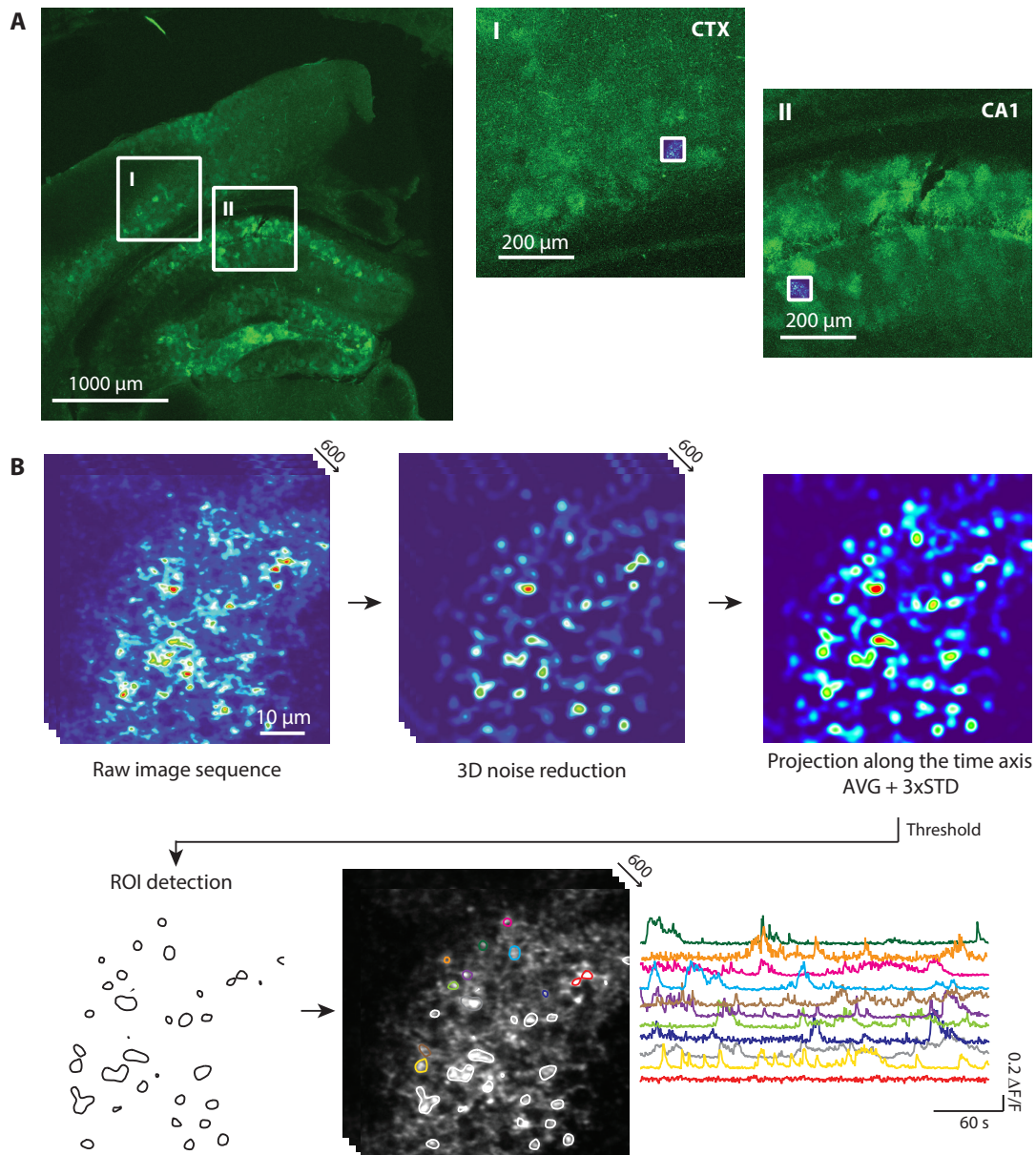


Figure 2.7. Analysis of astrocytic Ca^{2+} transients in the hippocampus and cortex. (A) Expression pattern of astrocytic GCaMP6 after AAV transduction in dentate gyrus and CA1 of the hippocampus and the somatosensory cortex. Squared insets: zoomed view of the imaging area in the cortex (I) and CA1 area (II). Blue insets: imaging acquisition areas of 67 \times 67 μm . (B) Analysis for microdomain detection and Ca^{2+} transient extraction: The background noise in 3D is subtracted from the raw image sequence. Next, average (AVG) and standard deviation (STD) projections along the time axis are used for the individual activity threshold definition (AVG + 3 \times STD). The threshold is employed for ROI detection from which Ca^{2+} traces are extracted from the raw image sequence. Exemplified subset of transients in colour.

Spontaneous astrocytic Ca²⁺ transients are impaired in the cortex of APP-KO animals

Astrocytic active microdomain composition and their Ca²⁺ transients were imaged in layer I/II of the somatosensory cortex in acute brain slices of WT and APP-KO animals. The analysis revealed no difference in the number of active domains within the image acquisition area (Figure 2.8A,B). Moreover, the microdomain size revealed no significant alterations due to the lack of APP (mean \pm SEM in μm^2 : WT = $85.92 \mu\text{m}^2 \pm 7.389$; APP-KO = $78.73 \mu\text{m}^2 \pm 6.846$, $p > 0.05$) (Figure 2.8C,D).

The extracted Ca²⁺ transients (Figure 2.8E-J) displayed significantly reduced frequency Ca²⁺ events in APP-KO animals (mean \pm SEM in evt/min/domain: WT = 2.449 ± 0.207 ; APP-KO = 1.629 ± 0.1813 ; $p < 0.005$) (Figure 2.8E,F). The amplitude of the events ($\Delta F/F$) remained unchanged (Figure 2.8G) (mean \pm SEM: WT = 0.08017 ± 0.006467 ; APP-KO = 0.09327 ± 0.01338 , $p > 0.05$). The rise time was significantly increased (mean \pm SEM in ms: WT = 2281 ± 120.8 ; APP-KO 3046 ± 308.9 ; $p < 0.05$) in APP-KO while the decay time was not altered (Figure 2.8I) (mean \pm SEM in ms: WT = 4780 ± 377.4 ; APP-KO = 5126 ± 552.4 ; $p > 0.05$). The area under the curve (AUC) was also not changed (Figure 2.8J) (mean \pm SEM in a.u.: WT = 5333834 ± 610869 ; APP-KO = 6692575 ± 1532647 ; $p > 0.05$).

These findings illustrate a role of APP in regulating spontaneous Ca²⁺ transients in the perisynaptic astrocytic protrusions in the cortex and might be an explanation for synaptic plasticity dysfunctions in APP-KO.

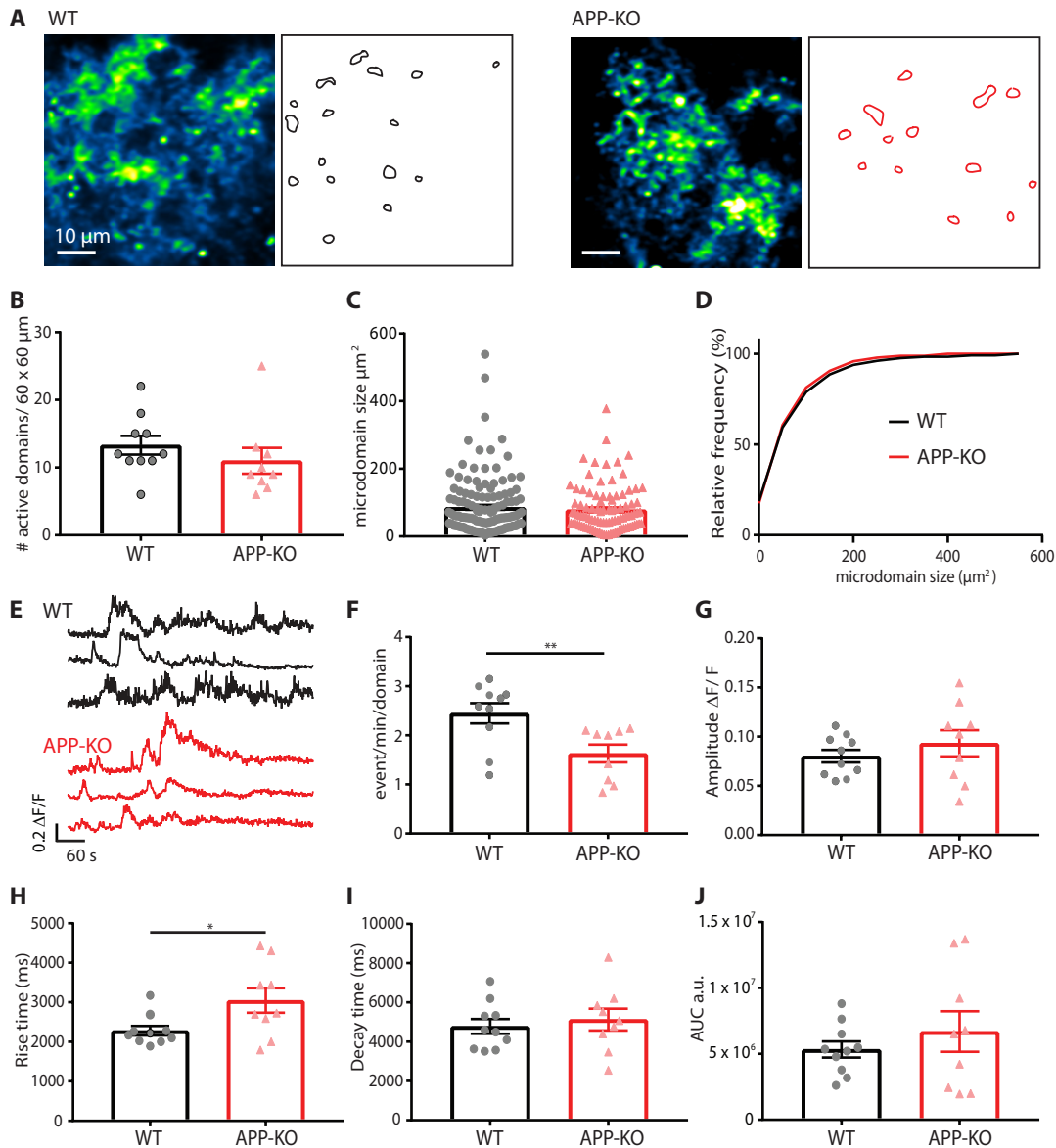


Figure 2.8. Altered spontaneous astrocytic Ca^{2+} transients in APP-KO cortex. (A) Exemplified activity profiles and distribution of active microdomains in WT and APP-KO cortex. Scale bar = 10 μm . (B) Neither the number of active domains (Mann-Whitney test: $p = 0.1373$; $U = 26.5$; $n = 9-10$ slices) nor the microdomain size (C) is altered in APP-KO cortex ($p = 0.9175$; $U = 6399$; $n = 97-133$ microdomain). (D) Frequency distribution of microdomain size (Kolmogorov-Smirnov comparison: $D = 0.0656$; $p = 0.964$). (E) Example Ca^{2+} traces. (F) The frequency of Ca^{2+} events is reduced in the APP-KO ($p = 0.0041$ (**); $U = 11$). (G) The amplitude of the events ($\Delta F/F$) remains unchanged (two-tailed t -test. $p = 0.3752$; $t(17) = 0.9107$). (H) The rise time is increased ($p = 0.0281$ (*); $t(17) = 2.401$), (I) decay time ($p = 0.6054$; $t(17) = 0.5264$), and (J) area under the curve (AUC) are unchanged in APP-KO ($p = 0.4037$; $t(17) = 0.8564$; $n = 9-10$ slices).

Spontaneous astrocytic Ca^{2+} transients are impaired in the hippocampus of APP-KO animals

Astrocytic active microdomain composition and their Ca^{2+} transients were imaged in the stratum radiatum of the hippocampal CA1 area in acute brain slices of WT and APP-KO animals. Analysis of the image sequences revealed no difference in the number of active microdomains (mean \pm SEM: WT = 10 ± 1.604 ; APP-KO = 12.09 ± 1.455 ; $p > 0.05$) (Figure 2.9A,B). However, the average microdomain size was larger in APP-KO animals (Figure 2.9C) (mean \pm SEM: WT = 80.97 ± 6.666 ; APP-KO = 95.91 ± 7.397 ; $p < 0.05$) which became evident in the shift of the frequency distribution (Figure 2.9D) ($p < 0.05$). With regard to the kinetics of the Ca^{2+} transients, APP-KO animals displayed reduced event frequency per active microdomain (Figure 2.9F) (evt/min/domain mean \pm SEM: WT = 2.189 ± 0.1541 ; APP-KO = 1.557 ± 0.2455 ; $p < 0.05$). The amplitude of the events ($\Delta F/F$) (Figure 2.9G)(mean \pm SEM in $\Delta F/F$: WT = 0.09677 ± 0.008027 ; APP-KO = 0.07745 ± 0.0115 ; $p > 0.05$), the rise time (Figure 2.9H)(mean \pm SEM in ms: WT = 2732 ± 136.1 ; APP-KO = 2756 ± 184.5 ; $p > 0.05$) and decay time (Figure 2.9I)(mean \pm SEM in ms: WT = 5375 ± 561.4 , APP-KO 5529 ± 634 , $p > 0.05$) remained unchanged between WT and APP-KO. The area under the curve was also unaltered among the two genotypes (Figure 2.9J)(mean \pm SEM in a.u.: WT = 6527615 ± 1046761 ; APP-KO = 4940486 ± 1163954 , $p > 0.05$).

These results depict a role of APP in regulating spontaneous Ca^{2+} transients in the perisynaptic astrocytic protrusions in the hippocampus and might be associated with the synaptic plasticity dysfunctions in APP-KO.

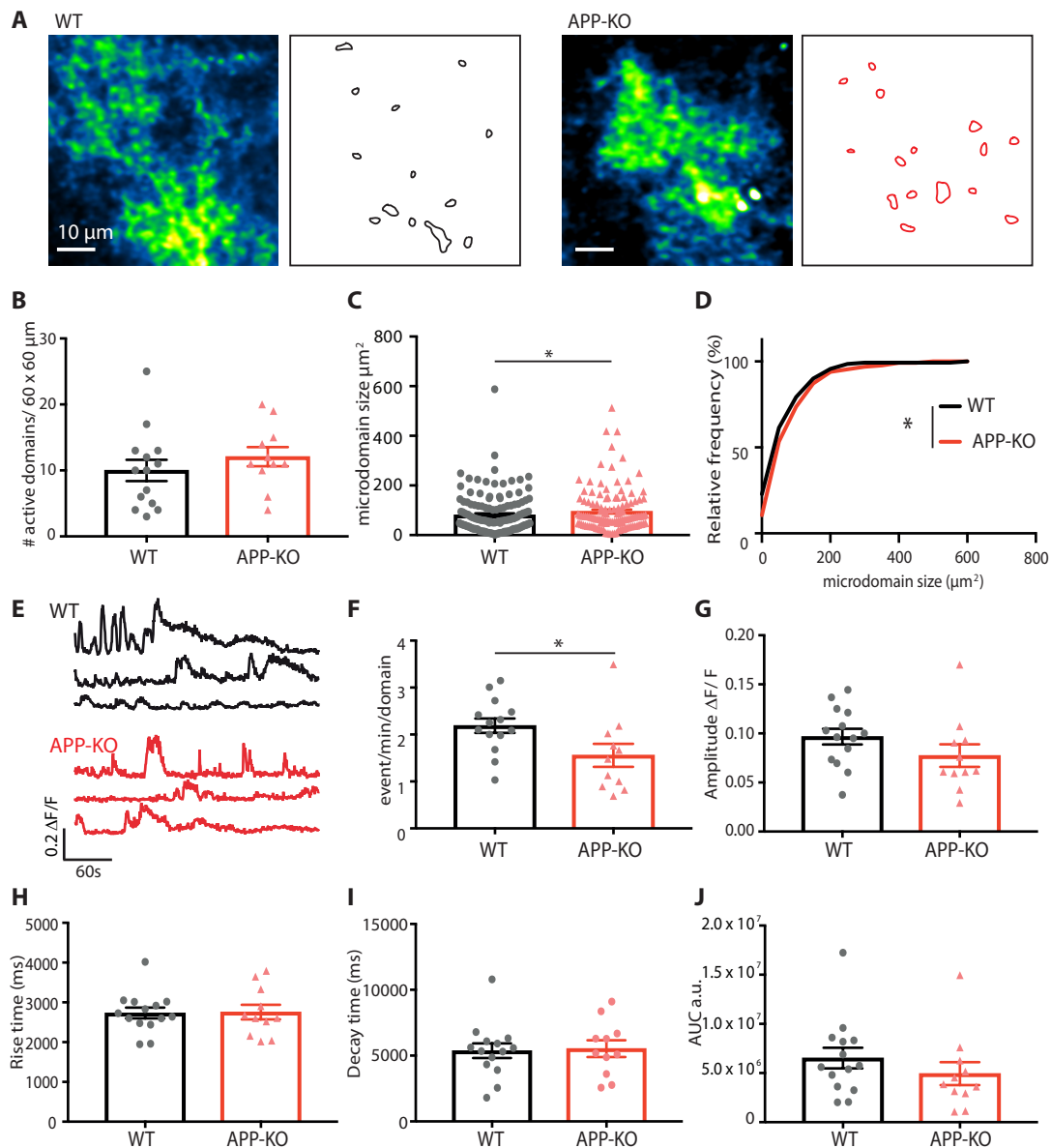


Figure 2.9. Altered spontaneous astrocytic Ca^{2+} transients in APP-KO hippocampus. (A) Illustrative activity profiles and distribution of active microdomains in WT and APP-KO CA1. **(B)** There is no difference in the number of active microdomains (two-tailed t -test: $p = 0.3570$; $t(23) = 0.9401$; $n = 11-14$ slices). **(C)** APP-KO animals display increase in microdomain size (Mann-Whitney test: $p = 0.036$; $U = 7942$; $n = 133-140$ microdomains.) and **(D)** a frequency distribution shift (Kolmogorov-Smirnov comparison of two data sets: $D = 0.1722$; $p = 0.031$). **(E)** Example Ca^{2+} traces. **(F)** The frequency is reduced in APP-KO ($p = 0.0328$; $t(23) = 2.272$). **(G)** The rise time ($p = 0.9174$; $t(23) = 0.1049$), **(H)** the decay time ($p = 0.8573$; $t(23) = 0.1818$), and **(J)** the area under the curve ($p = 0.1492$; $U = 50$; $n = 11-14$ slices) are unchanged in APP-KO.

2.2.2 Altered mitochondrial network integrity in APP-KO astrocytes

In the brain, astrocytes interact with closely associated synapses and with each other. Within this complex network they show alterations of spontaneous Ca^{2+} transients as a consequence of lack of APP.

The integrity of Ca^{2+} transients in the microdomains of astrocytes is strongly associated with mitochondrial localisation and function [195],[210]. In order to better understand the cause of this finding, primary astrocytic cultures were investigated for a potential mitochondrial phenotype. First of all, astrocytes were isolated from three pups at postnatal day 3 (p3) (Figure 2.10A) and the lack of APP was confirmed with western blot analysis by immunolabelling against the C-terminus and N-terminus of APP (Figure 2.10B). The slight bands in APP-KO immunoblotting against the N-terminus of APP result from cross reaction with the other APP family members APLP1 and APLP2.

Mitochondrial dynamics are suggested to be crucial for Ca^{2+} homeostasis and local energy supply [211]. Hence, investigation of mitochondrial morphology is providing information about the network integrity of mitochondria and shedding light on mitochondria function.

Primary cultured astrocytes from WT and APP-KO animals were passaged twice, fixed, and immunohistologically stained for the mitochondrial housekeeping protein translocase of the outer mitochondrial membrane 20 (TOM20). The culture was

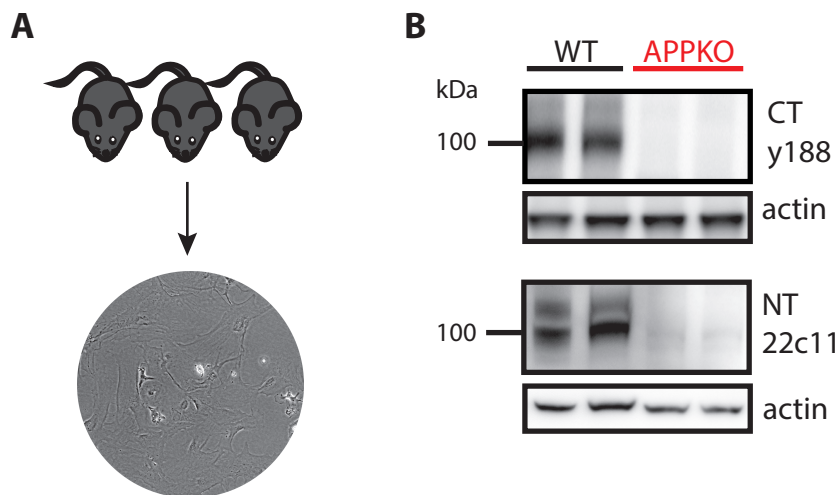


Figure 2.10. Primary astrocytes harvested from APP-KO mice do not express APP. (A) Illustration of primary astrocyte culture preparation from p3 pups of WT and APP-KO. **(B)** Western-blot of primary astrocyte culture lysate from WT and APP-KO pups. Antibodies against C-terminus (CT, Y188) and N-terminus (NT, 22c11) of APP confirm lack of APP in primary astrocytes from APP-KO mice. The cytoskeleton protein β -actin serves as loading control.

scanned for isolated, labelled astrocytes to image the mitochondrial network of a single astrocyte with a confocal microscope (Figure 2.11A). The quantification of mitochondrial morphology was based on the fluorescent signal of TOM20 that was categorised in three different morphology classes depending on the pixel connectivity (Figure 2.11B)[212]. Therefore, a threshold mask was generated with the programme ImageJ and the "Analyze Particles" function grouped the signal into puncta (0.1 - 2.7 μm), rods (2.8 - 8.8 μm) and network (from 8.9 μm). The morphology classes were then normalised to the total TOM20 signal and displayed in percentage (Figure 2.11C). Mitochondria of APP-KO astrocytes displayed a more fragmented morphology visualised by a reduction in network class (mean \pm SEM in %: Wt = 87.96 ± 0.9643 ; APP-KO = 78.7 ± 1.351) but an increase in puncta (mean \pm SEM in %: Wt = 3.293 ± 0.319 ; APP-KO = 7.823 ± 0.592) and rod (mean \pm SEM in %: Wt = 8.745 ± 0.6879 ; APP-KO = 13.47 ± 0.8753) morphology (Figure 2.11C).

In order to test if the lack in network type mitochondria does not derive from loss of mitochondria, western blot analysis was performed: no change in mitochondrial housekeeping protein content was detectable (Figure 2.11D)(mean \pm SEM: WT = 1 ± 0.07449 ; APP-KO = 1.096 ± 0.1026 ; $p > 0.05$).

To ascribe the fragmented phenotype to the presence of APP, APP fused to eGFP was reintroduced into a subset of APP-KO astrocytes via transient transfection. The eGFP expression enabled suitable detection of APP-expressing astrocytes (Figure 2.11A). These astrocytes were also subjected to morphological characterisation based on the TOM20 signal (Figure 2.11B) and displayed a mitochondrial morphology comparable to WT astrocytes (mean \pm SEM in % APP rescue: network = 89.43 ± 1.542 ; rods = 6.25 ± 0.9791 ; puncta = 4.321 ± 0.5902)(Figure 2.11C). Reintroduction of APP into APP-KO astrocytes was able to restore the mitochondrial network.

The observed fragmented morphology of mitochondria in APP-KO astrocytes provides another hint that APP function sustains normal mitochondria network integrity and that its depletion disrupts mitochondrial morphology and eventually function in regulating Ca^{2+} homeostasis.

2. Results

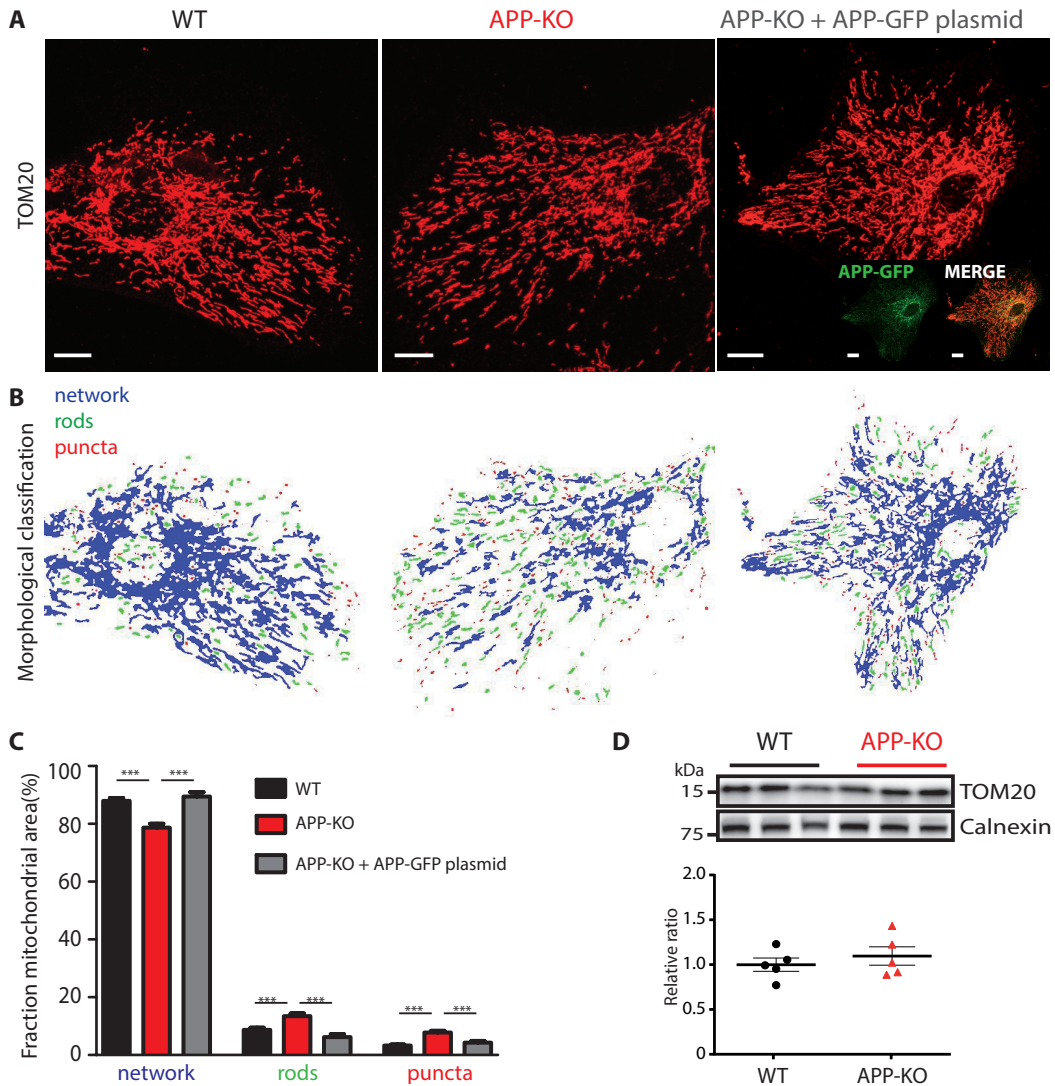


Figure 2.11. APP-KO astrocytes display fragmented mitochondrial morphology that can be rescued by reintroduction of APP. **(A)** Confocal images of immunofluorescently labelled mitochondria stained with mitochondrial housekeeping protein TOM20 in WT, APP-KO and APP-KO + APP-GFP plasmid astrocytes. Scale bar = 10 μ m. **(B)** Morphological classification of mitochondria into network, rods and puncta based on their TOM20 signal pixel integrity in astrocytes of WT, APP-KO and APP-KO expressing APP-GFP plasmid. **(C)** Quantification of mitochondrial morphology classes of WT, APP-KO and APP-KO expressing APP-GFP plasmid. APP-KO astrocytes have ~ 10 % reduction in mitochondria network (One-way ANOVA, $F_{(2,87)} = 19.78$, $p < 0.0001$), ~ 5 % increase in rods ($F_{(2,87)} = 18.38$, $p < 0.0001$) and puncta ($F_{(2,87)} = 21.14$, $p < 0.0001$) in comparison to WT, that can be rescued by expression of APP-GFP. *** $p < 0.0001$, $n = 30$. **(D)** Western blot of primary astrocyte culture reveals no changes in TOM20 level between WT and APP-KO (two-tailed Students t -test, $p = 0.4686$, $t(8)$; $n = 5$).

2.2.3 Altered mitochondrial Ca^{2+} transients in APP-KO astrocytes

To further link the observed fragmented phenotype to the functional Ca^{2+} alterations observed in the intact tissue, astrocytic mitochondria were characterised in terms of Ca^{2+} uptake behaviour. For this purpose, cultured primary astrocytes were transfected with a plasmid encoding the Ca^{2+} indicator GCaMP6 together with a mitochondrial targeting sequence (mitoGCaMP) (Figure 2.12A) under an astrocytic promoter [213]. Application of 100 μM ATP stimulates Ca^{2+} influx into astrocytes [213] via G-protein coupled receptor (GPCR) on the cell surface. Mitochondria, in turn, take up the cytosolic Ca^{2+} via mitochondrial Ca^{2+} uniporter (MCU). The elevated levels of mitochondrial Ca^{2+} can be detected by increase in fluorescence of mitoGCaMP. Here, two-photon microscopy was performed to image mitochondrial Ca^{2+} dynamics in astrocytes in response to stimulation. The image series was acquired with 1 Hz over 300 s during which a 60 s baseline (Figure 2.12BI), an initial ATP response (Figure 2.12BII) and the subsequent decay (Figure 2.12BIII) were imaged. A ROI encircling the entire mitochondrial Ca^{2+} signal was drawn and traces of WT and APP-KO astrocytic mitochondria (Figure 2.12C) were analysed in terms of response size and kinetics.

The baseline (Figure 2.12D)(mean \pm SEM in a.u.: WT = 566.7 ± 222.4 ; APP-KO = 378.8 ± 144.3 ; $p > 0.05$) and amplitude (Figure 2.12E)(mean \pm SEM in $\Delta\text{F}/\text{F}$: WT = 7.639 ± 2.049 ; APP-KO = 9.456 ± 3.295 ; $p > 0.05$) of the stimulated mitochondrial Ca^{2+} signal was not changed in APP-KO astrocytes. However, the kinetics of the response was slower in APP-KO mitochondria, as they exhibited a longer rise time (Figure 2.12F)(mean \pm SEM in ms: WT = 9000 ± 2171 ; APP-KO = 16500 ± 2121 ; $p < 0.05$) and slower decay of the first (fast) slope (mean \pm SEM tau (fast) in ms: WT = 50791 ± 14985 ; APP-KO = 130670 ± 35905 ; $p < 0.05$) but not the second slope (mean \pm SEM tau (slow) in ms: WT = 14184 ± 2629 ; APP-KO = 18679 ± 4975 ; $p > 0.05$) of the two-phase decay analysis (Figure 2.12G).

Next, the stimulation response amplitude $\Delta\text{F}/\text{F}$ was analysed depending on the mitochondrial morphology. Thus, a ROI was positioned close to the nucleus where mitochondria are arranged in the network conformation. Another ROI was placed close to the edge of the cell where rod and puncta shaped mitochondria are located (Figure 2.13A). As the amplitude of the response differed considerably across astrocytic mitochondria, a cell-internal ratio of $\Delta\text{F}/\text{F}$ network/edge ROI was formed and taken into account for comparison between APP-KO and WT astrocytes. Ca^{2+} signals of APP-KO mitochondria showed a significant decrease in the $\Delta\text{F}/\text{F}$ network/edge ratio in comparison to WT (Figure 2.13B). The more detailed analysis of $\Delta\text{F}/\text{F}$ network/edge ratio revealed spatially dependent alterations in APP-KO Ca^{2+} amplitude as a consequence of either increased response of rod and puncta mitochondria or decreased Ca^{2+} signal in network-shaped mitochondria (mean \pm SEM $\Delta\text{F}/\text{F}$ network/edge ratio: WT = 2.691 ± 0.2324 ; APP-KO = 1.415 ± 0.3087 ; $p < 0.05$)(Figure 2.13C).

2. Results

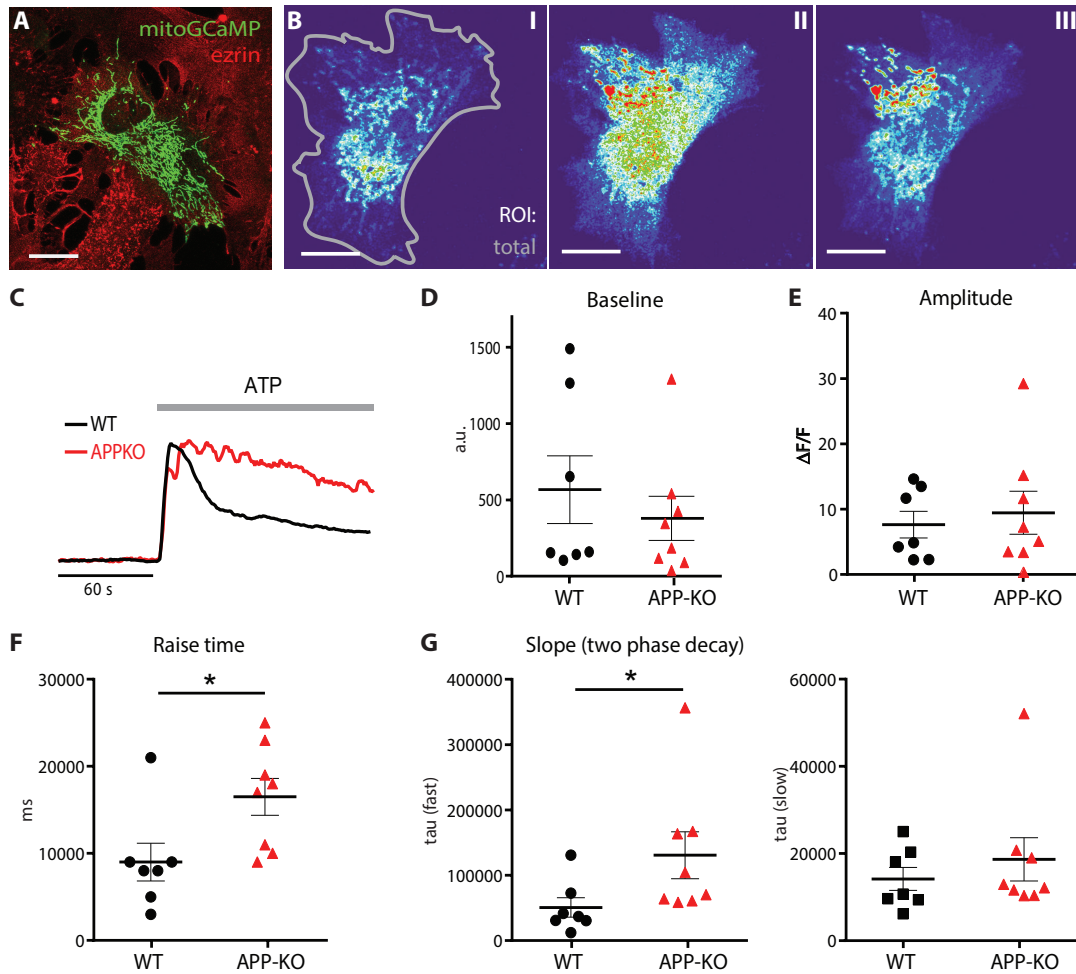


Figure 2.12. Stimulated mitochondrial Ca^{2+} signals of APP-KO astrocytes display slower kinetics. **(A)** Confocal image of an astrocyte transfected with mitochondria-targeted GCaMP (green, mitoGCaMP). Astrocytic cytoskeleton protein ezrin (red) confirms the cell identity. Scale bar = 20 μm . **(B)** Illustration of the stimulation procedure (ATP) and region of interest (ROI) encircling total mitochondrial Ca^{2+} signal (grey border). 1st picture: baseline, 2nd: peak; 3rd: decay. Scale bar = 20 μm . **(C)** Averaged mitochondrial Ca^{2+} traces in WT and APP-KO astrocytes during 100 μM ATP application. **(D)** The baseline fluorescence (10 s before the peak) (Mann-Whitney test, $p = 0.6126$; $U = 23$) and **(E)** the amplitude ($p = 0.8665$; $U = 26$) of the Ca^{2+} response of mitochondria in APP-KO astrocytes is not changed. **(F)** The rise time of Ca^{2+} traces of mitochondria is longer in APP-KO astrocytes, ($p = 0.0129$; $U = 7$). **(G)** The decay of mitochondrial Ca^{2+} traces was divided into two phases: The 1st fast tau lasts longer in APP-KO mitochondria ($p = 0.0289$; $U = 9$). The 2nd slow tau displayed no difference in APP-KO mitochondria, ($p = 0.3969$; $U = 20$; $n = 7-8$).

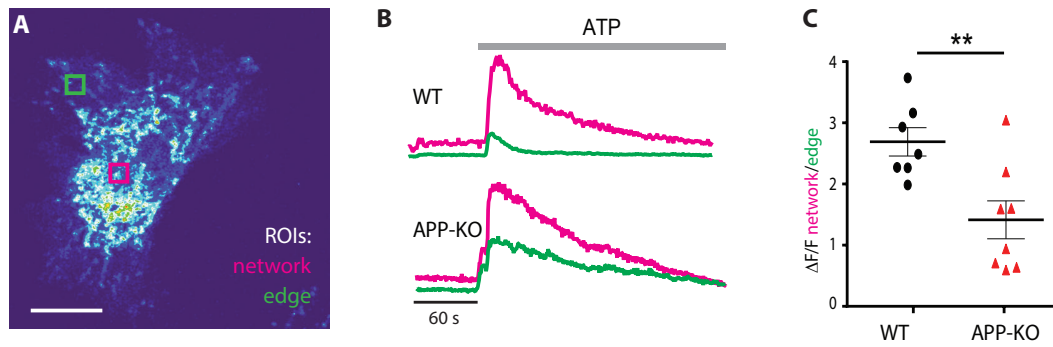


Figure 2.13. Stimulated mitochondrial Ca^{2+} signals of APP-KO astrocytes differ in distribution within the mitochondria network. Analysis of $\Delta\text{F}/\text{F}$ network $\Delta\text{F}/\text{F}$ edge ROI ratio. **(A)** Illustration of ROI position of network (magenta) and edge (green) in the astrocytic mitochondria. **(B)** Example traces of network and edge traces of WT (top) and APP-KO (bottom) mitochondrial Ca^{2+} traces. **(C)** Mitochondria from APP-KO astrocytes display a smaller $\Delta\text{F}/\text{F}$ network/edge ratio (two-tailed Students t -test, $p = 0.0067$; $t(13) = 3.223$; $n = 7-8$ astrocytes.)

Examination of mitochondrial Ca^{2+} signal in APP-KO astrocytes revealed substantial differences in mitochondrial Ca^{2+} influx expressed by slower kinetics and morphology-dependent uptake.

2.2.4 Investigation of mitochondrial proteins in primary astrocytes

In order to further understand the morphological and functional deficits of mitochondria in APP-KO astrocytes, primary astrocyte cultures from APP-KO and WT pups were lysed and employed for investigation of proteins involved in mitochondrial fission, Ca^{2+} transport and energy supply (Figure 2.14A,B). Cytochrome C is the proton pump of the respiratory chain in the inner membrane of mitochondria (Figure 2.14A). Increased levels of cytochrome C and its release from mitochondria are associated with a caspase mediated apoptotic mechanism [214]. The protein levels of cytochrome C were significantly increased in APP-KO astrocytes when normalised to cellular housekeeping protein (mean \pm SEM: WT = 1 ± 0.03227 ; APP-KO = 1.989 ± 0.3455 ; $p < 0.05$) and mitochondrial housekeeping protein TOM20 (mean \pm SEM: WT = 1 ± 0.02545 ; APP-KO = 1.802 ± 0.3355 ; $p < 0.05$) (Figure 2.14C). The ratio phosphorylated dynamin related protein 1/dynamin related protein 1 (pDRP1/DRP1) is a mitochondrial fission indicator [215]. The ratio of pDRP1/DRP1 was not changed in APP-KO astrocytes (Figure 2.14D) (mean \pm SEM: WT = 1 ± 0.07963 ; APP-KO = 1.136 ± 0.121 ; $p > 0.05$) suggesting that the fragmented mitochondrial morphology in APP-KO might result from other aberrant proteins. The voltage dependent anion channel (VDAC) and mitochondrial calcium uniporter (MCU) transports Ca^{2+} over the mitochondria membrane into mitochondria (Figure 2.14A) and are therefore important for clearing Ca^{2+} from the cytosol [216]. The protein levels of MCU, normalised to cellular (mean \pm SEM: WT = 1 ± 0.09092 ; APP-KO = 1.208 ± 0.08404) and mitochondrial housekeeping protein (mean \pm SEM: WT = 1 ± 0.03245 ; APP-KO = 1.133 ± 0.09828 ; $p > 0.05$), were slightly but not significantly increased in APP-KO astrocytes in comparison to WT (Figure 2.14B,E). TOM20 is part of the TOM complex on the outer mitochondria membrane and serves as mitochondrial housekeeping protein. The results of normalisation over TOM20 are similar to the results of normalisation over cellular housekeeping protein calnexin (Figure 2.14C,E).

Mitochondrial protein levels of MCU and TOM20 and the ratio pDRP1/DRP1 are not altered in the absence of APP suggesting that these proteins are not associated with the mitochondrial phenotype in APP-KO. The elevated levels of cytochrome C point towards malfunction and apoptosis which deserves further study.

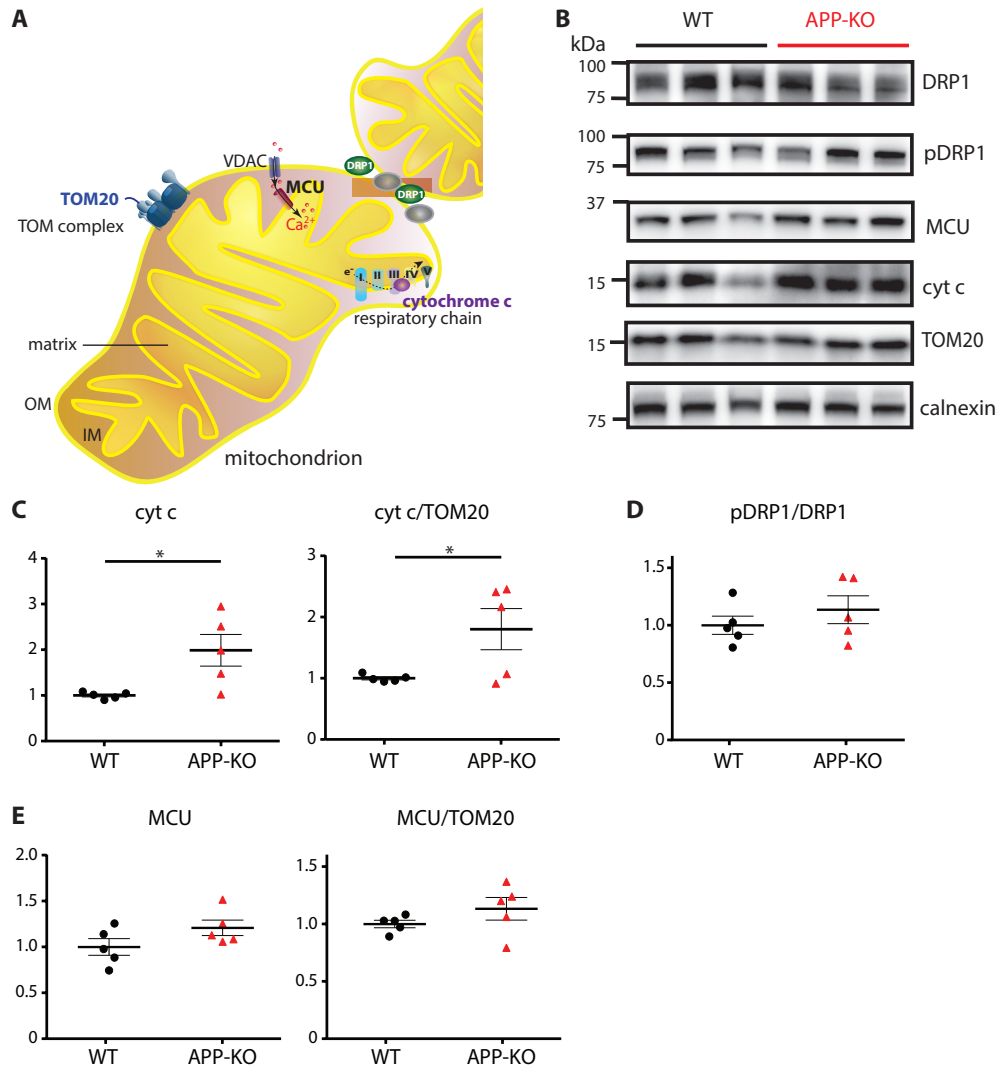


Figure 2.14. Investigation of mitochondrial proteins in primary astrocytes. (A) Illustrative drawing of a mitochondrion and associated proteins. Cytochrome C (cyt c) is part of the respiratory chain. DRP1 mediates outer mitochondrial membrane fission. MCU transports Ca^{2+} over the inner membrane (IM) into the lumen. TOM20 is part of the TOM complex, transports proteins over the outer membrane (OM), and serves as a mitochondrial housekeeping protein (hkprot). (B) Western blots of primary astrocyte lysates of $3 \times$ WT and APP-KO against DRP1, p-DRP1, MCU, cyt c, TOM20, and cellular hkprot calnexin. (C-E) Western blot quantifications. (C) Cyt c level is increased in APP-KO: Cyt c normalised to hkprot (left) (Students *t*-test: $p = 0.0215$ (*); $t(8) = 2.849$) normalised to TOM20 (right) ($p = 0.0443$ (*); $t(8) = 2.383$). (D) Ratio of the phosphorylated DRP1 (pDRP1)/DRP1 signal ($p = 0.3764$; $t(8) = 0.9366$) and (E) MCU levels normalised to hkprot (left) ($p = 0.1317$; $t(8) = 1.679$) and to TOM20 (right) ($p = 0.2351$; $t(8) = 1.284$; $n = 5$) are not altered in APP-KO astrocytes.

2.2.5 Isolation and protein investigation of astrocytes derived from the adult mouse brain

For the investigation of cell specific molecule levels that resemble *in vivo* conditions, astrocytes were acutely isolated from the intact adult mouse brain.

For this purpose, the mouse brain was quickly dissected after decapitation of the mouse (Figure 2.15I). The cortex was isolated and chopped into small cubes that were gently digested and homogenised with the GentleMACS with heaters machine (Figure 2.15II). Subsequently, the single cell solution was purified from cellular debris and red blood cells before binding magnetic beads to astrocytes (Figure 2.15III). Next, the cell solution was applied onto a column that was attached to a magnetic field. The labelled astrocytes got stuck in the magnetic field while other unlabelled cell types flushed through the column. When the column was removed from the magnetic field, the astrocytes were flushed out and collected in a separate falcon (Figure 2.15IV). The yield of isolated astrocytes derived from the adult mouse brain was very little: Cortices from 2 adult mouse brains result in ~ 3 mio total astrocyte number account for ~ 60 μg protein lysate. The isolated astrocytes were either employed for astrocyte culture confirming cell type identity and viability or for protein analysis via western blotting (Figure 2.15V).

For cell culture, astrocytes were plated onto coated 6-well plates, one well containing cortical astrocytes of one entire brain. After two days *in vitro* (DIV) some astrocytes started to adhere on the dish and to form protrusions. After 9 DIV, the cells spread out to a size larger than 100 μm . Staining against astrocytic markers such as $\text{s100}\beta$, GFAP and ezrin confirmed the identity of astrocytes (Figure 2.16A).

Moreover, isolated astrocytes derived from the adult brain were lysed for subse-

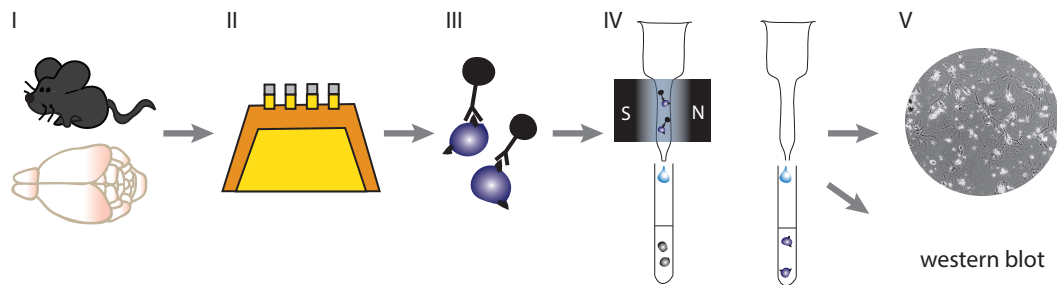


Figure 2.15. Isolation of astrocytes derived from the adult mouse brain. Procedure of astrocyte isolation from brains of 6 months old mice. **(I)** The brain is quickly harvested from the mouse and the cortex is dissected. **(II)** Cortical brain tissue is incubated and homogenised in the GentleMACS machine. **(III)** Antibodies coupled to magnetic beads are added to cell homogenate and bind to astrocytes. **(IV)** Cell homogenate with magnetic beads bound to astrocytes is applied onto a column attached to a magnetic field. Astrocytes stay in the magnetic field while other cell types are flushed through the column. Then, the column is removed from the magnetic field and astrocytes are collected. **(V)** Isolated astrocytes are either used for growing in a cell culture dish or lysed and further employed for protein analysis by western blot.

quent western blot analysis. Due to the small yield of the isolation, the cortices of two animals were taken for one replicate. The western blot analysis confirmed the lack of APP in astrocytes isolated from the adult cortex and hippocampus by immunoblotting against APP CT and APP NT (Figure 2.16B,D). Furthermore, blotting against GFAP indicated astrocytic identity of the lysate (Figure 2.16B). As cytochrome C levels were increased and MCU seemed slightly elevated in primary astrocyte cultures from APP-KO pups, the results are comparable to astrocytes derived from the adult brain: Indeed, adult astrocytes displayed slightly increased levels of MCU (mean \pm SEM in a.u.: WT = 4212 ± 716.4 ; APP-KO = 5225 ± 455.3 ; $p > 0.05$) and cytochrome C (mean \pm SEM in a.u.: WT = 4446 ± 673.7 ; APP-KO = 4649 ± 1327 ; $p > 0.05$) (Figure 2.16B,C). The statistical test was a paired *t*-test, as samples differed a lot between biological replicates. Hence, protein concentrations were compared over the same preparation procedure of the same day.

Isolation of astrocytes from the adult brain is a suitable tool for the investigation of astrocytes that matured in the intact brain. However, the small yield requires large amounts of tissue, respectively.

2. Results

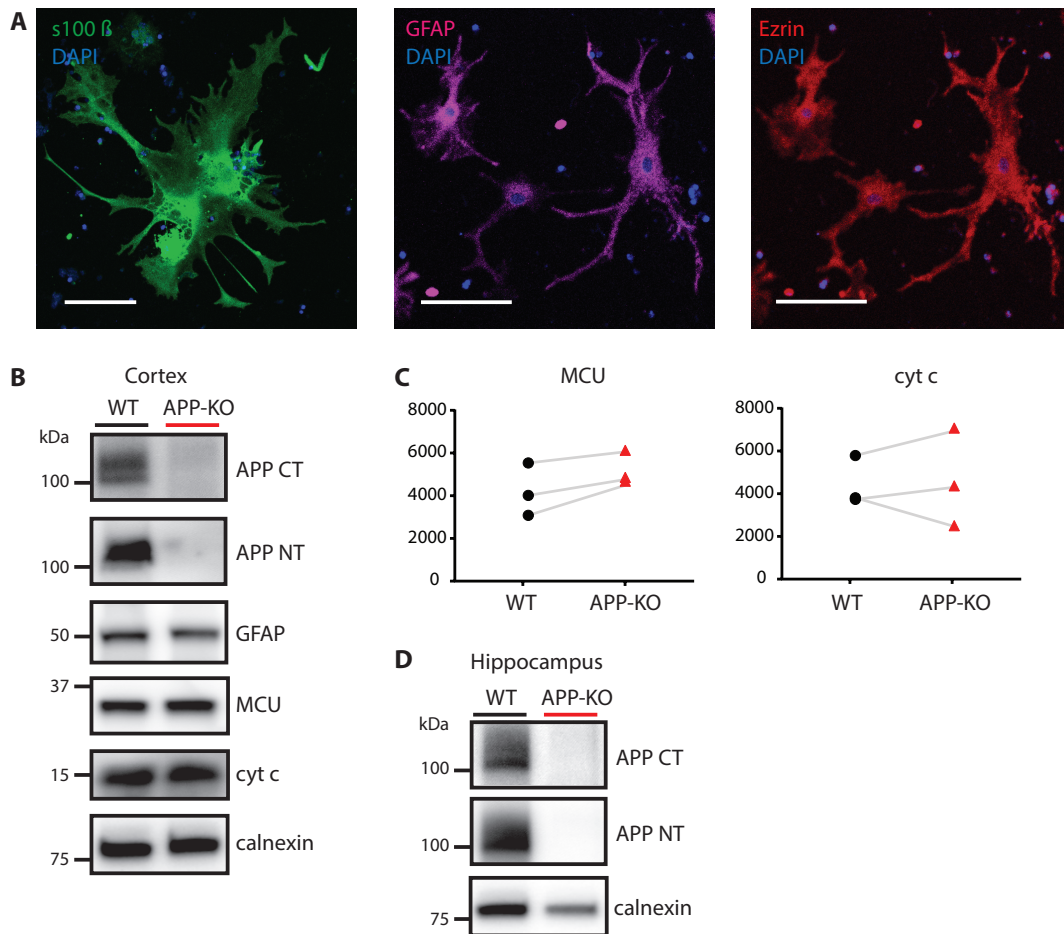


Figure 2.16. Characterisation of astrocytes isolated from the adult brain and investigation of mitochondrial proteins. **(A)** Immunohistochemical analysis of astrocytes isolated from the adult brain and grown in a cell culture dish for 9 days after isolation proves astrocytic identity: Staining against s100 β and DAPI (left); glial fibrillary acidic protein (GFAP) and DAPI (middle); ezrin and DAPI (right). Scale bar = 100 μ m. **(B)** Western blots of lysates from astrocytes of adult cortices from WT and APP-KO mice (two animals each). Antibodies against APP CT and APP NT prove the lack of APP in isolated cortical astrocytes from APP-KO mice. Antibody against GFAP verifies astrocytic identity. Calnexin serves as housekeeping protein. **(C)** Quantification of MCU and cytochrome c signal paired over one preparation day (grey connecting line between data points) does not reveal significant differences between WT and APP-KO astrocytes (paired Student's *t*-test, MCU: $p = 0.0795$, $t(2) = 3.33$; $n = 3$. cytochrome c: $p = 0.8185$, $t(2) = 2.61$; $n = 3$). **(D)** Antibodies against APP CT and APP NT prove the lack of APP in astrocytes isolated from the hippocampus of APP-KO mice.

Chapter 3

Discussion

3.1 The role of APP in synaptic plasticity in the cortex and hippocampus

The pathology of AD is characterised by the excessive abundance of the $A\beta$ peptide that aggregates and forms extracellular amyloid plaques [19],[76] and intracellular neurofibrillar tangles [217]. The amyloid-cascade hypothesis states that accumulation of $A\beta$ is the central step in the etiology of the disease [33],[218] whereupon soluble oligomeric $A\beta$ is suggested to be the harmful factor causing synaptic and cognitive deficits [36].

The amyloid precursor protein (APP) is crucially involved in the generation of the pathology of AD, as $A\beta$ is the proteolytic cleavage product of APP [35]. Current therapeutic strategies aim to decrease $A\beta$ production by targeting APP cleavage, for instance via BACE1 inhibition. This interference with levels of APP and its cleavage products demands understanding of the role of APP in the brain.

APP has been shown to be important for many brain functions [64]. So far, the role of APP has been mainly investigated in neurons. However, there is emerging evidence that complex brain functions derive from the interplay of neuronal and astrocytic activity [144]. Astrocytes play an active role in regulating brain networks by refining synapses, clearing the extracellular space and modulating trafficking of neuro- and gliotransmitters [153],[144].

Therefore, understanding the physiological function and subcellular action sites of APP in astrocytes is crucial for shedding light on basic physiological brain function and on AD related aspects.

3.1.1 Lack of APP does not result in altered NMDA/AMPA receptor currents

In vivo imaging of dendritic spines in the cortex of APP-KO animals revealed impaired neuronal plasticity that was manifested by reduced spine turnover and reduced thin spines. When neuronal plasticity was stimulated by placing the animals into enriched environment, WT animals displayed increased spine density while the spine density in APP-KO animals remained unchanged. These observations came along with decreased extracellular levels of the gliotransmitter D-serine which in turn could rescue the spine plasticity deficits when orally applied to the animals. Together, APP maintains spine plasticity via D-serine [96] and this raised the question whether NMDAR density is reduced in APP-KO animals, as D-serine potentiates as an endogenous co-agonist NMDAR [219]. As the presence of NMDAR is associated with spine stability and certain spine types [202], reduced NMDAR density might be a potential consequence of reduced extracellular D-serine levels and decreased thin spines. Moreover, APP has been shown to regulate NMDAR levels at the postsynapse [220],[92],[221].

To approximate the density of NMDAR, patch clamp recording of stimulated NMDAR and AMPAR currents were performed in neurons of cortical layer V. The ap-

proach revealed no difference in the NMDA/AMPA receptor current ratio between APP-KO and WT mice suggesting no changes in the receptor composition due to the lack of APP. Paired-pulse facilitation recordings additionally showed unaffected presynaptic transmission despite the lack of APP. These findings suggest that the effect on spine plasticity might derive from a different source or region.

APP has been shown to enhance synaptic activity, synapse formation, and dendritic spine formation [94]. In cell culture, enhanced NMDAR currents and NR2B-containing receptors on the postsynaptic membrane were linked to overexpression of APP [221] while APP 695 was associated with increased NMDAR subunits NR2A and NR2B to the surface [92]. In contrast, autaptic hippocampal neurons lacking APP display enhanced amplitudes of evoked AMPAR- and NMDAR-mediated EPSCs, increased mEPSC frequency and more vesicles in their readily release pool [95].

In the intact brain, APP AICD has been shown to regulate GluN2B levels that are associated with immature excitatory synapses [220]. Accordingly, it would not be surprising, if lack of APP results in reduced NMDAR on the cell surface and therefore reduced currents. The reduced NMDAR currents would result in a shift of NMDA/AMPA receptor ratio, assuming unchanged AMPAR density. However, changed protein levels of postsynaptic NMDAR in APP-KO have never been reported probably also because isolation of postsynapses from brains is challenging.

Additionally, APP-deficient mice show decreased glutamate levels and increased GABA levels, in addition to upregulated GluR2 subunit of AMPAR [206]. Both are hints that APP plays a role in excitatory synaptic transmission. The observed unchanged NMDA/AMPA ratio in the cortex of APP-KO animals from the present study does not exclude parallel changes of both NMDAR and AMPAR levels. However, basic synaptic transmission is reported to be not changed in APP-KO animals [64].

As the APP family members APLP1 and APLP2 are also associated with increased levels of NMDAR subunits on the cell surface [93], a compensatory mechanism could explain the unchanged NMDA/AMPA receptor ratio in the absence of APP.

As APPs α has been shown to facilitate NMDAR currents both *ex vivo* and *in vivo* in the hippocampus [203], lack of APP could also result in decreased NMDA currents, as its cleavage product APPs α cannot be generated from APLP1 and APLP2. Hence, the recorded NMDA/AMPA current ratio is independent of APPs α or other parameters compensate the lack of the neurotrophic factor APPs α .

Moreover, a difference in morphological distribution of dendritic spines was reported between WT and APP-KO (less thin, more mushroom spines in APP-KO) [96]. As morphology of spines is associated with plasticity and activity [202], a change of receptor density would not be surprising. Still, the investigated spines in the cortical layer I are not the synaptic input from the recorded NMDA/AMPA receptor currents, as the stimulation electrode was placed around layer III while positioning it in layer I would have been technically cumbersome and would be subject to the space clamp problem [222]. The space clamp problem means that controlled voltage at the soma with the voltage clamp only partially controls the membrane voltage distant from the

soma. Hence, one cannot exclude different postsynaptic constitution along the entire cortical layer V neurons.

The experiment describes no differences in the NMDA/AMPA receptor current ratio. Thus, the morphological changes in spine plasticity in the cortex of APP-KO animals cannot be related to alterations in the postsynaptic excitatory receptor composition. However, selective protein investigations of the postsynaptic membrane would further elucidate, if there is an alteration in the receptor density or if the spine plasticity alterations might derive from a different synaptic component such as astrocytes.

3.1.2 Reduced LTP in APP-KO animals cannot be rescued by D-serine application

Long-term potentiation (LTP) is a long-lasting strengthening of synaptic transmission that is considered to be the underlying mechanism of learning and memory [131]. LTP depends on the presence of extracellular D-serine which is released in a Ca^{2+} dependent manner from astrocytes [159]. As APP-KO animals have been shown to display decreased extracellular D-serine levels [96] and reduced LTP in old animals [223],[224],[205],[101], a potential rescue of the reduced LTP was tested by D-serine application. Firstly, the reduction of LTP was shown in young adult mice. The acute and chronic application of D-serine, in the recording bath containing the brain slice and orally to the animal, failed to rescue the reduced LTP. This result clearly shows that D-serine alone is not capable to rescue the reduced LTP in APP-KO animals.

Previous studies show that bath application of D-serine rescues LTP in an astrocytic Ca^{2+} dependent manner [167],[159]. As mentioned, APP plays a fundamental role in the homeostasis of D-serine in the cortex thereby being important for spine plasticity [96]. As the simple application of D-serine to APP-KO animals and brain slices does not rescue the reduction of LTP in the hippocampus, the plasticity impairment in the hippocampus of APP-KO animals is supposedly more complex.

For instance, the presence of APP cleavage products could be important for hippocampal plasticity. Accordingly, the absence of the cleavage product APPs α could have an impact, as it has been shown to positively influence NMDAR current, LTP and spatial memory [203] and rescue abnormalities in behaviour and LTP of APP-KO mice [101]. APPs α promotes NMDAR level increase by increased recruitment of NMDAR to the postsynaptic site [100],[92]. Additionally, APPs α has been shown to facilitate NMDAR currents both *ex vivo* and *in vivo* in the hippocampus [203] which would not be detectable by I/O and paired-pulse recordings (solely AMPAR currents). Hence, the reduction in LTP might be caused by NMDAR impairment in the absence of APPs α . Moreover, physiological levels of A β were shown to potentiate LTP [98], while another cleavage product such as A η has opposite effects on hippocampal LTP [225]. Both peptides are also absent in APP-KO animals.

The reduction in LTP in young adult mice is not in line with previous studies in which decreased LTP was only described in old (13 months) but not in young APP-

3.1 The role of APP in synaptic plasticity in the cortex and hippocampus

KO animals [205],[223],[224],[101]. However, in these studies the LTP was elicited with a different (tetanic) stimulation protocol potentially explaining the differences in the experimental outcomes. Surprisingly, D-serine application on WT slices in the recording chamber resulted in a LTP that was not significantly different to LTP in APP-KO. A previous study reports no change of LTP after D-serine bath application to the WT [167] which could again derive from a different stimulation protocol. In the present study 1×1 s trains of 100 Hz stimulation was applied, while Shigetomi and colleagues [167] used 2×1 s trains of 100 Hz stimulation with intertrain interval of 10 s.

APP is suggested to be involved in glutamate synthesis, as APP-KO mice displayed a decreased pool size of glutamate, while the pool was increased by APP overexpression [206]. Decreased glutamate could explain the decreased LTP and also ineffectiveness of D-serine application. However, the I/O and paired pulse facilitation were not affected in APP-KO which excepts altered glutamate release in basic synaptic transmission. Notably, the I/O and paired-pulse facilitation at all tested intervals were also shown to be unchanged between aged APP-KO and WT [223],[224],[226] in accordance with the observations in this study in young adult mice. Hence, a basic synaptic transmission deficit can be excluded in the hippocampus of APP-KO and the defect is consequently plasticity related.

It is known that astrocytes are highly involved in synaptic plasticity. Especially, increased astrocyte-synapse interactions have been reported during LTP induced by theta-burst stimulation [150]. Thereby, astrocytes respond to increased neuronal activity by changing their morphology to promote astrocytic synapse coverage. This process requires glutamate release from the presynapse and receptors on the astrocytic membrane and intracellular elevations of Ca^{2+} in the astrocyte, respectively [150]. The reduction of LTP in the hippocampus of APP-KO brains might also result from an activity dependent imbalance of glutamate release and uptake within the tripartite synapse, also suggested for AD [227]. The imbalance of glutamate release would be confined to plasticity related activity, e.g. after tetanic stimulation, as the AMPAR-related stimulation/response (I/O) curve was not changed between WT and APP-KO. The unchanged I/O also implies no change in AMPAR density.

To sum up, reduced LTP was also observed in young adult APP-KO animals. Application of the gliotransmitter D-serine, which rescued spine plasticity deficits in the cortex of these animals, failed to rescue LTP in the hippocampus. The reason for that could be an array of possibilities including decreased NMDAR density, aberrant glutamate levels, and altered astrocytic involvement.

In a prospective study, *in vivo* investigations of spine plasticity via a hippocampal window and plasticity stimulation via hippocampus-related learning tasks would shed light on the role of APP in hippocampal structural plasticity. Moreover, examination of NMDA receptor density and D-serine levels in the APP-KO hippocampus would help to understand the cause of reduced LTP in APP-KO mice.

3.1.3 Astrocytic APP impacts spine density and morphology in the cortex and hippocampus

Dendritic spine plasticity and morphology are closely related to synaptic function. For instance, structural remodeling of dendrites is a learning dependent process [124]. Moreover, the stability of dendritic spines is important for accurate brain function and destabilisation is associated with psychiatric or neurodegenerative diseases [123].

In order to investigate the role of astrocytic APP on excitatory synapse density and composition in the cortex and hippocampus, a confocal *ex vivo* investigation of dendritic spine density and morphology after conditional knock-out of *APP* (cAPP-KO) in a subset of adjacent astrocytes was performed. Intriguingly, the changes in dendrite appearance differed among the distinct brain areas. cAPP-KO in cortical astrocytes did not change the total spine density in adjacent WT neurons. But, the number of thin spines was reduced that are considered to be more plastic and transient [202]. This is in line with the *in vivo* observation of constitutive APP-KO animals that lack APP in neurons and astrocytes [96]. Consequently, the less transient spine composition observed in the cortex might be due to lack of astrocytic APP, as it can be detected in both cAPP-KO in astrocytes and constitutive KO (neuronal and astrocytic)[96]. In contrast, increased spine density in the cortex of APP-KO was reported in an *in vivo* approach in which spines of any morphological type were increased in number [97].

In contrast to the cortex, selective cAPP-KO in the hippocampus of adult mice resulted in increased dendritic spine density. Both dendrites of the stratum oriens (basal) and stratum radiatum (apical) displayed increased number of mushroom spines. Noteworthy, mushroom spines are considered to be more stable postsynapses, important for learning [202].

In *in vitro* studies, loss of APP in neurons was shown to reduce spine density in cultured hippocampal neurons and *in vivo* in CA1 region of 13-months old but not in young animals [205]. In line with this, another study on cultured hippocampal neurons showed that overexpression of APP resulted in increased spine number, while knockdown of APP reduced spine density [206]. An additional study showed that hippocampal neurons from APP-KO mice *in vitro* display reduced viability and impaired neurite development [91]. Moreover, the astrocytic role of APP was investigated by co-culturing WT neurons with APP-KO astrocytes. The neurons co-cultured with APP-KO astrocytes displayed decreased branching and length than those co-cultured with WT astrocytes [91]. In order to relate these studies to the findings of this thesis, cAPP-KO in astrocytes of the intact brain might elicit a compensatory effect by which neurons increase spine density and change spine morphology. The cell culture experiments are not applicable to *in vivo* conditions because neurons were either isolately investigated or in terms of neuron-astrocyte coculture astrocytes which is entirely isolated from the physiological brain environment.

The cell-adhesion function of APP can connect synaptic components and thereby play an important role in the stability of synapses [228],[229]. This feature can explain

the spine-promoting effect in APP overexpressing neurons which depends on the E1 extracellular domain of APP [206]. It is reasonable to assume that reduced interaction of astrocytes with dendritic spines results from disrupted cell adhesion when APP is lacking in one interaction partner. Additionally, this might result in decreased glio-neuron communication and decreased potentiation of neuronal synapses, e.g. via gliotransmitters such as D-serine, to which the neurons react by forming more stable excitatory synapses that are observable by more mushroom spines in the hippocampus. In contrast, the neurons of the cortex respond differently, as they decrease the fraction of transient thin spines without change in overall spine number.

Investigations of the neuropil in the hippocampus have shown that thin spines are covered more by astrocytes than larger spines [154] and the spine morphology also determines NMDAR density and Ca^{2+} influx into the spine and the dendritic compartment [230]. Hence in the cortex, neurons have less thin spines because astrocytes might retract from the synapse affecting mostly thin spines. On the contrary, neurons from the hippocampus behave differently. Potentially, different expression levels of APP depending on the brain region and different compensatory mechanism respond to the lack of APP, respectively.

In the hippocampus, lack of astrocytic APP could lead to elevated neuronal activity by increasing and reshaping dendritic spines, in particular mushroom spines which, because of their large head surface, can generate stronger postsynaptic signals [125],[126]. This could be a compensatory mechanism as a response to loose proximity of astrocytic protrusions that usually supports synaptic function [144] when APP acts as an cell adhesion molecule [228],[229].

It remains elusive why lack of astrocytic APP results in distinct phenotypes in different brain regions. This discrepancy might be caused by different protein expression levels in distinct brain regions [231] and in different astrocyte populations [232],[233]. Thus, the impact of APP-KO absence and thus the role of APP might differ accordingly.

It has been shown that astrocytes express glutamate transporters at different levels in distinct brain areas during development and adulthood [234],[235]. Hence, these region-specific differences in protein expression in astrocytes might lead to diverse phenotypes in the absence of APP [236]. For instance, GFAP expression in astrocytes of the hippocampus and cortex is described as diverse. While almost all hippocampal astrocytes express GFAP, only astrocytes of the upper and lower layers of the cortex express GFAP [233]. Even within one brain area such as the hippocampus, a heterogeneity is suggested among GFAP positive astrocytes that might participate in or differently modulate glutamate synaptic transmission [237].

In the present approach, the expression of Cre recombinase was depending on GFAP promotor activation in astrocytes. The fluorescent protein expression confirms the presence of active Cre recombinase and thus potential KO of APP. A proof of KO is missing in the experimental design. However, it is very difficult to immunohistologically confirm KO of APP and particularly in the ramified processes of astrocytes in 50 μm thick brain slices. KO of APP in astrocytes resulted in changed density and

morphology of dendritic spines suggesting a crucial role of APP in astrocytes in CA1 of the hippocampus and even assign a function in terms of synaptic integrity.

A further experiment linking astrocytic APP to excitatory synapse integrity would be the treatment of astrocytic conditional KO animals with the gliotransmitter D-Serine [238] that has been shown to compensate the deficits in dendritic spine plasticity in the cortex of constitutive APP-KO mice [96]. Moreover, generation of a global conditional KO of astrocytic APP would allow approaches such as chronic spine imaging *in vivo* in the cortex and hippocampus, D-serine level measurements, astrocytic Ca^{2+} imaging, behaviour tests and LTP recordings in the acute slice. This would further elucidate the role of astrocytic APP in the adult brain.

3.1.4 Conclusion I

Without doubt, the function of APP at synapses and adjacent astrocytes is puzzling and quite likely not uniform across neurons, astrocytes and brain regions. While in the cortex of APP-KO animals the reduced spine plasticity could not be linked to altered levels of excitatory receptor composition (NMDA/AMPA), it could be rescued by application of the gliotransmitter D-serine. Hippocampal LTP is reduced in APP-KO animals but cannot be rescued by D-serine application suggesting additional mechanisms important for synaptic plasticity that lack in the hippocampus in the absence of APP.

Selective and conditional KO of APP in a subset of astrocytes within the cortex and hippocampus resulted in brain region specific alterations of dendritic spine morphology and density in the adjacent neuron. Decreased thin spines without effects on the spine number were observed in the cortex, while hippocampal dendrites displayed increased spine density due to increased fraction of mushroom spines. The brain region specific consequences of astrocytic APP-KO on dendritic spines might be attributed to different astrocytic subpopulations and thus, receptor composition.

These findings accentuate not only the role of astrocytes in synaptic plasticity and integrity but also clearly assign a crucial physiological function to APP for the tripartite synapse that differs across brain regions.

3.2 The role of APP in astrocytic function

Astrocytes are highly involved in synaptic plasticity [150] that is aberrant in the absence of APP. In particular, KO of APP affects structural plasticity in neurons linked to decreased levels of gliotransmitter D-serine [96]. Hence, the role of APP was further investigated in astrocytes.

To decipher the role of APP in astrocytic function, Ca^{2+} transients in astrocytes were investigated, as Ca^{2+} is implicated in a variety of cellular processes. For instance, intracellular Ca^{2+} promotes gliotransmitter release important for the modulation of neuronal function [238]. More specifically, interference with Ca^{2+} signals in astrocytes

has been shown to reduce D-serine release with consequences on synaptic plasticity such as LTP [167],[159].

As previous studies described alterations in Ca^{2+} signalling and homeostasis in astrocytes that lack APP [110],[112], the role of APP in terms of astrocytic Ca^{2+} activity was deeper investigated within the course of this study.

3.2.1 APP plays a role in perisynaptic Ca^{2+} signalling in astrocytes

To understand the role of APP in astrocytic function during basal activity in the brain, spontaneous intracellular Ca^{2+} transients were investigated in astrocytes of the hippocampus and cortex in acute brain slices of WT and APP-KO animals. More specifically, the Ca^{2+} transients in small astrocytic protrusions were assessed, as they form the contact sites to synapses participating in neuronal signalling.

Astrocytic expression of a membrane-tethered Ca^{2+} indicator [194] allowed to detect alterations of Ca^{2+} transients in the hippocampus and cortex of APP-KO animals. The analysis of spontaneous Ca^{2+} activity within the ramified processes of astrocytes involves an elaborate protocol that filters the background noise and detects active areas that display changes in fluorescence. These active areas are termed microdomains [239] and act as ROI for Ca^{2+} trace extraction from the raw image sequence.

In the cortex of APP-KO animals, the number and size of active microdomains was not changed indicating no alterations in the composition of active sites within the protrusions of APP-KO astrocytes during spontaneous activity. However, the frequency (evt/min/domain) of Ca^{2+} transients within the microdomains was significantly reduced in APP-KO. These findings suggest that the lack of APP does not result in a spatial restriction of active microdomains but rather locally confined decreased Ca^{2+} activity potentially resulting in insufficient synaptic support. The amplitude and area under the curve of the astrocytic Ca^{2+} events were not changed, indicating that the amount of Ca^{2+} within one event is not altered despite the lack of APP. Furthermore, the rise time of astrocytic Ca^{2+} transients is longer in APP-KO in comparison to WT denoting a latency in reaching the Ca^{2+} transient peak. This latency shows prolonged increase of intracellular Ca^{2+} that might be due to delayed release of Ca^{2+} from intracellular stores. In contrast, the transient decay time remained unaffected proposing no alterations in the clearance of Ca^{2+} from the cytosol.

In the hippocampus of APP-KO animals spontaneous astrocytic Ca^{2+} activity exhibits different features in comparison to the cortex. While the number of active microdomains was unaltered, APP-KO animals displayed increased size in their active microdomains in the astrocytes of the hippocampus. The frequency of Ca^{2+} events was also reduced in hippocampus of APP-KO mice. Hence, the active microdomains of APP-KO astrocytes are larger and less active. This result suggests a spatial expansion of Ca^{2+} signals within astrocytic protrusions with less frequent emergence. The amplitude, rise and decay time and the area under the curve of the Ca^{2+} events remained unchanged in APP-KO suggesting no differences in the release, uptake and

3. Discussion

amount of intracellular Ca^{2+} events.

It is important to understand the local function of astrocytic microdomains in order to evaluate the contribution of APP to the communication between astrocytes and neurons [144].

Astrocytes have been shown to display structural plasticity depending on neuronal activity [150]. Since APP acts as a cell-adhesion molecule [228],[229], the lack of APP might disrupt the close proximity of synapses and astrocytic protrusions, resulting in altered communication. Consequently, APP-KO astrocytes might not be able to be adequately sensitive to adjacent neuronal activity e.g. via transmitters in the extracellular space which might result in decreased Ca^{2+} signalling and gliotransmitter release.

Additionally, NMDAR and AMPAR on the surface of astrocytes modulate astrocytic currents [240],[241]. As APP cleavage products interfere with these receptors [64], the lack of APP and its cleavage products might also influence astrocytic Ca^{2+} transients via these glutamate receptors. The aforementioned heterogeneity of astrocytes across the brain and in brain regions [236] can also explain the differences in microdomain size and kinetics that were observed between cortex and hippocampal GFAP positive astrocytes. The heterogeneity in neocortical astrocytes is exemplified by layer-specific morphological, molecular and Ca^{2+} activity differences [242],[243].

Astrocytes are electrically coupled via gap junctions that are important for the propagations of Ca^{2+} signals. The major gap junction component in astrocytes is connexin 43 which has been shown to be downregulated *in vitro* when the intracellular domain of APP was missing [244] or elevated levels of connexin 43 were found in AD mouse models associated with increased amounts of $\text{A}\beta$ [245],[246]. Hence, APP might be crucial for physiological composition of gap junctions and thus adequate inter-astrocyte communication.

APP has been shown to be crucial for intracellular Ca^{2+} homeostasis in cultured astrocytes [110],[112] suggesting interactions of APP with the endoplasmic reticulum and mitochondria that are involved in intracellular Ca^{2+} homeostasis. Moreover, APP localises at these organelles where it fulfills different functions [106],[69],[247],[107].

In acute slices, astrocytes exhibit intrinsic signalling independently of neuronal activity [248]. In contrast, in the experiments of the present study neuronal activity was not blocked by any specific blockers. Hence, the neurons were spontaneously active within the brain network of the acute brain slice. Consequently, it cannot be concluded that the observed frequency alterations of astrocytic Ca^{2+} transient in APP-KO are purely due to intrinsic astrocytic activity or an interplay of spontaneous neuronal and astrocytic activity. However, no changes in basal neuronal network activity have been reported in APP-KO [64],[249]. Investigations in the stratum radiatum of the hippocampus in acute slice showed that astrocytic Ca^{2+} signals can derive in the absence of neuronal activity and extracellular Ca^{2+} implicating a crucial contribution of Ca^{2+} from intracellular stores to Ca^{2+} signalling [250]. Moreover, this study showed that increased amounts of $\text{A}\beta$ (100 nM) lead to increased Ca^{2+} event frequency [250]. However, these approaches were not conducted in the ramified processes but in the

main branches of astrocytes. But still, physiological levels of $A\beta$ might positively effect the reduced frequency in APP-KO animals, similar to physiological levels of $A\beta$ (picomolar range) positively impact reduced LTP in APP-KO hippocampus [98]. This could easily be tested by incubating the brain slice in $A\beta$ containing ACSF prior to astrocytic Ca^{2+} recordings.

The Ca^{2+} source within astrocytes differ depending on the localisation. Hence, it has been shown that KO of Ip3r2 in the ER results in lack of somatic Ca^{2+} signalling in astrocytes. In contrast, the Ca^{2+} signals within the fine processes of astrocytes were not abolished [251]. Generally, majority of Ca^{2+} transients have been shown to occur in astrocytic processes and not in the soma [251]. Within these processes mitochondria are crucially involved in the generation of local Ca^{2+} transients [211],[195],[252].

Another study showed that spontaneous and evoked astrocyte Ca^{2+} signalling in the mossy fiber terminals of the hippocampus is tightly regulated by glutamate and even more specifically by glutamate uptake via glutamate transporters (GLT-1 and GLAST) [253]. Moreover, mitochondrial positioning within astrocytic microdomains appeared to be close to glutamate transporters and related to neuronal activity [254]. This suggests to investigate the extracellular glutamate levels in APP-KO animals in order to understand whether APP is crucially influencing glutamate in any aspect.

It is clear that experimental manipulation of astrocytic Ca^{2+} is not a straightforward practice and can produce different results depending on approach and context [165]. As astrocytic Ca^{2+} imaging in the hippocampal slice has been proven to be a suitable tool, a future approach could be the investigation of astrocytic Ca^{2+} transients during the induction of LTP and afterwards. This could shed light on the role of APP on astrocytic function during synaptic plasticity. This can be related to glutamate release and/or uptake by the astrocytes, as the present study has proven that the LTP deficit is not rescuable by D-serine application.

The close proximity of astrocytes and neurons in APP-KO animals and animals with conditional astrocytic KO of APP could be investigated by a recently developed method allowing the measurement of neuron - astrocyte proximity via Förster resonance energy transfer (FRET) between astrocyte processes and presynaptic terminals [255]. This technique could be applied *in vivo* during behaviour and in the acute brain slice during LTP recordings and could answer the question whether APP-KO animals have a neuron-astrocyte proximity problem during plasticity that could be responsible for the deficit. One could further speculate whether this might be due to the cell-adhesion function. Even further, the reduced proximity could result in defective neuron-glia communication such as the reduced D-serine release/levels [96].

In a broader sense, a function in astrocytic Ca^{2+} signalling can be attributed to APP, as the frequency of astrocytic Ca^{2+} transients were reduced in both cortex and CA1 of the hippocampus. Interestingly, there are region-specific differences in astrocytic Ca^{2+} signalling as consequences of APP-KO between hippocampus and cortex: microdomain size enlarged in APP-KO hippocampus and rise time prolonged in APP-KO cortex. These differences across brain regions could result from a heterogeneity of astrocytes.

3.2.2 APP is crucial for mitochondrial network integrity

The Ca^{2+} transient along the fine processes of astrocytes are defined by mitochondria mediated ion homeostasis [195],[210]. As aberrations of Ca^{2+} transients in delicate protrusions of astrocytes were detected, the question was raised whether the absence of APP directly affects mitochondrial integrity. Indeed, fragmented mitochondria have been observed in primary APP-KO astrocyte cultures. Convincingly, this phenotype could be rescued to WT level by reintroduction of APP.

Mitochondria morphology is very divers and dynamic [256]. Mitochondrial fusion and fission events in astrocytes are getting imbalanced in the incidence of injury or pro-inflammatory stimuli in acute slices [257]. Here, it can be assumed that APP-KO astrocytes are in a constant state of inflammation, which could explain the fragmented mitochondrial morphology. In support of this hypothesis, APP-KO mice have been described to develop reactive gliosis [89].

Mutations in the C-terminus region of KPI-APPs caused decreased localisation of APP to mitochondria together with mitochondrial fragmentation and dysfunction in HeLa cells [115]. Thereby, KPI-APPs harbour a mitochondrial localisation signal that is important for localisation of APP to mitochondria and mitochondria function. Overexpression of WT APP and APP harbouring the Swedish mutation leads to mitochondrial fragmentation resulting from imbalanced fission/fusion which is suggested to drive mitochondrial and cellular dysfunction [109]. Based on the findings that either missing mitochondrial localisation [115] or overproduction of APP [109] or full APP-KO in astrocytes exhibit a fragmented phenotype of mitochondria, at this point the conclusion can be drawn that a physiological level of APP in the cell is important for mitochondrial integrity. This is in line with the findings of this study in which reintroduction of APP via expression by the EF1 α promoter resulted in a rescued mitochondrial morphology in APP-KO astrocytes.

AD has been linked to malfunction of mitochondria [258],[259], as structurally and functionally aberrant mitochondria have been found in AD [260],[114] and in neurons of animal models of AD [261],[262]. Even though these studies are confined to neurons, also mitochondria of astrocytes could be highly affected in AD which in turn influences local energy demands and Ca^{2+} buffering important for synaptic support.

Recent findings in AD research delineate mitochondria dysfunction which is closely associated with phosphatase and tensin homolog (PTEN)-induced kinase 1 (PINK1) signalling [263]. PINK1 was reported to be implicated in mitofusin ubiquitination important for mitophagy [264]. It has been shown that the modulation of AICD levels or γ -secretase activity affects PINK1-related control of mitophagy and mitochondrial dynamics [265]. Hence, APP-KO astrocytes might display altered mitophagy and mitochondrial dynamics due to missing interaction of PINK1 and AICD. Therefore, reintroduction of AICD alone would be a potential approach for targeting this question.

The fragmented mitochondria might be one reason why intracellular Ca^{2+} is aberrant in the protrusions of APP-KO astrocytes in the acute brain slice. Consequences are the altered release of transmitters such as D-serine [96],[238] and potentially also

glutamate [174].

A future experiment could be a morphological investigation of mitochondria in astrocytes within the intact brain by expressing mitochondrial marker [257]. This would further elucidate whether APP-KO leads to mitochondrial abnormalities within astrocytes that are actively participating in the cellular network, for instance during glutamate take up and appropriate localisation of mitochondria [254].

3.2.3 Mitochondrial Ca^{2+} imaging in primary astrocytes

The lack of APP results in alterations of astrocytic microdomain Ca^{2+} transients which depend on mitochondria function and localisation [195],[211]. As mitochondria of APP-KO astrocytes displayed a fragmented phenotype, the function in terms of Ca^{2+} uptake was further tested. Therefore, stimulated Ca^{2+} elevations within the mitochondria of cortical astrocytes were visualised by mito-GCAMP and triggered by bath applications of GPCR agonist ATP. The elevations in the mitochondrial Ca^{2+} levels originated from the influx of Ca^{2+} through the mitochondrial uniporter (MCU).

Primary APP-KO astrocytes displayed slower kinetics of mitochondrial Ca^{2+} signals but unchanged amplitude ($\Delta\text{F}/\text{F}$) when the entire mitochondrial Ca^{2+} signal was taken into account. Moreover, the lack of APP does not change the basic Ca^{2+} level in astrocytes, as no change was observed in the basal Ca^{2+} signal in mitochondria. These findings are in line with a study that describes unchanged basal Ca^{2+} levels in the cytosol of APP-KO astrocytes [112]. The observed prolonged kinetics might derive from insufficient clearing of Ca^{2+} from the intracellular space by mitochondria, but can also come from slower Ca^{2+} release from the ER. APP fragment C99 has been shown to be localised at the ER-mitochondria contact site [106]. Consequently, the lack of APP might impair the proximity of ER and mitochondria resulting in altered Ca^{2+} signalling.

The more detailed analysis of $\Delta\text{F}/\text{F}$ network/edge ratio revealed spatially dependent alterations in APP-KO Ca^{2+} amplitude as a consequence of either increased response of rod and puncta mitochondria or decreased network Ca^{2+} signal. These findings further confirm that mitochondrial morphology closely relates to appropriate Ca^{2+} signalling in which APP plays a crucial role.

Together with slower kinetics of mitochondrial Ca^{2+} signals, these findings in primary astrocyte cultures partially resemble the decreased astrocytic Ca^{2+} transient kinetics observed in microdomains in the cortical slice.

3.2.4 Mitochondrial proteins

Mitochondrial proteins in primary astrocyte culture

Mitochondrial fragmentation and altered stimulated Ca^{2+} response in primary astrocyte culture of APP-KO animals were observed prompting the question which mitochondrial mechanism is affected in the absence of APP. Hence, mitochondrial proteins

3. Discussion

associated with mitochondrial features related to energy production, Ca^{2+} uptake and fission/fusion were analysed from primary astrocyte culture lysates by western blot. The levels of the electron transport chain component cytochrome C were increased in APP-KO astrocytes. Elevated levels and release of cytochrome C are a sign of apoptosis [214]. However, one of the mitophagic markers TOM20 [266], which also serves as an mitochondrial housekeeping protein, is not reduced in the tissue culture lysates. Thus, mitochondria in APP-KO astrocytes are not reduced. The elevated cytochrome C levels probably come along with the mitochondrial dysfunction but without mitochondrial loss. Whether cytochrome C is actually released by mitochondria and apoptosis is initiated in APP-KO astrocytes would have to be examined in a prospective study.

The uptake of Ca^{2+} from the cytosol is performed by the mitochondrial Ca^{2+} uniporter (MCU) [267]. As stimulated mitochondrial Ca^{2+} responses were altered in APP-KO astrocytes, the levels of MCU were examined in astrocyte lysates. No significant alteration was observed. As the stimulated response amplitudes in mitochondrial Ca^{2+} signalling differed within areas of one cell (edge/network ratio) and did not reveal any significant change when the entire mitochondrial Ca^{2+} signal was taken into account, a whole cell western blot approach might not be sensitive enough to detect potential local differences in protein concentrations. For instance, it could be possible that fragmented mitochondria differ in protein composition and therefore function in comparison to mitochondria of the network type.

The ratio of phosphorylated DRP1 (pDRP1) and DRP1 is a common mechanism to evaluate fission events in mitochondria [268],[269]. Mitochondrial fusion and fission events are getting imbalanced in the incidence of injury or pro-inflammatory stimuli in acute slices. Thereby, an increased mitochondrial fission and increase in the activated (phosphorylated) form of Drp1 were detected [257]. APP-KO astrocytes did not exhibit any change in the pDRP1/DRP1 ratio indicating no involvement of DRP1 in the observed mitochondrial fragmentation in APP-KO astrocytes. However, altered DRP1 levels have been reported in the context of AD [270],[271],[114] and APP [109]. DRP1 has been shown to be reduced when AICD is overexpressed in SH-SY5Y cells [265]. The protein Mitofusin-2 was also decreased in this study. The decrease in these proteins was associated with decreased levels of mitochondrial housekeeping proteins TOM20 and TIM23 suggesting reduced protein levels as a consequence of mitochondria loss.

Mitofusin 1 and mitofusin 2 are implicated in mitochondrial fission and fusion and also allocated to ER via MAM [272]. It has been shown that decreased levels of Mitofusin-2 promote ER-mitochondria contact sites followed by increased Ca^{2+} transfer from ER to mitochondria and decreases intra- and extracellular levels of $\text{A}\beta$ [273]. APP and BACE1 expression were not altered as a consequence to knock-down of mitofusin-2. However, γ -secretase complex function was impaired suggesting ER-mitochondria contacts as regulatory unit for APP processing and $\text{A}\beta$ generation. Maybe within this interplay, the presence of APP might be important for mitofusin levels. Hence, it would be of interest to check the levels of mitofusin-1 and -2 in

APP-KO astrocytes.

Generally, further investigations of mitochondrial function such as mitochondrial membrane potential [110], ATP production, cytochrome C release, measurements of mitochondrial membrane potential and of other electron transport chain proteins (e.g. OXPHOS) will shed light on the mechanisms in which APP plays a crucial role.

Notably, cultured astrocytes are uncoupled from the complex cellular interaction within the brain. Hence, examination of astrocytes interacting with neurons and other cell types in the intact brain would be of great value for unravelling the role of astrocytes and their proteins.

Isolation and protein investigation of astrocytes derived from the adult mouse brain

Primary astrocyte cultures mature by time and get purified by passaging from culture dish to culture dish. Findings from cell cultures cannot be related to the whole brain condition, as important signalling among different cell types is missing. Therefore, astrocytes were isolated from the adult brain in order to assess the changes in protein concentration due to the lack of APP. The elaborate protocol succeeded and the astrocytes isolated from the adult brain were maintained in a culture dish or lysed for western blot analysis. However, it is a work-intensive procedure that requires a lot of biological material resulting in very small yield.

Although the yield of this approach is quite small, the value is of great importance, as it allows selective analysis of astrocytes matured in the brain. Hence, experiments should be adjusted to the little amount of astrocytes in culture and small protein concentration in the lysate. A western blot machine for small protein concentrations and little volume (e.g. proteinsimple Wes) would be an option. Additionally, the protein content of astrocytes isolated from the adult brain could be analysed with proteomic analysis such as mass spectrometry which does not require large amounts of protein and potentially reveals additional proteins that are related to APP. Mitochondria of adult astrocytes could also be further isolated and functionally or molecularly analysed. Furthermore, astrocytes isolated from the adult brain could be plated on coated glass coverslips and employed for mitochondrial morphology investigations testing comparability to primary astrocyte culture. Moreover, this experiment would be closer to *in vivo* or slice conditions, as the astrocytes matured in an intact tissue environment.

Surprisingly, a study has shown that APP is predominantly expressed by pyramidal neurons but not in GFAP-positive astroglial cells in the adult mouse hippocampus [274]. In the aforementioned study, the presence of APP was investigated by immunofluorescence and *in situ* hybridisation. Here, expression of APP in hippocampal astrocytes was confirmed by western blot analysis of astrocytes derived from the adult hippocampus. Additionally, as dendritic spine alterations could be observed after GFAP promoter dependent cAPPKO in the hippocampus, the presence of APP in GFAP-positive astrocytes can be assumed.

Isolation of astrocytes from the adult brain is a reliable but work-intensive tool for

culturing adult astrocytes that matured in the brain and for protein analysis. But, the method requires large amounts of biological tissue in relation to very small yield. A further step in selective isolation of biological material from the intact brain could be the isolation of astrocytic mitochondria from the adult APP-KO brain. Subsequently, proteomic and EM analysis could provide information about the function of APP in mitochondria *in vivo*. These investigations could more closely link the observed microdomain size and Ca^{2+} transients to a mitochondrial phenotype.

3.2.5 Conclusion II

This study describes a plasticity deficit in APP-KO animals within the cortex and hippocampus that is associated with malfunction of astrocytes as part of the tripartite synapse. The task of astrocytes within this interplay are among others release of D-serine for potentiation of the NMDAR at the postsynapse in order to strengthen the signal. Moreover, astrocytes are highly involved in clearance and release of glutamate. Both D-serine and glutamate have been shown to be regulated by elevations in intracellular Ca^{2+} within astrocytic microdomains. Even further, it has been shown that neuronal activity and glutamate localisation and level are associated with the localisation and mobility of mitochondria in astrocytic protrusions [254]. APP-KO astrocytes might be in an inflammatory state [89] that involves mitochondrial fragmentation in astrocytes [257] and consequently directly affects gliotransmission involving D-serine release [96] and glutamate uptake [254]. Thereby, neurons display altered functional and structural plasticity which differs among cortex and hippocampus. The differences in neuronal plasticity across brain regions might derive from involvement of astrocytes of different populations across brain regions.

Within the APP-KO astrocyte perisynaptic Ca^{2+} transient changes might be linked to the disturbed mitochondria integrity manifested by mitochondrial fragmentation and disturbed Ca^{2+} signalling. Physiological levels of APP are important for mitochondrial morphology [115] and localisation [69], high abundance of APP cleavage products such as C99 are associated with mitochondria-ER contact sites [106], $\text{A}\beta$ is localised in mitochondria [70] and can inhibit mitofusin levels [275], and full-length APP can localise in TOM40 interfering with protein import into mitochondria [107]. Hence, APP and its cleavage products can interfere at several action sites in mitochondria e.g. fission and fusion proteins, ER-mitochondria proximity, protein import into mitochondria that influence Ca^{2+} homeostasis (Figure 3.1). It remains elusive to which extend physiological levels of APP and its cleavage products contribute to appropriate mitochondrial function.

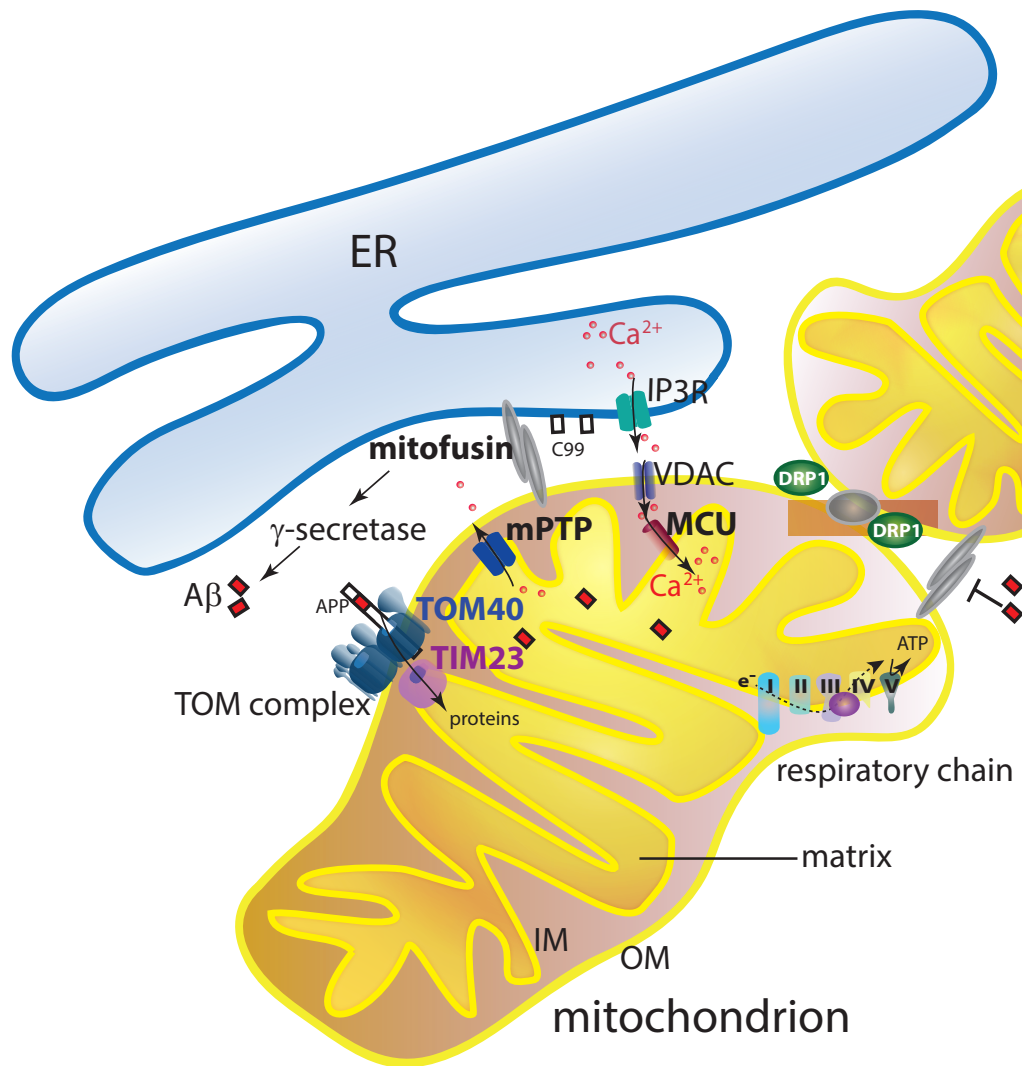


Figure 3.1. Potential interaction sites of APP with the ER and mitochondria that affect Ca²⁺ homeostasis. APP and its cleavage products have been shown to effect ER and mitochondria function which are potential explanations why Ca²⁺ homeostasis is altered and mitochondria are fragmented in APP-KO astrocytes. Thereby, potential sites of actions are the ER-mitochondria contact sites involving mitofusin. Close proximity of ER and mitochondria is important for appropriate Ca²⁺ signalling. Secondly, levels of mitochondrial fission and fusion proteins DRP1 and mitofusin were shown to be affected by the lack of APP and have been shown to be aberrant in AD. Furthermore, full-length APP can control import of mitochondrial proteins through the TOM complex which might also affect the protein composition within the mitochondria. Aβ can localise in the mitochondrial lumen where it can cause mitochondrial dysfunction.

3.3 Relevance of APP studies for understanding AD

The physiological role of APP for neuronal plasticity and associated astrocytic function is further investigated in the present thesis. As it has been shown that protease BACE is elevated in AD patients and full-length APP and neurotrophic APPs α are reduced in brains of AD patients [276], it is reasonable to assume that reduction of full-length APP and the imbalance of its cleavage products might be an additional causative factor for the disease besides the accumulation of A β . The memory deficits in AD patients correlate best with synapse loss and not with A β plaque burden or neurofibrillary tangles [23]. Hence, it is crucial to understand the physiological role of APP on synapses including astrocytic contribution for the development of therapeutic strategies. For instance, BACE1 inhibitors reduce the level of A β but also implicate a change in increased levels of full-length APP and other APP cleavage products.

Astrocytes should also be clearly considered in therapeutic approaches for the treatment of AD, as APP plays a crucial role in astrocytic Ca²⁺ signalling which is essential for associated neuronal function.

Regarding the features and physiological consequences of astrocyte-neuron signalling, important questions remain, as molecular and cellular events and consequences on whole brain function and further on animal behaviour are not fully understood. Moreover, the implication of astrocyte-neuron signalling integrity in any brain pathology requires further research [144]. This study provides further steps on the way to comprehend the physiological role of APP at the tripartite synapse which is crucial for brain network function. In addition to that, the findings highlight critical aspects of APP function which need to be considered for AD therapy.

Chapter 4

Materials and Methods

4.1 Genetically modified mouselines, genotyping and husbandry

4.1.1 Mouse lines

The following genetically modified mouse lines were used:

APP-KO

Constitutive KO of the amyloid precursor protein: APP-KO [198],[101], [277].
App^{tm2Cwe}; MGI:2154535

APP flox

Conditional null allele for APP: APP fl [207]
App^{tm3.1Umu}; MGI:4822174

GFP-M

Labelled subset of principal neurons in hippocampus and cortex: GFP-M [208]
Tg(Thy1-EGFP)# Jrs; MGI:4941461

Wild type

Control animals were either WT littermates or C57BL/6J from Jackson Laboratory.

4.1.2 Genotyping

The genomic DNA of the mice was isolated from ear or tail biopsies by the pegGold Tissue DNA Mini Kit (Peglab) in 96-well plates. The tissue was incubated in 400 μ l lysis buffer containing proteinase K and RNase at 50°C over night. Subsequently, a supernatant was generated by centrifugation (1 min, 10000 rpm, Eppendorf Centrifuge 5804) which was mixed with 400 μ l DNA binding buffer. Next, the solution was loaded onto DNA binding columns (PerfectBind) and centrifuged (1 min, 10000 rpm). The DNA bound to the columns was washed twice (washing buffer followed by 1 min centrifugation 10000 rpm) and eluted (200 μ l elution buffer, 3 min incubation, and 1 min centrifugation 6000 rpm). Subsequently, the isolated DNA was amplified by polymerase chain reaction (PCR, Thermocycler Eppendorf) by using specific primer and PCR protocols for mouse line genotyping (see below). Following, the genotype of the mice was defined by the electrophoresis of the DNA bands on an agarose gel which depends on the size of the amplified DNA fragment.

APP-KO

Fragments: ca. 650-700bp (WT) und ca. 430 (KO)

Primer:

Name	Sequence 5' → 3'	T _m (°C)
1	CGA GAT CAG CAG CCT CTG TTC CAC A	57,4
2	ATC ACC TGG TTC TAA TCA GAG GCC C	59,2
3	GAG ACG AGG ACG CTC AGT CCT AGG G	56

PCR sample:

Volume (µl)	Product	Concentration
12.5	OneTaq HotStart QuickLoad, NEB (x2 MM)	
0.5	Primer 1	10 µM
0.5	Primer 2	10 µM
0.5	Primer 3	10 µM
1	Template DNA	
10	H ₂ O	

PCR programme:

Step	Temperature (°C)	Time (s)	Repeats
Denaturation	94	180	1 ×
Denaturation	94	30	27 ×
Hybridisation	60	60	
Elongation	68	50	
Elongation	68	300	1 ×
	10	unlimited	

4. Materials and Methods

APP flox

Fragments: 342bp (WT) und 388bp (APPflox)

Primer:		
Name	Sequence 5' → 3'	Tm (°C)
1	TGC ATG TCA GTC TAA TGG AGG C	58
2	ATC TGC CCT TAT CCA GTG AAA TGA ACC C	60

PCR sample:		
Volume (µl)	Product	Concentration
12.5	OneTaq HotStart QuickLoad, NEB (x2 MM)	
0.5	Primer 1	10 µM
0.5	Primer 2	10 µM
0.5	Template DNA	
11	H ₂ O	

PCR programme:			
Step	Temperature (°C)	Time (s)	Repeats
Denaturation	94	180	1 ×
Denaturation	94	30	27 ×
Hybridisation	59	60	
Elongation	68	30	
Elongation	68	120	1 ×
	10	unlimited	

4.1 Genetically modified mousetines, genotyping and husbandry

eGFP-M

Fragments: Transgene 173 bp

Primer:		
Name	Sequence 5' → 3'	Tm (°C)
1	AAG TTC ATC TGC ACC ACC G	56,7
2	TCC TTG AAG AAG ATG GTG CG	57,3

PCR sample:			
Volume (µl)	Product		Concentration
12.5	OneTaq HotStart QuickLoad, NEB (x2 MM)		
0.5	Primer 1		10 µM
0.5	Primer 2		10 µM
1	Template DNA		
10.5	H ₂ O		

PCR programme:			
Step	Temperature (°C)	Time (s)	Repeats
Denaturation	94	180	1 ×
Denaturation	94	30	27 ×
Hybridisation	60	60	
Elongation	68	20	
Elongation	68	120	1 ×
	10	unlimited	

4.1.3 Husbandry

All animals were bred in the animal housing facility of the Center for Neuropathology and Prion Research and the Center for Stroke and Dementia of the Ludwig Maximilian University Munich. Mice were group-housed with up to six individuals in standard cages (30 × 15 × 20 cm), with standard bedding and additional nesting material under pathogen-free conditions, with food and water provided ad libitum. Mice were kept under a 12/12-hr light/dark cycle. At the age of 2 months, virus injections were performed.

4.2 Genetic modifications via viruses and plasmids

4.2.1 Viruses

Conditionally inducible Cre recombinase expressed under the GFAP promoter

AAV GFAPCreERT2 Penn Vector, Philadelphia, PA, USA.
GFAPCreERT2 virus (AAV5Penn Vector)

Conditional reporter fluorophore

AAV Brainbow Penn Vector, Philadelphia, PA, USA.
AAV9.hEF1a.lox.mCherry.lox.mTFP1.lox.WPRE.hGH-InvCheTF (Harvard)

4.2.2 Plasmids

Primary astrocytic cultures were transfected with plasmids for reintroduction of APP and for astrocytic specific expression of a Ca²⁺ indicator in mitochondria.

APP-GFP plasmid

The plasmid was kindly provided by Prof. Dr. Stefan Lichtenthaler.
Full name of the plasmid: p12/HA-APP-GFP.
APP CT is fused to GFP and NT fused to HA tag enabling CT (GFP) and NT (HA) detection of the protein. The expression is controlled by the EF1 α promoter. The plasmid consists of 9871 bp.

Astrocytic-specific expression of mitochondrial-targeted GCaMP6

The astrocytic mitochondrial Ca²⁺ indicator GCaMP6 (mitoGCaMP6) was kindly provided by Prof. Shinghua Ding, PhD [278].

Full Name of the plasmid: pZac2.1-ABC1D-mito-GCaMP6s.

The plasmid was amplified by bacterial inoculation followed by DNA extraction using a Qiagen Midiprep kit. Plasmid information: Mitochondrial matrix (MM)-targeting sequence (mito-) ATGT CCGTCCTGAC GCCGCTGCTG CTGCGGGGCT TGACAGGCTC GGCCCGGCGG CTCCCAGTGC CGCGCGCCAA GATCCATTCG TTG [279].

Sequencing Primer:

Seq-ABC1D F: TCTAGCCCCTCCTTCATAAAG;

Seq-ABC1D R: ATTTACACAAATAAAGCATTTTTT

The plasmid consist of 5630 bp.

4.3 Stereotactic virus injection

Surgery tools (Fine Science Tools, FST) were sterilised (Hot Bead Sterilizer, FST) before start of the injection. Mice were anaesthetised before undergoing surgery by intraperitoneal injection of ketamine/xylazine (120 and 10 $\mu\text{g/g}$ body weight, respectively; WDT/Bayer HealthCare). The depth of the anaesthesia was checked by pinch-withdrawl reflex on the hind limb of the mouse. Additionally, the anti-inflammatory drug Rimadyl (7.5 $\mu\text{g/g}$; Pfizer) and the antibiotic Baytril (7 $\mu\text{g/g}$ body weight, Bayer HealthCare) were subcutaneously administered. During the surgery the body temperature of the mouse was kept at 37°C, as the mouse was lying on a heating pad (FST). The eyes of the mouse were prevented from drying by application of Bepanthen eye ointment (Bayer). The head of the mouse was fixed between two ear bars of a stereotactic injection setup. The head of the mouse was orientated planar for stereotactic injection and cleaned with 70 % ethanol. The surgery was conducted through binoculars with a cold light source. The skin over the skull was longitudinally cut with a scalpel in order to expose the skull over the cortex. The skull and edges of the skin were cleaned with a scalpel, forceps and cotton sticks by removing loose hair, blood and connecting tissue. A hole was drilled in the skull on top of the right somatosensory cortex, 2 mm posterior and 2 mm lateral of bregma. The injection glass capillary (pulled with vertical puller, Narishige) mounted on the stereotactic device was loaded with the virus, respectively. The capillary was inserted into the brain for virus injections at three different injection depths from the brain surface: 1) 2 mm hippocampus dentate gyrus, 2) 1.4 mm hippocampus CA1 and 3) 0.3 mm cortex. In each injection site 300 nl virus was released with a speed of 30 nl/min. After each injection, the capillary was kept for 1 min at the injection site before moving to the next one. After virus application, the hole in the skull was closed with bone wax and the skin sewed with sutures. The animals were transferred into a 37°C incubator or onto a heating pad to allow waking up under warm conditions. The recovery of the animal was checked daily and the brain was harvested after several months depending on the experiment.

4.3.1 Investigation of the role of APP in astrocytic Ca²⁺ transients

For perisynaptic astrocytic Ca²⁺ imaging the AAV2/5_ GfaABC1D_ Lck-GCaMP6f virus (# 52924, Penn Vector, Philadelphia, PA, USA) with a strong membrane targeting dual acylation motif from Lck protein tyrosine kinase, in a of 10% virus (titer 10¹² vg/ml, 45% PBS (1x) and 11.25 % mannitol solution, for a final volume of 300 nl/injection site was injected into the hippocampus and cortex of APP-KO and WT animals. Due to the low expression of the virus, the expression duration was defined to 4-5 months before astrocytic Ca²⁺ imaging of acute brain slices was commenced with a two-photon microscope.

4.3.2 Investigation of the role of APP in dendritic spine density and morphology

For conditional KO of APP in a subset of astrocytes and simultaneous labelling of those, Cre recombinase and a conditional reporter fluorophore were introduced in a subset of astrocytes: GFAPCreERT2 AAV & Brainbow AAV (2 × 10% virus (titer 10¹² vg/ml, 45% PBS (1 ×) and 35% of 8.75% mannitol solution were injected in the hippocampus and cortex of *APP^{fl/fl}* × GFP-M and *APP^{+/+}* × GFP-M mice. The virus was expressed for 10 weeks followed by one week of tamoxifen application (intraperitoneal injection of tamoxifen (Sigma) in miglyol (Caesar & Lorentz) 20 mg/ml; 40 mg/kg bodyweight) and another 10 weeks of the Cre recombinase (CreERT2, tamoxifen inducible) activity and fluorophore expression. Finally, the animals were perfused and the brain harvested for immunohistochemical investigations and confocal microscopy.

4.4 Electrophysiology in acute brain slices

4.4.1 Patch clamp recordings

Acute brain slice preparation for patch clamp recordings

Animals were deeply anaesthetised by 5% isoflurane inhalation. The depth of the anaesthesia was checked by the pinch-withdrawl reflex of the hind limb. The animals were quickly decapitated and the head was immediately placed into ice-cold cutting solution (in mM: 75 sucrose, 85 NaCl, 2.5 KCl, 1.25 NaH₂PO₄, 25 NaHCO₃, 25 D-glucose, 4 MgCl₂, 0.5 CaCl₂; pH = 7.4) which contained ice crystals and was bubbled with carbogen (95% O₂, 5% CO₂) for >20 min. The brain was quickly and carefully dissected and placed in fresh cutting solution. Subsequently, the brain was trimmed by disconnecting the cerebellum and forebrain. In order to obtain coronal sections, the brain was glued on the cutting surface of the cerebellum. 300 μm thick slices were

prepared with the Leica VT1200S with integrated cooling chamber filled with ice cold cutting solution. The slices were taken with the numb end of a Pasteur pipette and transferred in a submerged holding chamber containing aCSF (in mM: 125 NaCl, 2.5 KCl, 1.25 NaH₂PO₄, 25 NaHCO₃, 25 D-glucose, 2 MgCl₂, 2 CaCl₂) that was warmed in a water bath at 34°C. Slices were kept at 34°C for 30 min followed by transfer of the holding chamber to RT where the temperature was slowly decreasing. After 1 h at RT the slices were employed for patch clamp recordings in aCSF.

Cortical NMDA/AMPA patch clamp recordings

Stimulated NMDA/AMPA recordings were performed in layer V cortical pyramidal cells of 3-months old mice of both sexes. For recordings, a glass microelectrode (3-5 MΩ, produced by P-97 Puller, Sutter Instruments) was filled 1/3 with intracellular solution (in mM: 140 CsCl, 5 Lidocaine N-ethyl bromide (QX-314, Sigma), 10 KCl, 5 NaCl, 0.01 EGTA, 10 HEPES, 2 MgATP; pH=7.4; Osmol/kg=300) and aCSF (in mM: 125 NaCl, 2.5 KCl, 1.25 NaH₂PO₄, 25 NaHCO₃, 25 glucose, 2 MgCl₂, 2 CaCl₂). Low MgCl₂ conditions (0.5 mM) were obtained to facilitate the release of the Mg²⁺ block in the NMDAR. Stimulation (bipolar electrode) steps at different holding potentials in mV: -90, -80, -70, -60, -50, -40, -30, -20, -10, 0, 10, 20, 30, 40, 50, 60, 70 served for the optimisation of the NMDAR response recording conditions. In the presence of Picrotoxin (Sigma, GABA_A receptor antagonist) 50 μM and low Mg²⁺ (0.5 mM) aCSF the AMPAR response was recorded at -90 mV holding potential. Subsequently, the cell was clamped at +40 mV for the additional NMDAR current present through the depolarisation of the membrane. The ratio of NMDA/AMPA current was calculated from the response at +40 mV. Thereby, the AMPAR response was considered at the timepoint of the peak at -90 mV and the NMDAR component 40 ms after the stimulus artifact. The resistance was checked before the measurements at -90 mV and after at +40 mV with a 10 mV test pulse, respectively.

4.4.2 LTP recordings

Acute brain slice preparation for local field potential recordings

Animals were deeply anaesthetised by 5% isoflurane inhalation. The depth of the anaesthesia was checked by pinching the mouse between the toes of the hind limb. The animals were quickly decapitated and the head was immediately placed into ice-cold cutting solution (in mM: 125 NaCl, 2.5 KCl, 1.25 NaH₂PO₄, 25 NaHCO₃, 25 D-glucose, 6 MgCl₂, 0.5 CaCl₂; pH = 7.4) was contained ice crystals and were bubbled with carbogen (95% O₂, 5% CO₂) for >20 min. The brain was quickly and carefully dissected and placed in fresh and bubbled cutting solution. Subsequently, the brain was trimmed by disconnecting the cerebellum and forebrain. In order to obtain coronal sections, the brain was glued on the cutting surface of the cerebellum. 350 μm thick slices were performed with the Leica VT1200S with integrated cooling chamber filled

4. Materials and Methods

with ice cold cutting solution. The slices were taken with the numb end of a Pasteur pipette and transferred in a submerged holding chamber containing aCSF (in mM: 125 NaCl, 2.5 KCl, 1.25 NaH₂PO₄, 25 NaHCO₃, 25 glucose, 2 MgCl₂, 2 CaCl₂) that was warmed in a water bath at 34°C. Slices were kept in at 34°C for 30 min followed by transfer of the holding chamber to RT where the temperature was slowly decreasing. After 1 h at RT the slices were employed for LTP recordings.

Hippocampal LTP recordings

Animals of 3-4 months of age of both sexes were used for acute slice preparation followed by LTP recordings. Experimental groups: WT and APP-KO, both either non-treated or treated with D-serine supplemented to the drinking water (0.55 mg/ml D-serine (Sigma) dissolved in drinking water for 4 weeks starting when animals were 3 months of age, preparing a fresh bottle every second day). In another experiment, 10 μ M D-serine was washed into the recording chamber containing the acute brain slice.

Prepared brain slices were transferred into a submerged recording chamber for recordings of field excitatory postsynaptic potentials (fEPSPs). Therefore, two platinum/iridium concentric electrodes (PI2CEA3, Life Science) were placed on the surface of the slice on the Schaffer-collaterals in the stratum radiatum of the CA1. For recording a glass microelectrode (1-3 M Ω , produced by P-97 Puller, Sutter Instruments) was filled 1/3 with aCSF and placed in the CA1 stratum radiatum between the two stimulation electrodes. The stimulation electrodes sent a single pulse in an alternating manner with 15 s inter-stimulation interval and 30 s from one side. This interval is necessary for preventing paired facilitation responses. After positioning the electrodes, the initial stimulation was mild and just enough to elicit a fEPSP of <0.5 mV for \sim 10 min. Following, the setting was used for input/output (I/O) curve generation. Therefore, the stimulator was set to a value that no fEPSP was detectable. This value differed among slices and electrode position (1.5 -3.5 mV). Then, the stimulation was raised in 0.5 mV steps until a fiber volley appeared. Afterwards, it was raised one more time for 0.5 mV. The fEPSPs of a range of 4.5 mV were employed for generating an I/O curve. Next, the stimulus was set to a value that generates half of the maximum response for paired pulse facilitation (PPF) experiments. The intervals between the two stimuli were 20, 30, 50, 75, 100 ms.

Subsequently, the LTP recordings were performed. Therefore, the stimulus intensity was individually adjusted for each experiment to produce fEPSPs, which are 30-40% of the maximal responses. Every 30 s a stimulus from each site was elicited alternating with each other, resulting in fEPSP every 15 sec. Once the response was stable and no longer raising, the baseline was recorded for 20 min. In order to induce LTP, 100 stimuli of high frequency stimulation (HFS) of 100 Hz was applied. Stimulated fEPSP recordings (with stimulation intervals as during baseline recordings) were continued for 60 min after HFS.

The field potentials were amplified 100 \times using an EXT-10C amplifier (National Instruments) and digitised with BNC-2090A (National Instruments). 1-4 LTP record-

ings were performed per animal from two setups. Data were analysed with WinLTP 2.10 programme. For the analysis of the LTP, fEPSP from one site were averaged over one minute, to obtain one data point per minute (2 stimuli per minute from one site). This enabled two independent LTP recordings from one slice.

4.5 Astrocytic Ca^{2+} imaging in acute brain slices

4.5.1 Two-photon Ca^{2+} imaging in astrocytic protrusions

The acute brain slices were prepared as for LTP recordings. For astrocytic Ca^{2+} imaging, the Ca^{2+} content of the aCSF in the imaging chamber was slightly increased (2.5 mM) in order to favour Ca^{2+} activity in the slice. For two-photon imaging of acute slices the incubated brain slices were transferred in a submerged chamber under a two-photon microscope (LaVision). Constant perfusion of aCSF saturated with carbogen ensured survival of the slice. The bath temperature was set to 32°C and the perfusion rate was 4 ml/min. Before image acquisition, the orientation in the slice and expression of the Ca^{2+} indicator was checked bright field microscopy. When an imaging region was chosen time-lapse image series of GCaMP6f fluorescence were acquired in the hippocampus or cortex. The fluorescence image series were obtained by LaVision Trim Scope with a Spectra-Physics femtosecond pulsed Ti:Sa laser (Mai Tai, DeepSee) tuned to 920 nm and W Plan-Apochromat 20×/1.0 DIC objective water immersion (Zeiss). The microscope was controlled by using LaVision Inspector software (LaVision BioTec GmbH, Bielefeld, DE) while the laser was regulated by the Mai Tai software. The image series were acquired at a rate of 2 Hz in a frame of $69 \times 69 \mu\text{m}$ with a resolution of 1024×1024 pixel. Every image series lasted for 300 sec. The laser power was kept below 20 mW.

4.5.2 Analysis of astrocytic Ca^{2+} transients

After image acquisition, the image series were further processed for analysis of the Ca^{2+} transients. The protocol used for astrocytic Ca^{2+} activity investigations was adapted from the protocol CaSCaDe (Ca^{2+} Signal Classification and Decoding) [195]. Thereby, the detection of microdomains and extraction of Ca^{2+} traces was performed with Fiji, while the trace analysis was semi-automatically done with MiniAnalysis Software (Synaptosoft Inc., Decatur, GA, USA). Firstly, x-y drift of the image series was corrected by using Igor 7 Pro software (WaveMetrics Inc., Lake Oswego, OR, USA), followed by cropping to $60 \times 60 \mu\text{m}$. The aligned and cropped image series was further processed with Fiji: The background noise was subtracted by performing 3D convolutions (average and Gaussian filters of size $25 \times 25 \times 25$ pixels (x,y,t)) on the image series. Subsequently, Gaussian filtering product was subtracted from the average image stacks resulting in a noise-filtered image stack ($I(x,y,t)$). In order to identify regions that exhibit frequent dynamic changes in fluorescence, the mean

4. Materials and Methods

intensity (AVG) and standard deviation (STD) of noise-filtered image series were performed resulting in a 2D (x-y) projection. From the sum intensity of $AVG + 3 \times STD$ a threshold value was generated that was used for binarising sum and STD projections (2D) of the image series. The sum of the two binarised (sum and STD) pictures was the mask for detected microdomains/ROIs, again Gaussian filtered (25) for core detection. Number and size of active microdomains was taken into account for analysis. The ROIs were finally applied on the raw image series for extraction of Ca^{2+} traces. Only active microdomains were taken into account. Spontaneous Ca^{2+} events were analysed and characterised with the MiniAnalysis 6.0.07 software (Synaptosoft, Inc., Decatur, GA, USA): Spontaneous events were manually marked, event amplitudes, area under the curve, rise and decay time and event frequency per ROI/min were determined.

4.6 *Ex vivo* analysis of dendritic spines

4.6.1 Perfusion

Mice were anaesthetised by intraperitoneal injection of ketamine/xylazine (120 and 10 $\mu\text{g/g}$ body weight, respectively; WDT/Bayer HealthCare) before undergoing perfusion. They were transcardially perfused with phosphate buffered saline ($1 \times \text{PBS}$) until blood was washed out (5 min) followed by 4% paraformaldehyde in 0.12 M PBS (15 min), pH: 7.4. The brain was dissected and post-fixed for 24 h at 4°C in the same fixative. The next day, the brain was placed in $1 \times \text{PBS} + 0.05\%$ sodium azide until slicing and immunohistochemistry.

4.6.2 Brain slicing

For staining with antibodies, the brain was coronally cut with a vibratome Leica VT 1000S (Leica Mikrosysteme Vertrieb GmbH, Wetzlar, Germany) from Bregma 1.4 - 2.2 with a thickness of 50 μm and transferred into 24-well plates containing $1 \times \text{PBS} + 0.05\%$ sodium azide. The immunohistochemical stainings were performed on free-floating sections in 24-well plates.

4.6.3 Immunohistochemical staining

Slices were permeabilised (2% Triton X-100 in $1 \times \text{PBS}$, Life Science, Darmstadt, DE) on the horizontal shaker overnight at 4°C. In order to prevent unspecific binding of the antibodies, the slices were blocked in blocking solution (10% normal goat serum in $1 \times \text{PBS}$, Thermo Fisher Scientific Messtechnik GmbH, Munich, DE) for 2 h at RT. Slices were incubated with primary antibodies (see list) in blocking solution (10% normal goat serum, 0,03% Triton-X, 0,05% sodium azide in $1 \times \text{PBS}$) overnight at 4°C. The next day, slices were washed $3 \times$ with $1 \times \text{PBS}$ for 10 min at RT and the secondary

antibody was applied for 2h at RT. After $3 \times$ washing with $1 \times$ PBS brain slices were mounted on polysine slides and embedded in Dako Fluorecent Mounting Medium (# S3023, Thermo Fisher Scientific Messtechnik GmbH, Munich, DE).

4.6.4 Confocal microscopy

Images of the dendrites and astrocytes were obtained in the cortex and hippocampus with the confocal microscope Zeiss LSM 780 with a Plan Apochromat $40\times$ / NA 1.4 Oil DIC objective with the pinhole set to 1 airy unit for high resolution image acquisition. First a region where an astrocyte expresses mCherry and thus lacks APP was chosen and imaged as a small overview (pixel: 512×512 ; zoom around 2.5 depending on astrocyte size; pixel dwell: $1.58 \mu\text{s}$; $1 \mu\text{m}$ z-resolution; example size of an overview picture: x: $84.85 \mu\text{m}$, y: $84.85 \mu\text{m}$, z: $31.00 \mu\text{m}$) for orientation of the dendrites. This picture served for choosing the dendrites for detailed acquisition: the zoom function was used for a more detailed image of the dendrite (pixel: x: 1024, y: 256; z= depending on dendrite orientation. $0.5 \mu\text{m}$ z-scaling; picture size: x: $59.93 \mu\text{m}$, y: $14.94 \mu\text{m}$; zoom: 3.5; pixel dwell: $1.58 \mu\text{s}$, 2x avg.; 8-bit; Channel 1: 488 nm, 1.5%; Channel 2: 561 nm, 2.0%). Overview tile scans for illustration on the expression pattern were obtained with a $20\times$ /NA 0.8Plan Apochromat Air objective and in the tile scan mode.

4.6.5 Dendritic spine counting and morphological investigation

Images were analysed with ZEN software as 3 dimensional image stacks and a built-in overlay (.ovl) mask in combination with the SpineMiner programme by Simon Ochs. All data was blindly and manually analysed. Firstly, the length of the dendrite surrounded by the mCherry expressing astrocyte was determined by drawing an Open Bezier along the part of the dendrite that was surrounded by red fluorescent signal. Next, the spines along the measured dendrite segment were counted and classified in the morphological spine classes stubby, thin and mushroom spine in z-stacks by manually scrolling through the images. In the somatosensory cortex basal dendrites were taken into account, as it was impossible to find enough dendrites passing through mCherry-positive astrocytes in layer I of the cortex. In the hippocampus basal and apical dendrites of the CA1 region were analysed.

4.7 Primary astrocyte culture

4.7.1 Preparation

Primary cortical astrocyte cultures were prepared on postnatal day 3 (P3) from APP-KO and WT animals. The brain was isolated and placed in HBSS (Gibco, cat.

4. Materials and Methods

24020091, Thermo Fisher Scientific) + HEPES (3.5 ml 1M in 500 ml HBSS) at RT. Meninges were removed and the cortex was dissected. Cortices from 3 animals were pooled, cut into pieces, washed with HBSS, and digested in 5 ml Trypsin containing 0.05% EDTA (Gibco; cat. 25300062, Thermo Fisher Scientific) at 37°C for 15 min. The reaction was stopped by adding 5 ml of medium (MEM (Gibco cat. 31095029, Thermo Fisher Scientific), 0.6% Glucose (Merck # 1083371000, CAS 50-99-7), 5% heat-inactivated FBS (PAN Biotech P40-37500)). After washing with HBSS, cells were mechanically dissociated by pipetting in culture medium to obtain a single-cell suspension and plated on a T-75 flask (Nunc EasY Flask cat. 156499, Thermo Fisher Scientific). The medium was changed the next day in order to remove unattached cells. Cultures were grown in an incubator with humid environment at 37°C and 5% CO₂ (Hereaus, HERAcell 150i). Astrocytic cultures were split at 90% confluency by transferring the cells equally in T-175 flasks (Nunc EasY Flask cat.159910, Thermo Fisher Scientific).

For transfection and immunofluorescence experiments astrocytes were plated on coverslips: During the second passaging procedure cells were plated on 15 mm glass coverslips (Marienfeld) in a 12-well plate (Nunc cat. 150628, Thermo Fisher Scientific) at a density of 70 000 cells per well. Before plating the cells, the coverslips were pretreated overnight (o/n) in nitric acid (Merck), washed 3 × with H₂O, and sterilised in an oven (Mettert UF30) for 8 h.

For cell lysis followed by protein investigation via western blot, astrocytes were kept in flasks.

4.7.2 Plasmid transfection

Astrocytes grown on coverslips for 72 h were washed once with 1 × PBS. Cells were transfected by incubating 1 µg plasmid encoding a mitochondria-targeted Ca²⁺ indicator GCaMP6 (mitoGCaMP6) or APP-GFP plasmid with 1.5 µl lipofectamine (lipofectamine 2000 reagent, Invitrogen) in OptiMEM (Gibco, cat. 51985026, Thermo Fisher Scientific) + 2.5% FBS over night in the incubator at 37°C and 5% CO₂. The medium was changed the following day.

Day 5 after transfection with APP-GFP plasmid, the cells were washed with 1 × PBS and fixed for 15 min with 4% PFA (Merck, 4% PFA (w/v) in 1 × PBS) at RT. After washing with 1 × PBS, cells were used for immunofluorescence stainings.

Day 2 after transfection with mitoGCaMP6, the stimulated mitochondrial Ca²⁺ response was investigated.

4.7.3 Investigation of mitochondrial morphology

Immunohistochemistry

Cover glasses were placed into a humid chamber, quenched for 10 min with 50 mM ammonium chloride, and extracted with 0.1% Triton-X 1 × PBS (Live Sciences) for 3

min at RT. In order to prevent unspecific binding, a 10% blocking solution (2% FCS, 2% BSA, 0.2% fish gelatin) diluted in $1 \times$ PBS was applied on the coverslips for 1 h at RT. The coverslips were incubated 1 hour at RT with the primary antibody diluted in 10% blocking solution / $1 \times$ PBS (for a complete primary antibodies list see table). After rinsing the coverslips $3 \times$ with $1 \times$ PBS we applied secondary antibodies diluted in 10% blocking solution / $1 \times$ PBS. The secondary antibody applied, raised in goat or donkey, were: Alexa 594, Alexa 488, and Alexa 647 diluted 1:500 in 10% blocking solution / $1 \times$ PBS.

Confocal microscopy

Mitochondria of cultured astrocytes were stained against TOM20 (see table for protocol) and embedded with Dako Fluorescent Mounting Medium (S3023) on polysine slides (Thermo Scientific, P4981). Confocal microscopy z-stack images were acquired (x and y depending on size of mitochondria, z: between 3-6 μm , 0.5 μm interval; Zeiss $40\times/1.4$, oil immersion) and 2D deconvolved (AutoQuantX3, Media Cybernetics). Projection on the z-axis was performed to obtain a single in-focus field projection. Mitochondria were selected by thresholding the pictures and classifying them using the software Fiji. Classification of mitochondria morphology in network (from 8.9 μm^2), rods (rods area: 2.7 - 8.8 μm^2) and puncta (0.1 - 2.7 μm^2) was based on the pixel coherence. A colour-coded image was generated to visualise mitochondrial morphology distribution in red puncta, in green rods and in blue the network. The eGFP signal of APP-GFP transfected cells was amplified by anti-GFP staining which allowed visual identification of APP transfected astrocytes and investigation of their mitochondria. For statistical analysis the morphological class is shown as fraction (%) of the total mitochondria area (TOM20) of an astrocyte, $n = 30$ astrocytes.

4.8 Mitochondrial Ca^{2+} signals in cultured astrocytes

4.8.1 Two-photon imaging of mitochondrial Ca^{2+} signals

Primary astrocytes on cover slips were transferred to the imaging setup in a Petri dish with $1\times$ PBS. The coverslip was divided with a scalpel in three parts in order to conduct more recordings from one coverslip and fit into the recording chamber. The recording chamber was under constant perfusion of aCSF (in mM: 125 NaCl, 2.5 KCl, 1.25 NaH_2PO_4 , 25 NaHCO_3 , 25 D-glucose, 2 MgCl_2 , 2 CaCl_2) pH = 7.4, constantly bubbled with carbogen (95% O_2 , 5% CO_2) and the temperature was set to 32°C. With transmission light the coverslip was screened for green fluorescently labelled mitochondria. Subsequently, the fluorescence image series were obtained by LaVision Trim Scope with a Spectra-Physics two-photon Ti:Sa laser (Mai Tai, DeepSee) tuned to 920 nm and W Plan-Apochromat $20\times/1.0$ DIC water immersion objective (Zeiss).

4. Materials and Methods

The microscope was controlled by using LaVision Inspector software (LaVision BioTec GmbH, Bielefeld, DE) while the laser was regulated by the Mai Tai software. A resonant scanner in unidirectional scanning mode was used. The laser was set to 1.5% laser power and 77 gain for the PMT (photon multiplier tube). The image series were acquired at a rate of 1 Hz in a frame of $69 \times 69 \mu\text{m}$ with 1024×1024 pixel resolution for 300 s. The settings were chosen in a way that fluorescent changes were detectable with moderate bleaching rate. For stimulating a mitochondrial Ca^{2+} signal, either $10 \mu\text{M}$ ATP (adenosine 5'-triphosphate di(tris) salt hydrate, Sigma) were applied in the perfusion system. When the substance reached the cells, they responded with an increase of fluorescence signal in the mitochondria. This takes place due to Ca^{2+} release into the cytosol and subsequent influx of Ca^{2+} into the mitochondria via the MCU (mitochondrial Ca^{2+} uniporter).

4.8.2 Data analysis of mitochondrial Ca^{2+} signals

The fluorescence signals were quantified by measuring the mean pixel intensities of the regions of interest (ROI) around the entire mitochondrial signal. The first minute before the rise of the fluorescent signal was employed as baseline. The drop of the curve of the first minute was corrected on the entire image series to subtract the bleach rate. Two exponential fits were applied on the decay of the signal. For fluorescence baseline signal comparison, the fluorescence signal of the mitochondria was subtracted by the baseline (two 55 pixel squared ROIs on the background). For analysis of the Ca^{2+} response of network and rod/puncta mitochondria, the amplitude ($\Delta F/F$) from a ROI close to the nucleus and close to the cell edge were taken into account.

4.9 Protein extraction and immunoblotting

Western blot

Westernblot analysis was performed with 2x passaged astrocyte cultures. 5 cultures prepared from 3 pups each were taken to obtain 5 biological replicates. After cells reached 90% confluency they were detached by trypsinisation and lysed with STET buffer (50 mM Tris (pH 7.5), 150 mM NaCl, 2 mM EDTA, 1% Triton-X-100,) containing 1:100 freshly added protease inhibitor (P8340, Sigma-Aldrich Chemie GmbH Munich, De) and 1:100 phosphatase inhibitor (# 5870 Cell signaling) for 30 min on ice. Protein concentration was determined with bicinchoninic acid (BCA) assay (Uptima Interchim) and samples were mixed 1 in 4 with $4 \times$ Laemmli buffer (8% SDS, 40% Glycerol, 0.025% Bromophenol blue, 10% β -mercaptoethanol, 125 mM Tris, pH 6.8). 10-15 μg protein was loaded on a gradient gel (M42015, Genscript ExpressPlus PAGE gel 4-20%) and SDS-PAGE was performed with Tris-MOPS-SDS Buffer (M00138, GenScript,). Proteins were transferred onto a PVDF membrane (IPVH 00010, Merck) in transfer buffer (25 mM Tris, 240 mM Glycin, 10% Methanol). The membrane was

blocked with 5% skim milk (Sigma-Aldrich Chemie GmbH Munich, De) in PBS-T (1x Phosphate buffered saline + 0.05% Tween) for at least 30 min at RT with horizontal rotation. After washing with PBS-T, the following antibodies were used for WB analysis: primary antibodies in PBS-T, 0.25% BSA and incubated o/n at 4°C APPY188 1:1000, TOM20 1:1000 (see antibody list), 1h at RT β -actin 1:10000 (A5316, clone AC-74, Sigma), 1 h at RT calnexin 1:10000 (ADI-SPA-860, Enzo); secondary antibodies were diluted in 0.25% BSA in PBS-T and incubated for 1h at RT anti-mouse-horseradish peroxidase (HRP) 1:10000 (Promega, Mannheim, De), anti-rabbit-HRP 1:10000 (Promega). Protein signals were developed with enhanced chemiluminescence (ECL) (ECL-substrate, RPN3243, GE Healthcare) and visualised using ImageQuant LAS4000 (GE Healthcare).

Membrane stripping

The membrane was placed in 1 M glycine in 1 × PBS and boiled 2 × for 10 min on a heating plate. Following, it was cooled down at RT on the horizontal shaker and washed 3 × for 15 min with PBS-T (0.1%) at RT.

4.10 Isolation of astrocytes from the adult mouse brain

The isolation of astrocytes derived from the adult mouse brain was performed by following the suggested protocol for the kit (Adult Brain Dissociation Kit and Anti-ACSA-2 MicroBead Kit) of Miltenyi Biotec, Gladbach, Germany. Samples were kept on ice or at 4°C and fastly processed. The cortex and hippocampus were quickly harvested and placed in a gentleMAC C tube, thereby, pooling two brains in one tube containing enzyme mix 1 then enzyme mix 2 was added. The gentle incubation and homogenisation was conducted by the gentleMACS Octo Dissociator with Heaters with the programme 37C_ ABDK_ 01. After ~30 min programme duration the sample was collected at the bottom of the tube by centrifugation 300 rpm for 10 min at 4°C. The resuspended sample was run through a cell strainer (70 μ m) in order to select for single cells and small cell debris. The cells were centrifuged for 10 min at 4°C and supernatant was discarded. Next, cell debris and red blood cells were removed according to the protocol with solutions provided in the kit. Following, cells were resuspended in a cold buffer containing 0.5% BSA, 0.08 mM EDTA in PBS before the sorting procedure that was subsequently performed. The cell number was determined in order to choose the appropriate volume for the binding of the magnetic beads. At that stage, the cell suspension contained about 1.3×10^7 cells of the cortex and about 6×10^6 cells of the hippocampus of which 40-70% were living. The cells were blocked by adding FcR Blocking reagent to the cell suspension. After 10 min incubation in the fridge, Anti-ACSA-2 MicroBeads were added and again incubated for 15 min in the fridge. Cells with bound MicroBeads were washed (adding buffer, centrifugation

4. Materials and Methods

and resuspension) and were ready for magnetic sorting in LS Columns. The columns were placed into the magnetic field of the quadro MACS Separator, rinsed with buffer and cell suspension was loaded. The flow-through contained the unlabelled cells. The column was $3 \times$ washed. Subsequently, the cells were collected by removing the column from the separator and putting buffer onto the column. Firm usage of the plunger helped to flush the cells in a collection tube. About 3×10^6 astrocytes from the cortex and 9×10^4 astrocytes from the hippocampus were collected, of which 40-80% were living. Isolated astrocytes were further used for cell culture in 6-well plate or western blot similar to the procedure of primary astrocytes.

4.11 Antibody list

Various antibodies were used for immunohistochemical (IHC) stainings or western blot (WB). For convenience all antibodies are listed here:

Antibody	IHC	WB	Company	#
APP CT Y188		1:10000	abcam	ab32136
APP NT		1:500	Lichtenthaler's lab	22c11
TOM20	1:200	1:1000	abcam	ab186735
antiGFP	1:500		life technologies	A21311
DRP1		1:1000	cell signaling	8570
pDRP1 S616		1:1000	cell signaling	3455
Ezrin	1:500		Sigma	E8897
mCherry	1:500		Biologend	clone 8c5.5
β actin		1:10000	Sigma	A5316
calnexin		1:10000	Enzo	ADI-SPA-860
GFAP	1:500	1:1000	abcam	53554
S100 β	1:500		DAKO	A21311
Cytochrome C		1:1000	abcam	90529

4.12 Statistics

For statistical evaluation of the data the programme GraphPad Prism 5.04 (GraphPad Software, Inc., La Jolla, CA USA) was used. Each data set was tested, if the values are normally distributed (Gaussian distribution). Therefore, the data was checked with the Shapiro-Wilk normality test. For normally distributed data, parametric tests were used (unpaired and paired two-tailed Students *t*-test and two-way ANOVA followed by Bonferroni post-hoc test), otherwise non-parametric tests were used (Mann Whitney test). For comparison of the frequency distribution, Kolmogorov-Smirnov test was applied. *P*-value > 0.05 was defined as statistically significant.

Bibliography

- [1] Alzheimer, A. über eine eigenartige Erkrankung der Hirnrinde. *Allg Zeitschr Psychiatr* 146–148 (1907).
- [2] Sütterlin, S., Hoßmann, I. & Klingholz, R. *Demenz-Report: wie sich die Regionen in Deutschland, Österreich und der Schweiz auf die Alterung der Gesellschaft vorbereiten können* (Berlin-Institut für Bevölkerung und Entwicklung, Berlin, 2011). OCLC: 778268128.
- [3] Abbott, A. Dementia: A problem for our age. <https://www.nature.com/emedien.ub.uni-muenchen.de/articles/475S2a> (2011).
- [4] World Alzheimer Report 2016 — Alzheimer’s Disease International. <https://www.alz.co.uk/research/world-report-2016>.
- [5] Weintraub, S., Wicklund, A. H. & Salmon, D. P. The Neuropsychological Profile of Alzheimer Disease. *Cold Spring Harb Perspect Med* **2** (2012).
- [6] Huang, Y. & Mucke, L. Alzheimer Mechanisms and Therapeutic Strategies. *Cell* **148**, 1204–1222 (2012).
- [7] Gómez-Isla, T. *et al.* Profound Loss of Layer II Entorhinal Cortex Neurons Occurs in Very Mild Alzheimer’s Disease. *J. Neurosci.* **16**, 4491–4500 (1996).
- [8] Frisoni, G. B., Fox, N. C., Jack, C. R., Scheltens, P. & Thompson, P. M. The clinical use of structural MRI in Alzheimer disease. *Nat Rev Neurol* **6**, 67–77 (2010).
- [9] Sperling, R. A. *et al.* Functional Alterations in Memory Networks in Early Alzheimer’s Disease. *Neuromol Med* **12**, 27–43 (2010).
- [10] Putcha, D. *et al.* Hippocampal hyperactivation associated with cortical thinning in Alzheimer’s disease signature regions in non-demented elderly adults. *J. Neurosci.* **31**, 17680–17688 (2011).
- [11] Amatniek, J. C. *et al.* Incidence and predictors of seizures in patients with Alzheimer’s disease. *Epilepsia* **47**, 867–872 (2006).
- [12] Dickerson, B. C. *et al.* Alzheimer-signature MRI biomarker predicts AD dementia in cognitively normal adults. *Neurology* **76**, 1395–1402 (2011).
- [13] Itagaki, S., McGeer, P. L., Akiyama, H., Zhu, S. & Selkoe, D. Relationship of microglia and astrocytes to amyloid deposits of Alzheimer disease. *Journal of Neuroimmunology* **24**, 173–182 (1989).
- [14] Beach T.G., Walker R. & McGeer E.G. Patterns of gliosis in alzheimer’s disease and aging cerebrum. *Glia* **2**, 420–436 (1989).

BIBLIOGRAPHY

- [15] Braak, H. & Braak, E. Neuropathological staging of Alzheimer-related changes. *Acta Neuropathol* **82**, 239–259 (1991).
- [16] Wischik, C. M. *et al.* Isolation of a fragment of tau derived from the core of the paired helical filament of Alzheimer disease. *Proc. Natl. Acad. Sci. U.S.A.* **85**, 4506–4510 (1988).
- [17] Drewes, G., Ebner, A. & Mandelkow, E.-M. MAPs, MARKs and microtubule dynamics. *Trends in Biochemical Sciences* **23**, 307–311 (1998).
- [18] Wang, Y. & Mandelkow, E. Tau in physiology and pathology. *Nature Reviews Neuroscience* **17**, 22–35 (2016).
- [19] Masters, C. L. *et al.* Amyloid plaque core protein in Alzheimer disease and Down syndrome. *Proc. Natl. Acad. Sci. U.S.A.* **82**, 4245–4249 (1985).
- [20] Nelson, P. T. *et al.* Correlation of Alzheimer Disease Neuropathologic Changes With Cognitive Status: A Review of the Literature. *J Neuropathol Exp Neurol* **71**, 362–381 (2012).
- [21] Palop, J. J., Chin, J. & Mucke, L. A network dysfunction perspective on neurodegenerative diseases. *Nature* **443**, 768 (2006).
- [22] Bezprozvanny, I. & Mattson, M. P. Neuronal calcium mishandling and the pathogenesis of Alzheimer’s disease. *Trends in Neurosciences* **31**, 454–463 (2008).
- [23] Terry Robert D. *et al.* Physical basis of cognitive alterations in alzheimer’s disease: Synapse loss is the major correlate of cognitive impairment. *Annals of Neurology* **30**, 572–580 (2004).
- [24] Ferri, C. P. *et al.* Global prevalence of dementia: A Delphi consensus study. *The Lancet* **366**, 2112–2117 (2005).
- [25] Bertram, L., Lill, C. M. & Tanzi, R. E. The Genetics of Alzheimer Disease: Back to the Future. *Neuron* **68**, 270–281 (2010).
- [26] Ulrich, J. D., Ulland, T. K., Colonna, M. & Holtzman, D. M. Elucidating the Role of TREM2 in Alzheimer’s Disease. *Neuron* **94**, 237–248 (2017).
- [27] Rovelet-Lecrux, A. *et al.* APP locus duplication causes autosomal dominant early-onset Alzheimer disease with cerebral amyloid angiopathy. *Nature Genetics* **38**, 24 (2006).
- [28] Mann, D. M. A. & Esiri, M. M. The pattern of acquisition of plaques and tangles in the brains of patients under 50 years of age with Down’s syndrome. *Journal of the Neurological Sciences* **89**, 169–179 (1989).
- [29] Lee, Y. *et al.* Systematic review of health behavioral risks and cognitive health in older adults. *International Psychogeriatrics* **22**, 174–187 (2010).
- [30] Savva, G. M., Stephan, B. C. M. & Alzheimer’s Society Vascular Dementia Systematic Review Group. Epidemiological studies of the effect of stroke on incident dementia: A systematic review. *Stroke* **41**, e41–46 (2010).
- [31] WHO — Dementia. <http://www.who.int/mediacentre/factsheets/fs362/en/>.
- [32] Timeline - APP and Amyloid-Related — ALZFORUM. <https://www.alzforum.org/therapeutics/timeline/app-and-amyloid-related>.
- [33] Hardy, J. & Allsop, D. Amyloid deposition as the central event in the aetiology of Alzheimer’s disease. *Trends in Pharmacological Sciences* **12**, 383–388 (1991).

-
- [34] Hardy, J. A. & Higgins, G. A. Alzheimer's disease: The amyloid cascade hypothesis. *Science* **256**, 184–185 (1992).
- [35] Beyreuther, K. & Masters, C. L. Amyloid Precursor Protein (APP) and beta A4 Amyloid in the Etiology of Alzheimer's Disease: Precursor-Product Relationships in the Derangement of Neuronal Function. *Brain Pathology* **1**, 241–251 (1991).
- [36] Haass, C. & Selkoe, D. J. Soluble protein oligomers in neurodegeneration: Lessons from the Alzheimer's amyloid β -peptide. *Nature Reviews Molecular Cell Biology* **8**, 101–112 (2007).
- [37] Glenner, G. G. & Wong, C. W. Alzheimer's disease: Initial report of the purification and characterization of a novel cerebrovascular amyloid protein. *Biochemical and Biophysical Research Communications* **120**, 885–890 (1984).
- [38] Glenner, G. G. & Wong, C. W. Alzheimer's disease and Down's syndrome: Sharing of a unique cerebrovascular amyloid fibril protein. *Biochemical and Biophysical Research Communications* **122**, 1131–1135 (1984).
- [39] Wisniewski, K. E., Wisniewski, H. M. & Wen, G. Y. Occurrence of neuropathological changes and dementia of Alzheimer's disease in Down's syndrome. *Annals of Neurology* **17**, 278–282 (1985).
- [40] Goldgaber, D., Lerman, M. I., McBride, O. W., Saffiotti, U. & Gajdusek, D. C. Characterization and chromosomal localization of a cDNA encoding brain amyloid of Alzheimer's disease. *Science* **235**, 877–880 (1987).
- [41] Kang, J. *et al.* The precursor of Alzheimer's disease amyloid A4 protein resembles a cell-surface receptor. *Nature* **325**, 733–736 (1987).
- [42] Goate, A. *et al.* Segregation of a missense mutation in the amyloid precursor protein gene with familial Alzheimer's disease. *Nature* **349**, 704–706 (1991).
- [43] Strooper, B. D., Iwatsubo, T. & Wolfe, M. S. Presenilins and γ -Secretase: Structure, Function, and Role in Alzheimer Disease. *Cold Spring Harb Perspect Med* **2**, a006304 (2012).
- [44] De Strooper, B. *et al.* Deficiency of presenilin-1 inhibits the normal cleavage of amyloid precursor protein. *Nature* **391**, 387–390 (1998).
- [45] Mutations — ALZFORUM. <https://www.alzforum.org/mutations>.
- [46] Corder, E. H. *et al.* Gene dose of apolipoprotein E type 4 allele and the risk of Alzheimer's disease in late onset families. *Science* **261**, 921–923 (1993).
- [47] Kim, J., Basak, J. M. & Holtzman, D. M. The Role of Apolipoprotein E in Alzheimer's Disease. *Neuron* **63**, 287–303 (2009).
- [48] Jonsson, T. *et al.* A mutation in *APP* protects against Alzheimer's disease and age-related cognitive decline. *Nature* **488**, 96–99 (2012).
- [49] Strooper, B. D. & Voet, T. Alzheimer's disease: A protective mutation. *Nature* **488**, 38–39 (2012).
- [50] Hardy, J. & Selkoe, D. J. The Amyloid Hypothesis of Alzheimer's Disease: Progress and Problems on the Road to Therapeutics. *Science* **297**, 353–356 (2002).

BIBLIOGRAPHY

- [51] Haass, C. *et al.* Amyloid β -peptide is produced by cultured cells during normal metabolism. *Nature* **359**, 322–325 (1992).
- [52] Bateman, R. J. *et al.* Human amyloid- β synthesis and clearance rates as measured in cerebrospinal fluid *in vivo*. *Nature Medicine* **12**, 856–861 (2006).
- [53] Lue, L.-F. *et al.* Soluble Amyloid β Peptide Concentration as a Predictor of Synaptic Change in Alzheimer’s Disease. *The American Journal of Pathology* **155**, 853–862 (1999).
- [54] Hampel, H. *et al.* Biomarkers for Alzheimer’s disease: Academic, industry and regulatory perspectives. *Nature Reviews Drug Discovery* **9**, 560–574 (2010).
- [55] Bateman, R. J. *et al.* Clinical and Biomarker Changes in Dominantly Inherited Alzheimer’s Disease. *New England Journal of Medicine* **367**, 795–804 (2012).
- [56] Citron, M. Alzheimer’s disease: Strategies for disease modification. *Nature Reviews Drug Discovery* **9**, 387–398 (2010).
- [57] Selkoe, D. J. Resolving controversies on the path to Alzheimer’s therapeutics. *Nature Medicine* **17**, 1060–1065 (2011).
- [58] Karran Eric & De Strooper Bart. The amyloid cascade hypothesis: Are we poised for success or failure? *Journal of Neurochemistry* **139**, 237–252 (2016).
- [59] Wasco, W. *et al.* Identification of a mouse brain cDNA that encodes a protein related to the Alzheimer disease-associated amyloid beta protein precursor. *Proc. Natl. Acad. Sci. U.S.A.* **89**, 10758–10762 (1992).
- [60] Wasco, W. *et al.* Isolation and characterization of APLP2 encoding a homologue of the Alzheimer’s associated amyloid β protein precursor. *Nature Genetics* **5**, 95 (1993).
- [61] Yamada, T. *et al.* Complementary DNA for the mouse homolog of the human amyloid beta protein precursor. *Biochemical and Biophysical Research Communications* **149**, 665–671 (1987).
- [62] Anliker, B. & Müller, U. The Functions of Mammalian Amyloid Precursor Protein and Related Amyloid Precursor-Like Proteins. *NDD* **3**, 239–246 (2006).
- [63] Aydin, D., Weyer, S. W. & Müller, U. C. Functions of the APP gene family in the nervous system: Insights from mouse models. *Experimental Brain Research* **217**, 423–434 (2012).
- [64] Müller, U. C., Deller, T. & Korte, M. Not just amyloid: Physiological functions of the amyloid precursor protein family. *Nature Reviews Neuroscience* **18**, 281–298 (2017).
- [65] Haass, C. Take five—BACE and the γ -secretase quartet conduct Alzheimer’s amyloid β -peptide generation. *The EMBO Journal* **23**, 483–488 (2004).
- [66] Koo, E. H. *et al.* Precursor of amyloid protein in Alzheimer disease undergoes fast anterograde axonal transport. *Proc. Natl. Acad. Sci. U.S.A.* **87**, 1561–1565 (1990).
- [67] Dawkins, E. & Small, D. H. Insights into the physiological function of the β -amyloid precursor protein: Beyond Alzheimer’s disease. *J. Neurochem.* **129**, 756–769 (2014).
- [68] Sambamurti, K., Refolo, L. M., Shioi, J., Pappolla, M. A. & Robakis, N. K. The Alzheimer’s Amyloid Precursor Is Cleaved Intracellularly in the Trans-Golgi Network or in a Post-Golgi Compartment. *Annals of the New York Academy of Sciences* **674**, 118–128 (1992).

-
- [69] Anandatheerthavarada, H. K., Biswas, G., Robin, M.-A. & Avadhani, N. G. Mitochondrial targeting and a novel transmembrane arrest of Alzheimer's amyloid precursor protein impairs mitochondrial function in neuronal cells. *The Journal of Cell Biology* **161**, 41–54 (2003).
- [70] Pagani, L. & Eckert, A. Amyloid-Beta interaction with mitochondria. *Int J Alzheimers Dis* **2011**, 925050 (2011).
- [71] Tanaka, S. *et al.* Tissue-specific expression of three types of β -protein precursor mRNA: Enhancement of protease inhibitor-harboring types in Alzheimer's disease brain. *Biochemical and Biophysical Research Communications* **165**, 1406–1414 (1989).
- [72] Haass, C., Hung, A. Y. & Selkoe, D. J. Processing of beta-amyloid precursor protein in microglia and astrocytes favors an internal localization over constitutive secretion. *J. Neurosci.* **11**, 3783–3793 (1991).
- [73] Rohan de Silva, H. A. *et al.* Cell-specific expression of β -amyloid precursor protein isoform mRNAs and proteins in neurons and astrocytes. *Molecular Brain Research* **47**, 147–156 (1997).
- [74] Kirazov, E., Kirazov, L., Bigl, V. & Schliebs, R. Ontogenetic changes in protein level of amyloid precursor protein (APP) in growth cones and synaptosomes from rat brain and prenatal expression pattern of APP mRNA isoforms in developing rat embryo. *International Journal of Developmental Neuroscience* **19**, 287–296 (2001).
- [75] Schubert, W. *et al.* Localization of Alzheimer β A4 amyloid precursor protein at central and peripheral synaptic sites. *Brain Research* **563**, 184–194 (1991).
- [76] Selkoe, D. J. Alzheimer's Disease: Genes, Proteins, and Therapy. *Physiological Reviews* **81**, 741–766 (2001).
- [77] Bhattacharyya, R., Barren, C. & Kovacs, D. M. Palmitoylation of Amyloid Precursor Protein Regulates Amyloidogenic Processing in Lipid Rafts. *J. Neurosci.* **33**, 11169–11183 (2013).
- [78] Haass, C., Kaether, C., Thinakaran, G. & Sisodia, S. Trafficking and Proteolytic Processing of APP. *Cold Spring Harb Perspect Med* **2**, a006270 (2012).
- [79] Lai, A., Sisodia, S. S. & Trowbridge, I. S. Characterization of Sorting Signals in the β -Amyloid Precursor Protein Cytoplasmic Domain. *J. Biol. Chem.* **270**, 3565–3573 (1995).
- [80] Haass, C., Koo, E. H., Mellon, A., Hung, A. Y. & Selkoe, D. J. Targeting of cell-surface β -amyloid precursor protein to lysosomes: Alternative processing into amyloid-bearing fragments. *Nature* **357**, 500 (1992).
- [81] Haass, C. & Selkoe, D. J. Cellular processing of β -amyloid precursor protein and the genesis of amyloid β -peptide. *Cell* **75**, 1039–1042 (1993).
- [82] Müller, S. A., Scilabra, S. D. & Lichtenthaler, S. F. Proteomic Substrate Identification for Membrane Proteases in the Brain. *Front Mol Neurosci* **9** (2016).
- [83] Chow, V. W., Mattson, M. P., Wong, P. C. & Gleichmann, M. An Overview of APP Processing Enzymes and Products. *Neuromolecular Med* **12**, 1–12 (2010).
- [84] Turner, P. R., O'Connor, K., Tate, W. P. & Abraham, W. C. Roles of amyloid precursor protein and its fragments in regulating neural activity, plasticity and memory. *Progress in Neurobiology* **70**, 1–32 (2003).

BIBLIOGRAPHY

- [85] Chen, K. *et al.* Synergic interaction between amyloid precursor protein and neural cell adhesion molecule promotes neurite outgrowth. *Oncotarget* **7**, 14199–14206 (2016).
- [86] Kang, J. *et al.* The precursor of Alzheimer’s disease amyloid A4 protein resembles a cell-surface receptor. *Nature* **325**, 733 (1987).
- [87] Rossjohn, J. *et al.* Crystal structure of the N-terminal, growth factor-like domain of Alzheimer amyloid precursor protein. *Nature Structural & Molecular Biology* **6**, 327 (1999).
- [88] Bukhari, H. *et al.* Small things matter: Implications of APP intracellular domain AICD nuclear signaling in the progression and pathogenesis of Alzheimer’s disease. *Progress in Neurobiology* **156**, 189–213 (2017).
- [89] Zheng, H. *et al.* β -amyloid precursor protein-deficient mice show reactive gliosis and decreased locomotor activity. *Cell* **81**, 525–531 (1995).
- [90] Wang, Z. *et al.* Presynaptic and Postsynaptic Interaction of the Amyloid Precursor Protein Promotes Peripheral and Central Synaptogenesis. *J. Neurosci.* **29**, 10788–10801 (2009).
- [91] Perez, R. G., Zheng, H., der Ploeg, L. H. T. V. & Koo, E. H. The β -Amyloid Precursor Protein of Alzheimer’s Disease Enhances Neuron Viability and Modulates Neuronal Polarity. *J. Neurosci.* **17**, 9407–9414 (1997).
- [92] Cousins, S. L., Hoey, S. E. A., Anne Stephenson, F. & Perkinson, M. S. Amyloid precursor protein 695 associates with assembled NR2A- and NR2B-containing NMDA receptors to result in the enhancement of their cell surface delivery. *J. Neurochem.* **111**, 1501–1513 (2009).
- [93] Cousins, S. L., Dai, W. & Stephenson, F. A. APLP1 and APLP2, members of the APP family of proteins, behave similarly to APP in that they associate with NMDA receptors and enhance NMDA receptor surface expression. *Journal of Neurochemistry* **133**, 879–885 (2015).
- [94] Hoe, H.-S., Lee, H.-K. & Pak, D. T. S. The Upside of APP at Synapses. *CNS Neuroscience & Therapeutics* **18**, 47–56 (2012).
- [95] Priller, C. *et al.* Synapse Formation and Function Is Modulated by the Amyloid Precursor Protein. *J. Neurosci.* **26**, 7212–7221 (2006).
- [96] Zou, C. *et al.* Amyloid precursor protein maintains constitutive and adaptive plasticity of dendritic spines in adult brain by regulating D-serine homeostasis. *The EMBO Journal* **35**, 2213–2222 (2016).
- [97] Bittner, T. *et al.* β -Secretase Inhibition Reduces Spine Density In Vivo via an Amyloid Precursor Protein-Dependent Pathway. *Journal of Neuroscience* **29**, 10405–10409 (2009).
- [98] Puzzo, D. *et al.* Picomolar Amyloid- β Positively Modulates Synaptic Plasticity and Memory in Hippocampus. *Journal of Neuroscience* **28**, 14537–14545 (2008).
- [99] Ishida, A., Furukawa, K., Keller, J. N. & Mattson, M. P. Secreted form of beta-amyloid precursor protein shifts the frequency dependency for induction of LTP, and enhances LTP in hippocampal slices. *Neuroreport* **8**, 2133–2137.

- [100] Hoey, S. E., Williams, R. J. & Perkinson, M. S. Synaptic NMDA Receptor Activation Stimulates α -Secretase Amyloid Precursor Protein Processing and Inhibits Amyloid- β Production. *J. Neurosci.* **29**, 4442–4460 (2009).
- [101] Ring, S. *et al.* The Secreted Beta-Amyloid Precursor Protein Ectodomain APPsAlpha Is Sufficient to Rescue the Anatomical, Behavioral, and Electrophysiological Abnormalities of APP-Deficient Mice. *Journal of Neuroscience* **27**, 7817–7826 (2007).
- [102] Hick, M. *et al.* Acute function of secreted amyloid precursor protein fragment APPs α in synaptic plasticity. *Acta Neuropathologica* **129**, 21–37 (2015).
- [103] Copanaki, E. *et al.* sAPP α antagonizes dendritic degeneration and neuron death triggered by proteasomal stress. *Molecular and Cellular Neuroscience* **44**, 386–393 (2010).
- [104] Weyer, S. W. *et al.* Comparative analysis of single and combined APP/APLP knockouts reveals reduced spine density in APP-KO mice that is prevented by APPs α expression. *Acta neuropathologica communications* **2**, 1 (2014).
- [105] Schon, E. A. & Area-Gomez, E. Mitochondria-associated ER membranes in Alzheimer disease. *Mol. Cell. Neurosci.* **55**, 26–36 (2013).
- [106] Pera, M. *et al.* Increased localization of APP-C99 in mitochondria-associated ER membranes causes mitochondrial dysfunction in Alzheimer disease. *The EMBO Journal* **36**, 3356–3371 (2017).
- [107] Devi, L., Prabhu, B. M., Galati, D. F., Avadhani, N. G. & Anandatheerthavarada, H. K. Accumulation of Amyloid Precursor Protein in the Mitochondrial Import Channels of Human Alzheimer’s Disease Brain Is Associated with Mitochondrial Dysfunction. *J. Neurosci.* **26**, 9057–9068 (2006).
- [108] Pavlov, P. F. *et al.* Mitochondrial γ -secretase participates in the metabolism of mitochondria-associated amyloid precursor protein. *The FASEB Journal* **25**, 78–88 (2010).
- [109] Wang, X. *et al.* Amyloid- β overproduction causes abnormal mitochondrial dynamics via differential modulation of mitochondrial fission/fusion proteins. *Proceedings of the National Academy of Sciences* **105**, 19318–19323 (2008).
- [110] Hamid, R. *et al.* Amyloid precursor protein intracellular domain modulates cellular calcium homeostasis and ATP content. *Journal of Neurochemistry* **102**, 1264–1275 (2007).
- [111] Leissring, M. A. *et al.* A physiologic signaling role for the γ -secretase-derived intracellular fragment of APP. *PNAS* **99**, 4697–4702 (2002).
- [112] Linde, C. I., Baryshnikov, S. G., Mazzocco-Spezia, A. & Golovina, V. A. Dysregulation of Ca²⁺ signaling in astrocytes from mice lacking amyloid precursor protein. *AJP: Cell Physiology* **300**, C1502–C1512 (2011).
- [113] Zhang, L. *et al.* Altered brain energetics induces mitochondrial fission arrest in Alzheimer’s Disease. *Scientific Reports* **6** (2016).
- [114] Wang, X. *et al.* Impaired Balance of Mitochondrial Fission and Fusion in Alzheimer’s Disease. *J. Neurosci.* **29**, 9090–9103 (2009).
- [115] Wang, Y. *et al.* Lost region in amyloid precursor protein (APP) through TALEN-mediated genome editing alters mitochondrial morphology. *Scientific Reports* **6**, srep22244 (2016).

BIBLIOGRAPHY

- [116] Ho, V. M., Lee, J.-A. & Martin, K. C. The Cell Biology of Synaptic Plasticity. *Science* **334**, 623–628 (2011).
- [117] Yuste, R. Dendritic Spines and Distributed Circuits. *Neuron* **71**, 772–781 (2011).
- [118] García-López, P., García-Marín, V. & Freire, M. The discovery of dendritic spines by Cajal in 1888 and its relevance in the present neuroscience. *Progress in Neurobiology* **83**, 110–130 (2007).
- [119] Hotulainen, P. & Hoogenraad, C. C. Actin in dendritic spines: Connecting dynamics to function. *The Journal of Cell Biology* **189**, 619–629 (2010).
- [120] Alvarez, V. A. & Sabatini, B. L. Anatomical and Physiological Plasticity of Dendritic Spines. *Annual Review of Neuroscience* **30**, 79–97 (2007).
- [121] Arellano, J. I., Espinosa, A., Fairén, A., Yuste, R. & DeFelipe, J. Non-synaptic dendritic spines in neocortex. *Neuroscience* **145**, 464–469 (2007).
- [122] Berry, K. P. & Nedivi, E. Spine Dynamics: Are They All the Same? *Neuron* **96**, 43–55 (2017).
- [123] Koleske, A. J. Molecular mechanisms of dendrite stability. *Nature Reviews Neuroscience* **14**, 536–550 (2013).
- [124] Fu, M. & Zuo, Y. Experience-dependent structural plasticity in the cortex. *Trends in Neurosciences* **34**, 177–187 (2011).
- [125] Yuste, R. & Bonhoeffer, T. Morphological Changes in Dendritic Spines Associated with Long-Term Synaptic Plasticity. *Annual Review of Neuroscience* **24**, 1071–1089 (2001).
- [126] Yuste, R. Electrical compartmentalization in dendritic spines. *Annu. Rev. Neurosci.* **36**, 429–449 (2013).
- [127] Trachtenberg, J. T. *et al.* Long-term *in vivo* imaging of experience-dependent synaptic plasticity in adult cortex. *Nature* **420**, 788 (2002).
- [128] Zuo, Y., Lin, A., Chang, P. & Gan, W.-B. Development of Long-Term Dendritic Spine Stability in Diverse Regions of Cerebral Cortex. *Neuron* **46**, 181–189 (2005).
- [129] Bliss, T. V. P. & Lømo, T. Long-lasting potentiation of synaptic transmission in the dentate area of the anaesthetized rabbit following stimulation of the perforant path. *The Journal of Physiology* **232**, 331 (1973).
- [130] Malenka, R. C. & Bear, M. F. LTP and LTD: An Embarrassment of Riches. *Neuron* **44**, 5–21 (2004).
- [131] Bliss, T. V. P. & Collingridge, G. L. A synaptic model of memory: Long-term potentiation in the hippocampus. *Nature* **361**, 31–39 (1993).
- [132] Huganir, R. L. & Nicoll, R. A. AMPARs and Synaptic Plasticity: The Last 25 Years. *Neuron* **80**, 704–717 (2013).
- [133] Collingridge, G. L., Kehl, S. J. & McLennan, H. Excitatory amino acids in synaptic transmission in the Schaffer collateral-commissural pathway of the rat hippocampus. *J. Physiol. (Lond.)* **334**, 33–46 (1983).
- [134] Shepherd, J. D. & Huganir, R. L. The Cell Biology of Synaptic Plasticity: AMPA Receptor Trafficking. *Annual Review of Cell and Developmental Biology* **23**, 613–643 (2007).

- [135] Lynch, G., Larson, J., Kelso, S., Barrionuevo, G. & Schottler, F. Intracellular injections of EGTA block induction of hippocampal long-term potentiation. *Nature* **305**, 719–721 (1983).
- [136] Koleske, A. J. Molecular mechanisms of dendrite stability. *Nature Reviews Neuroscience* **14**, 536–550 (2013).
- [137] Giaume, C., Kirchhoff, F., Matute, C., Reichenbach, A. & Verkhratsky, A. Glia: The fulcrum of brain diseases. *Cell Death & Differentiation* **14**, 1324–1335 (2007).
- [138] Kettenmann, H. & Verkhratsky, A. Neuroglia: The 150 years after. *Trends in Neurosciences* **31**, 653–659 (2008).
- [139] Dimou, L. & Götz, M. Glial Cells as Progenitors and Stem Cells: New Roles in the Healthy and Diseased Brain. *Physiological Reviews* **94**, 709–737 (2014).
- [140] Theis, M., Söhl, G., Eiberger, J. & Willecke, K. Emerging complexities in identity and function of glial connexins. *Trends Neurosci.* **28**, 188–195 (2005).
- [141] Rouach, N., Koulakoff, A., Abudara, V., Willecke, K. & Giaume, C. Astroglial Metabolic Networks Sustain Hippocampal Synaptic Transmission. *Science* **322**, 1551–1555 (2008).
- [142] Halassa, M. M. & Haydon, P. G. Integrated Brain Circuits: Astrocytic Networks Modulate Neuronal Activity and Behavior. *Annual Review of Physiology* **72**, 335–355 (2010).
- [143] Bushong, E. A., Martone, M. E., Jones, Y. Z. & Ellisman, M. H. Protoplasmic Astrocytes in CA1 Stratum Radiatum Occupy Separate Anatomical Domains. *J. Neurosci.* **22**, 183–192 (2002).
- [144] Perea, G., Navarrete, M. & Araque, A. Tripartite synapses: Astrocytes process and control synaptic information. *Trends in Neurosciences* **32**, 421–431 (2009).
- [145] Wang, X. *et al.* Astrocytic Ca²⁺ signaling evoked by sensory stimulation *in vivo*. *Nature Neuroscience* **9**, 816–823 (2006).
- [146] Araque, A., Parpura, V., Sanzgiri, R. P. & Haydon, P. G. Tripartite synapses: Glia, the unacknowledged partner. *Trends in Neurosciences* **22**, 208–215 (1999).
- [147] Navarrete, M. *et al.* Astrocyte Calcium Signal and Gliotransmission in Human Brain Tissue. *Cereb Cortex* **23**, 1240–1246 (2013).
- [148] Toni, N., Buchs, P.-A., Nikonenko, I., Bron, C. R. & Müller, D. LTP promotes formation of multiple spine synapses between a single axon terminal and a dendrite. *Nature* **402**, 421–425 (1999).
- [149] Maletic-Savatic, M., Malinow, R. & Svoboda, K. Rapid Dendritic Morphogenesis in CA1 Hippocampal Dendrites Induced by Synaptic Activity. *Science* **283**, 1923–1927 (1999).
- [150] Bernardinelli, Y. *et al.* Activity-Dependent Structural Plasticity of Perisynaptic Astrocytic Domains Promotes Excitatory Synapse Stability. *Current Biology* **24**, 1679–1688 (2014).
- [151] Chung, W.-S. *et al.* Astrocytes mediate synapse elimination through MEGF10 and MERTK pathways. *Nature* **504**, 394–400 (2013).
- [152] Perez-Alvarez, A., Navarrete, M., Covelo, A., Martin, E. D. & Araque, A. Structural and Functional Plasticity of Astrocyte Processes and Dendritic Spine Interactions. *J. Neurosci.* **34**, 12738–12744 (2014).

BIBLIOGRAPHY

- [153] Haber, M., Zhou, L. & Murai, K. K. Cooperative Astrocyte and Dendritic Spine Dynamics at Hippocampal Excitatory Synapses. *J. Neurosci.* **26**, 8881–8891 (2006).
- [154] Medvedev, N. *et al.* Glia selectively approach synapses on thin dendritic spines. *Philos. Trans. R. Soc. Lond., B, Biol. Sci.* **369**, 20140047 (2014).
- [155] Blanco-Suárez, E., Caldwell, A. L. M. & Allen, N. J. Role of astrocyte–synapse interactions in CNS disorders. *J Physiol* **595**, 1903–1916 (2017).
- [156] Scuderi, C., Stecca, C., Iacomino, A. & Steardo, L. Role of astrocytes in major neurological disorders: The evidence and implications. *IUBMB Life* **65**, 957–961.
- [157] Halassa, M. M. *et al.* Astrocytic Modulation of Sleep Homeostasis and Cognitive Consequences of Sleep Loss. *Neuron* **61**, 213–219 (2009).
- [158] Pascual, O. *et al.* Astrocytic Purinergic Signaling Coordinates Synaptic Networks. *Science* **310**, 113–116 (2005).
- [159] Henneberger, C., Papouin, T., Oliet, S. H. R. & Rusakov, D. A. Long-term potentiation depends on release of d-serine from astrocytes. *Nature* **463**, 232–236 (2010).
- [160] Butt, A. M. & Kalsi, A. Inwardly rectifying potassium channels (Kir) in central nervous system glia: A special role for Kir4.1 in glial functions. *J. Cell. Mol. Med.* **10**, 33–44 (2006 Jan-Mar).
- [161] Anderson, C. M. & Swanson, R. A. Astrocyte glutamate transport: Review of properties, regulation, and physiological functions. *Glia* **32**, 1–14 (2000).
- [162] Schousboe, A. Pharmacological and functional characterization of astrocytic GABA transport: A short review. *Neurochem. Res.* **25**, 1241–1244 (2000).
- [163] Hertz, L. & Zielke, H. R. Astrocytic control of glutamatergic activity: Astrocytes as stars of the show. *Trends Neurosci.* **27**, 735–743 (2004).
- [164] Nortley, R. & Attwell, D. Control of brain energy supply by astrocytes. *Current Opinion in Neurobiology* **47**, 80–85 (2017).
- [165] Volterra, A., Liaudet, N. & Savtchouk, I. Astrocyte Ca²⁺ signalling: An unexpected complexity. *Nature Reviews Neuroscience* **15**, 327–335 (2014).
- [166] Parpura, V. *et al.* Glutamate-mediated astrocyte–neuron signalling. *Nature* **369**, 744–747 (1994).
- [167] Shigetomi, E., Jackson-Weaver, O., Huckstepp, R. T., O’Dell, T. J. & Khakh, B. S. TRPA1 Channels Are Regulators of Astrocyte Basal Calcium Levels and Long-Term Potentiation via Constitutive D-Serine Release. *Journal of Neuroscience* **33**, 10143–10153 (2013).
- [168] Zhang, Q. *et al.* Fusion-related release of glutamate from astrocytes. *J. Biol. Chem.* **279**, 12724–12733 (2004).
- [169] Perea, G. & Araque, A. Properties of Synaptically Evoked Astrocyte Calcium Signal Reveal Synaptic Information Processing by Astrocytes. *J. Neurosci.* **25**, 2192–2203 (2005).
- [170] Parri, H. R., Gould, T. M. & Crunelli, V. Spontaneous astrocytic Ca²⁺ oscillations *in situ* drive NMDAR-mediated neuronal excitation. *Nature Neuroscience* **4**, 803–812 (2001).

- [171] Bindocci, E. *et al.* Three-dimensional Ca²⁺ imaging advances understanding of astrocyte biology. *Science* **356**, eaai8185 (2017).
- [172] Grosche, J. *et al.* Microdomains for neuron–glia interaction: Parallel fiber signaling to Bergmann glial cells. *Nature neuroscience* **2**, 139–143 (1999).
- [173] Boitier, E., Rea, R. & Duchen, M. R. Mitochondria Exert a Negative Feedback on the Propagation of Intracellular Ca²⁺ Waves in Rat Cortical Astrocytes. *The Journal of Cell Biology* **145**, 795–808 (1999).
- [174] Reyes, R. C. & Parpura, V. Mitochondria Modulate Ca²⁺-Dependent Glutamate Release from Rat Cortical Astrocytes. *J. Neurosci.* **28**, 9682–9691 (2008).
- [175] Yuste, R. Fluorescence microscopy today. <https://www.nature.com/emedien.ub.uni-muenchen.de/articles/nmeth1205-902> (2005).
- [176] Svoboda, K. & Yasuda, R. Principles of Two-Photon Excitation Microscopy and Its Applications to Neuroscience. *Neuron* **50**, 823–839 (2006).
- [177] Helmchen, F. & Denk, W. Deep tissue two-photon microscopy. *Nature Methods* **2**, 932–940 (2005).
- [178] Denk, W., Strickler, J. H. & Webb, W. W. Two-photon laser scanning fluorescence microscopy. *Science* **248**, 73–76 (1990).
- [179] Denk, W. & Svoboda, K. Photon Upmanship: Why Multiphoton Imaging Is More than a Gimmick. *Neuron* **18**, 351–357 (1997).
- [180] Marvin, M. Microscopy apparatus (1961).
- [181] Minsky, M. Memoir on inventing the confocal scanning microscope. *Scanning* **10**, 128–138.
- [182] Conchello, J.-A. & Lichtman, J. W. Optical sectioning microscopy. *Nature Methods* **2**, 920–931 (2005).
- [183] Berridge, M. J., Lipp, P. & Bootman, M. D. The versatility and universality of calcium signalling. *Nature Reviews Molecular Cell Biology* **1**, 11–21 (2000).
- [184] Berridge, M. J., Bootman, M. D. & Lipp, P. Calcium - a life and death signal. *Nature* **395**, 645–648 (1998).
- [185] Nedergaard, M., Rodríguez, J. J. & Verkhratsky, A. Glial calcium and diseases of the nervous system. *Cell Calcium* **47**, 140–149 (2010).
- [186] Shimomura, O., Johnson, F. H. & Saiga, Y. Extraction, purification and properties of aequorin, a bioluminescent protein from the luminous hydromedusan, *Aequorea*. *J Cell Comp Physiol* **59**, 223–239 (1962).
- [187] Miyawaki, A. *et al.* Fluorescent indicators for Ca²⁺ based on green fluorescent proteins and calmodulin. *Nature* **388**, 882–887 (1997).
- [188] Grienberger, C. & Konnerth, A. Imaging Calcium in Neurons. *Neuron* **73**, 862–885 (2012).
- [189] McCombs, J. E. & Palmer, A. E. Measuring calcium dynamics in living cells with Genetically Encodable Calcium Indicators. *Methods (San Diego, Calif.)* **46**, 152 (2008).

BIBLIOGRAPHY

- [190] Palmer, A. E. & Tsien, R. Y. Measuring calcium signaling using genetically targetable fluorescent indicators. *Nature Protocols* **1**, 1057–1065 (2006).
- [191] Nakai, J., Ohkura, M. & Imoto, K. A high signal-to-noise Ca^{2+} probe composed of a single green fluorescent protein. *Nature Biotechnology* **19**, 137–141 (2001).
- [192] Chen, T.-W. *et al.* Ultrasensitive fluorescent proteins for imaging neuronal activity. *Nature* **499**, 295–300 (2013).
- [193] Shigetomi, E., Kracun, S., Sofroniew, M. V. & Khakh, B. S. A genetically targeted optical sensor to monitor calcium signals in astrocyte processes. *Nature Neuroscience* **13**, 759–766 (2010).
- [194] Shigetomi, E. *et al.* Imaging calcium microdomains within entire astrocyte territories and endfeet with GCaMPs expressed using adeno-associated viruses. *The Journal of General Physiology* **141**, 633–647 (2013).
- [195] Agarwal, A. *et al.* Transient Opening of the Mitochondrial Permeability Transition Pore Induces Microdomain Calcium Transients in Astrocyte Processes. *Neuron* **93**, 587–605.e7 (2017).
- [196] Srinivasan, R. *et al.* New Transgenic Mouse Lines for Selectively Targeting Astrocytes and Studying Calcium Signals in Astrocyte Processes In Situ and In Vivo. *Neuron* **92**, 1181–1195 (2016).
- [197] Nimchinsky, E. A., Sabatini, B. L. & Svoboda, a. K. Structure and Function of Dendritic Spines. *Annual Review of Physiology* **64**, 313–353 (2002).
- [198] Magara, F. *et al.* Genetic background changes the pattern of forebrain commissure defects in transgenic mice underexpressing the β -amyloid-precursor protein. *Proceedings of the National Academy of Sciences* **96**, 4656–4661 (1999).
- [199] Madeira, C. *et al.* D-serine levels in Alzheimer’s disease: Implications for novel biomarker development. *Translational Psychiatry* **5**, e561 (2015).
- [200] Wu, S., Basile, A. S. & Barger, S. W. Induction of Serine Racemase Expression and D-Serine Release from Microglia by Secreted Amyloid Precursor Protein (sAPP) 9.
- [201] Wu, S.-Z. *et al.* Induction of serine racemase expression and D-serine release from microglia by amyloid β -peptide. *Journal of Neuroinflammation* **1**, 2 (2004).
- [202] Bourne, J. & Harris, K. M. Do thin spines learn to be mushroom spines that remember? *Current Opinion in Neurobiology* **17**, 381–386 (2007).
- [203] Taylor, C. J. *et al.* Endogenous secreted amyloid precursor protein- α regulates hippocampal NMDA receptor function, long-term potentiation and spatial memory. *Neurobiology of Disease* **31**, 250–260 (2008).
- [204] Sala, C. & Segal, M. Dendritic Spines: The Locus of Structural and Functional Plasticity. *Physiological Reviews* **94**, 141–188 (2014).
- [205] Tyan, S.-H. *et al.* Amyloid precursor protein (APP) regulates synaptic structure and function. *Molecular and Cellular Neuroscience* **51**, 43–52 (2012).
- [206] Lee, K. J. *et al.* Beta amyloid-independent role of amyloid precursor protein in generation and maintenance of dendritic spines. *Neuroscience* **169**, 344–356 (2010).

- [207] Mallm, J.-P., Tschäpe, J.-A., Hick, M., Filippov, M. A. & Müller, U. C. Generation of conditional null alleles for APP and APLP2. *genesis* **48**, 200–206 (2010).
- [208] Feng, G. *et al.* Imaging Neuronal Subsets in Transgenic Mice Expressing Multiple Spectral Variants of GFP. *Neuron* **28**, 41–51 (2000).
- [209] Takata, N. *et al.* Astrocyte Calcium Signaling Transforms Cholinergic Modulation to Cortical Plasticity In Vivo. *Journal of Neuroscience* **31**, 18155–18165 (2011).
- [210] Jackson, J. G. & Robinson, M. B. Reciprocal Regulation of Mitochondrial Dynamics and Calcium Signaling in Astrocyte Processes. *J. Neurosci.* **35**, 15199–15213 (2015).
- [211] Jackson, J. G. & Robinson, M. B. Regulation of mitochondrial dynamics in astrocytes: Mechanisms, consequences, and unknowns. *Glia* **66**, 1213–1234 (2018).
- [212] Leonard, A. P. *et al.* Quantitative analysis of mitochondrial morphology and membrane potential in living cells using high-content imaging, machine learning, and morphological binning. *Biochim. Biophys. Acta* **1853**, 348–360 (2015).
- [213] Li, H. *et al.* Imaging of mitochondrial Ca²⁺ dynamics in astrocytes using cell-specific mitochondria-targeted GCaMP5G/6s: Mitochondrial Ca²⁺ uptake and cytosolic Ca²⁺ availability via the endoplasmic reticulum store. *Cell Calcium* **56**, 457–466 (2014).
- [214] Jiang, X. & Wang, X. Cytochrome C-Mediated Apoptosis. *Annual Review of Biochemistry* **73**, 87–106 (2004).
- [215] Reddy, P. H. Inhibitors of Mitochondrial Fission as a Therapeutic Strategy for Diseases with Oxidative Stress and Mitochondrial Dysfunction. *J Alzheimers Dis* **40**, 245–256 (2014).
- [216] Mishra, J. *et al.* The Mitochondrial Ca²⁺ Uniporter: Structure, Function and Pharmacology. *Handb Exp Pharmacol* **240**, 129–156 (2017).
- [217] Duyckaerts, C., Delatour, B. & Potier, M.-C. Classification and basic pathology of Alzheimer disease. *Acta Neuropathol* **118**, 5–36 (2009).
- [218] Selkoe, D. J. The molecular pathology of Alzheimer’s disease. *Neuron* **6**, 487–498 (1991).
- [219] Panatier, A. *et al.* Glia-Derived d-Serine Controls NMDA Receptor Activity and Synaptic Memory. *Cell* **125**, 775–784 (2006).
- [220] Pousinha, P. A. *et al.* Physiological and pathophysiological control of synaptic GluN2B-NMDA receptors by the C-terminal domain of amyloid precursor protein. *eLife Sciences* **6**, e25659 (2017).
- [221] Hoe, H.-S. *et al.* The Effects of Amyloid Precursor Protein on Postsynaptic Composition and Activity. *J. Biol. Chem.* **284**, 8495–8506 (2009).
- [222] Bar-Yehuda, D. & Korngreen, A. Space-Clamp Problems When Voltage Clamping Neurons Expressing Voltage-Gated Conductances. *Journal of Neurophysiology* **99**, 1127–1136 (2008).
- [223] Dawson, G. R. *et al.* Age-related cognitive deficits, impaired long-term potentiation and reduction in synaptic marker density in mice lacking the β -amyloid precursor protein. *Neuroscience* **90**, 1–13 (1999).
- [224] Seabrook, G. R. *et al.* Mechanisms contributing to the deficits in hippocampal synaptic plasticity in mice lacking amyloid precursor protein. *Neuropharmacology* **38**, 349–359 (1999).

BIBLIOGRAPHY

- [225] Willem, M. *et al.* η -Secretase processing of APP inhibits neuronal activity in the hippocampus. *Nature* **526**, 443–447 (2015).
- [226] Phinney, A. L. *et al.* No hippocampal neuron or synaptic bouton loss in learning-impaired aged β -Amyloid precursor protein-null mice. *Neuroscience* **90**, 1207–1216 (1999).
- [227] Rudy, C. C., Hunsberger, H. C., Weitzner, D. S. & Reed, M. N. The Role of the Tripartite Glutamatergic Synapse in the Pathophysiology of Alzheimer's Disease. *Aging and Disease* **6**, 131 (2015).
- [228] Soba, P. *et al.* Homo- and heterodimerization of APP family members promotes intercellular adhesion. *The EMBO Journal* **24**, 3624–3634 (2005).
- [229] Stahl, R. *et al.* Shedding of APP limits its synaptogenic activity and cell adhesion properties. *Front Cell Neurosci* **8**, 410 (2014).
- [230] Noguchi, J., Matsuzaki, M., Ellis-Davies, G. C. R. & Kasai, H. Spine-Neck Geometry Determines NMDA Receptor-Dependent Ca²⁺ Signaling in Dendrites. *Neuron* **46**, 609–622 (2005).
- [231] Kwon, H.-B. *et al.* Neuroligin-1–dependent competition regulates cortical synaptogenesis and synapse number. *Nature Neuroscience* **15**, 1667–1674 (2012).
- [232] John Lin, C.-C. *et al.* Identification of diverse astrocyte populations and their malignant analogs. *Nature Neuroscience* **20**, 396–405 (2017).
- [233] Khakh, B. S. & Sofroniew, M. V. Diversity of astrocyte functions and phenotypes in neural circuits. *Nature Neuroscience* **18**, 942–952 (2015).
- [234] Regan, M. R. *et al.* Variations in Promoter Activity Reveal a Differential Expression and Physiology of Glutamate Transporters by Glia in the Developing and Mature CNS. *J. Neurosci.* **27**, 6607–6619 (2007).
- [235] Lehre, K. P., Levy, L. M., Ottersen, O. P., Storm-Mathisen, J. & Danbolt, N. C. Differential expression of two glial glutamate transporters in the rat brain: Quantitative and immunocytochemical observations. *J. Neurosci.* **15**, 1835–1853 (1995).
- [236] Schitine, C., Nogaroli, L., Costa, M. R. & Hedin-Pereira, C. Astrocyte heterogeneity in the brain: From development to disease. *Front. Cell. Neurosci.* **9** (2015).
- [237] Zhou, M. & Kimelberg, H. K. Freshly Isolated Hippocampal CA1 Astrocytes Comprise Two Populations Differing in Glutamate Transporter and AMPA Receptor Expression. *J. Neurosci.* **21**, 7901–7908 (2001).
- [238] Martineau, M., Parpura, V. & Mothet, J.-P. Cell-type specific mechanisms of D-serine uptake and release in the brain. *Frontiers in Synaptic Neuroscience* **6**, 12 (2014).
- [239] Rizzuto, R. & Pozzan, T. Microdomains of Intracellular Ca²⁺ : Molecular Determinants and Functional Consequences. *Physiological Reviews* **86**, 369–408 (2006).
- [240] Lalo, U., Pankratov, Y., Kirchhoff, F., North, R. A. & Verkhratsky, A. NMDA Receptors Mediate Neuron-to-Glia Signaling in Mouse Cortical Astrocytes. *J. Neurosci.* **26**, 2673–2683 (2006).
- [241] Matthias, K. *et al.* Segregated Expression of AMPA-Type Glutamate Receptors and Glutamate Transporters Defines Distinct Astrocyte Populations in the Mouse Hippocampus. *J. Neurosci.* **23**, 1750–1758 (2003).

- [242] Lanjakornsiripan, D. *et al.* Layer-specific morphological and molecular differences in neocortical astrocytes and their dependence on neuronal layers. *Nature Communications* **9** (2018).
- [243] Takata, N. & Hirase, H. Cortical Layer 1 and Layer 2/3 Astrocytes Exhibit Distinct Calcium Dynamics In Vivo. *PLoS ONE* **3** (2008).
- [244] Lynn, B. D., Marotta, C. A. & Nagy, J. I. Propagation of intercellular calcium waves in PC12 cells overexpressing a carboxy-terminal fragment of amyloid precursor protein. *Neuroscience Letters* **199**, 21–24 (1995).
- [245] Mei, X., Ezan, P., Giaume, C. & Koulakoff, A. Astroglial connexin immunoreactivity is specifically altered at β -amyloid plaques in β -amyloid precursor protein/presenilin1 mice. *Neuroscience* **171**, 92–105 (2010).
- [246] Koulakoff, A., Mei, X., Orellana, J. A., Sáez, J. C. & Giaume, C. Glial connexin expression and function in the context of Alzheimer’s disease. *Biochimica et Biophysica Acta (BBA) - Biomembranes* **1818**, 2048–2057 (2012).
- [247] Goiran, T. *et al.* β -Amyloid Precursor Protein Intracellular Domain Controls Mitochondrial Function by Modulating Phosphatase and Tensin Homolog–Induced Kinase 1 Transcription in Cells and in Alzheimer Mice Models. *Biological Psychiatry* **83**, 416–427 (2018).
- [248] Nett, W. J., Oloff, S. H. & McCarthy, K. D. Hippocampal Astrocytes In Situ Exhibit Calcium Oscillations That Occur Independent of Neuronal Activity. *Journal of Neurophysiology* **87**, 528–537 (2002).
- [249] Zhang, X. *et al.* Impaired theta-gamma coupling in APP-deficient mice. *Scientific Reports* **6** (2016).
- [250] Bosson, A. *et al.* TRPA1 channels promote astrocytic Ca²⁺ hyperactivity and synaptic dysfunction mediated by oligomeric forms of amyloid- β peptide. *Molecular Neurodegeneration* **12**, 53 (2017).
- [251] Srinivasan, R. *et al.* Ca²⁺ signaling in astrocytes from Ip3r2 ^{-/-} mice in brain slices and during startle responses in vivo. *Nature Neuroscience* **18**, 708–717 (2015).
- [252] Stephen, T.-L., Gupta-Agarwal, S. & Kittler, J. T. Mitochondrial dynamics in astrocytes. *Biochemical Society Transactions* **42**, 1302–1310 (2014).
- [253] Hausteijn, M. D. *et al.* Conditions and Constraints for Astrocyte Calcium Signaling in the Hippocampal Mossy Fiber Pathway. *Neuron* **82**, 413–429 (2014).
- [254] Jackson, J. G., O’Donnell, J. C., Takano, H., Coulter, D. A. & Robinson, M. B. Neuronal Activity and Glutamate Uptake Decrease Mitochondrial Mobility in Astrocytes and Position Mitochondria Near Glutamate Transporters. *J. Neurosci.* **34**, 1613–1624 (2014).
- [255] Oceau, J. C. *et al.* An Optical Neuron–Astrocyte Proximity Assay at Synaptic Distance Scales. *Neuron* **98**, 49–66.e9 (2018).
- [256] Rafelski, S. M. Mitochondrial network morphology: Building an integrative, geometrical view. *BMC Biology* **11**, 71 (2013).
- [257] Motori, E. *et al.* Inflammation-Induced Alteration of Astrocyte Mitochondrial Dynamics Requires Autophagy for Mitochondrial Network Maintenance. *Cell Metabolism* **18**, 844–859 (2013).

BIBLIOGRAPHY

- [258] Swerdlow, R. H., Burns, J. M. & Khan, S. M. The Alzheimer's disease mitochondrial cascade hypothesis: Progress and perspectives. *Biochimica et Biophysica Acta (BBA) - Molecular Basis of Disease* **1842**, 1219–1231 (2014).
- [259] Chen, H. & Chan, D. C. Mitochondrial dynamics-fusion, fission, movement, and mitophagy-in neurodegenerative diseases. *Human Molecular Genetics* **18**, R169–R176 (2009).
- [260] Baloyannis, S. J. Mitochondrial alterations in Alzheimer's disease. *Journal of Alzheimer's Disease* **9**, 119–126 (2006).
- [261] Trushina, E. *et al.* Defects in mitochondrial dynamics and metabolomic signatures of evolving energetic stress in mouse models of familial Alzheimer's disease. *PLoS ONE* **7**, e32737 (2012).
- [262] Calkins, M. J., Manczak, M., Mao, P., Shirendeb, U. & Reddy, P. H. Impaired mitochondrial biogenesis, defective axonal transport of mitochondria, abnormal mitochondrial dynamics and synaptic degeneration in a mouse model of Alzheimer's disease. *Hum. Mol. Genet.* **20**, 4515–4529 (2011).
- [263] Du, F. *et al.* PINK1 signalling rescues amyloid pathology and mitochondrial dysfunction in Alzheimer's disease. *Brain* **140**, 3233–3251 (2017).
- [264] Gegg, M. E. *et al.* Mitofusin 1 and mitofusin 2 are ubiquitinated in a PINK1/parkin-dependent manner upon induction of mitophagy. *Hum Mol Genet* **19**, 4861–4870 (2010).
- [265] Goiran, T. *et al.* β -Amyloid Precursor Protein Intracellular Domain Controls Mitochondrial Function by Modulating Phosphatase and Tensin Homolog-Induced Kinase 1 Transcription in Cells and in Alzheimer Mice Models. *Biological Psychiatry* **83**, 416–427 (2018).
- [266] Zhu, Y. *et al.* Monitoring Mitophagy in Mammalian Cells. In *Methods in Enzymology*, vol. 547, 39–55 (Elsevier, 2014).
- [267] Santo-Domingo, J. & Demaurex, N. Calcium uptake mechanisms of mitochondria. *Biochimica et Biophysica Acta (BBA) - Bioenergetics* **1797**, 907–912 (2010).
- [268] Ko, A.-R., Hyun, H.-W., Min, S.-J. & Kim, J.-E. The Differential DRP1 Phosphorylation and Mitochondrial Dynamics in the Regional Specific Astroglial Death Induced by Status Epilepticus. *Front Cell Neurosci* **10** (2016).
- [269] Frank, S. *et al.* The Role of Dynamin-Related Protein 1, a Mediator of Mitochondrial Fission, in Apoptosis. *Developmental Cell* **1**, 515–525 (2001).
- [270] Kandimalla, R. & Reddy, P. H. Multiple Faces of Dynamin-related Protein 1 and Its Role in Alzheimer's Disease Pathogenesis. *Biochim Biophys Acta* **1862**, 814–828 (2016).
- [271] Manczak, M., Calkins, M. J. & Reddy, P. H. Impaired mitochondrial dynamics and abnormal interaction of amyloid beta with mitochondrial protein Drp1 in neurons from patients with Alzheimer's disease: Implications for neuronal damage. *Human Molecular Genetics* **20**, 2495–2509 (2011).
- [272] de Brito, O. M. & Scorrano, L. Mitofusin 2 tethers endoplasmic reticulum to mitochondria. *Nature* **456**, 605 (2008).
- [273] Leal, N. S. *et al.* Mitofusin-2 knockdown increases ER-mitochondria contact and decreases amyloid β -peptide production. *Journal of Cellular and Molecular Medicine* **20**, 1686–1695 (2016).

-
- [274] Del Turco, D. *et al.* Region-Specific Differences in Amyloid Precursor Protein Expression in the Mouse Hippocampus. *Frontiers in Molecular Neuroscience* **9** (2016).
- [275] Park, J. *et al.* Loss of mitofusin 2 links beta-amyloid-mediated mitochondrial fragmentation and Cdk5-induced oxidative stress in neuron cells. *Journal of Neurochemistry* **132**, 687–702 (2015).
- [276] Wu, G., Sankaranarayanan, S., Hsieh, S. H.-K., Simon, A. J. & Savage, M. J. Decrease in brain soluble amyloid precursor protein β (sAPP β) in Alzheimer's disease cortex. *J. Neurosci. Res.* **89**, 822–832 (2011).
- [277] Li, Z. W. *et al.* Generation of mice with a 200-kb amyloid precursor protein gene deletion by Cre recombinase-mediated site-specific recombination in embryonic stem cells. *PNAS* **93**, 6158–6162 (1996).
- [278] Li, H. *et al.* Imaging of mitochondrial Ca²⁺ dynamics in astrocytes using cell-specific mitochondria-targeted GCaMP5G/6s: Mitochondrial Ca²⁺ uptake and cytosolic Ca²⁺ availability via the endoplasmic reticulum store. *Cell Calcium* **56**, 457–466 (2014).
- [279] Rizzuto, R., Brini, M., Pizzo, P., Murgia, M. & Pozzan, T. Chimeric green fluorescent protein as a tool for visualizing subcellular organelles in living cells. *Current Biology* **5**, 635–642 (1995).

List of Publications

Crux S, Herms J, Dorostkar MM. Tcf4 regulates dendritic spine density and morphology in the adult brain. *PLoS One* 13(6):e0199359 (2018)

Zhu K, Xiang X, Filser S, Marinkovi P, Dorostkar MM, **Crux S**, Neumann U, Shimshek DR, Rammes G, Haass C, Lichtenthaler SF, Gunnensen JM, Herms J. Beta-Site Amyloid Precursor Protein Cleaving Enzyme 1 Inhibition Impairs Synaptic Plasticity via Seizure Protein 6. *Biol Psychiatry* 83(5):428-437 (2018)

Zou C, **Crux S**, Marinesco S, Montagna E, Sgobio C, Shi Y, Shi S, Zhu K, Dorostkar MM, Mller UC, Herms J. Amyloid precursor protein maintains constitutive and adaptive plasticity of dendritic spines in adult brain by regulating D-serine homeostasis. *EMBO J* 35(20):2213-2222 (2016)

Poska H, Haslbeck M, Kurudenkandy FR, Hermansson E, Chen G, Kostallas G, Abelein A, Biverstl H, **Crux S**, Fisahn A, Presto J, Johansson J. Dementia-related Bri2 BRICHOS is a versatile molecular chaperone that efficiently inhibits A42 toxicity in Drosophila. *Biochem J*. 473(20):3683-3704 (2016)

Manuscripts in preparation

Montagna E*, **Crux S***, Luckner M, Herber J, Colombo AV, Tahirovic S, Wanner G, Lichtenthaler S, Sgobio C, Herms J. In vivo Ca²⁺ imaging of astrocytic microdomains reveals a critical role of the amyloid precursor protein for mitochondria. (*shared first authorship, in review)

Crux S, Pratsch K, Filser S, Herms J. The astrocytic amyloid precursor protein regulates dendritic spine density and morphology in the adult brain. (in preparation)

Scientific poster presentations

Crux S, Montagna E, Herber J, Sgobio C, Colombo AV, Tahirovic S, Lichtenthaler S, Herms J. The amyloid precursor protein is crucial for robust calcium activity in astrocytes. Poster, Society for Neuroscience 2017, November 11-15, Washington DC.

Acknowledgements

Firstly, I would like to express my sincere gratitude to my supervisor Prof. Dr. Jochen Herms for his continuous support during this interesting research project. With his patience, motivation and discussions he created an excellent scientific environment that helped me develop scientifically and personally.

Furthermore, I would like to deeply thank Prof. Dr. Martin Biel who agreed to represent this dissertation at the Faculty for Chemistry and Pharmacy. I would also like to thank the entire thesis committee for their time and interest in this work.

Moreover, I would like to acknowledge all collaborators for their material and/or teaching and fruitful discussions. Special thanks go to Prof. Dr. Gerhard Rammes, Prof. Dr. Stefan Lichtenthaler, Dr. Sabina Tahirovic, Prof. Dr. Gerhard Wanner, Dr. Alessio Colombo, Prof. Dr. Ulrike Müller and my collaborating colleagues in the lab Elena Montagna, Dr. Dr. Mario Dorostkar, Dr. Carmelo Sgobio, Julia Herber, Manja Luckner, Dr. Kaichuan Zhu, Dr. Chengyu Zou, Katrin Pratsch and Dr. Severin Filser. Moreover, I would like to thank Kathi, Sarah, Claudia, Marek and Nadine for their excellent technical support.

A big thank you goes to all colleagues from AG Herms, CSD U1 and ZNP who created a great working atmosphere in the lab and who were always helpful. Special thanks to all people who proofread this dissertation.

Finally, I would like to express my very profound gratitude to my parents, to Jojo and to Dennis for providing me with continuous support and encouragement throughout any episode of my life. I deeply thank you for constantly believing in me and always being there for me.